Chemical Ionization and Collision Induced Dissociation Mass Spectrometry

by

Andrew David Wright

Submitted to the University of Warwick in partial fulfillment of the degree of Doctor of Philosophy.

Department of Chemistry
University of Warwick
COVENTRY
CV4 7AL

October 1989

To Nicola.

Contents

Acknowledgements

I would like to thank my supervisor, Professor Keith Jennings, for his encouragement throughout my three years of study. I thank all of my colleagues at Kratos, especially Dr. David Milton, Peter Ryan, Rod Buchanan and Susan Coles, for their patience and assistance during my periods of study there. My thanks go to Professor Peter Derrick for the many discussions of the translational energy losses of ions. I thank the university of Warwick Chemistry Department's mechanical, glassblowing and electronic workshop staff for the many hours of work they have done to maintain the instruments and for their help with modification of the instruments. I would also like to thank all of my colleagues in the Chemistry Department, especially Dr. Richard Bowen for his encouragement and many fruitful discussions.

I acknowledge the Science and Engineering Research Council and Kratos Analytical for their financial support under the Cooperative Awards in Science and Engineering (CASE) scheme. I also acknowledge the British Mass Spectrometry Society for their assistance in meeting the cost of travel to several conferences which have been very rewarding.

Finally, I thank my wife, Nicola, without whose patience, encouragement and support, none of this would have been possible.

Declaration

Parts of this work have been presented at the following meetings either orally or in poster form.

British Mass Spectrometry Society Sixteenth Annual meeting, University of York, September 1987.

Eleventh International Mass Spectrometry Conference, Bordeaux Congrès, 1988.

American Society for Mass Spectrometry, Thirty-seventh meeting, Miami, May 1989.

The work contained in Chapter 3 is also presented in a paper in the Royal Society of Chemistry Perkin II journal, and is a result of collaboration with Dr Richard Bowen at the University of Warwick*.

* A.D. Wright, R.D. Bowen and K.R. Jennings, *J. Chem. Soc. Perk. Trans. II, in press.*

B	Magnetic Field Strength
CI	Chemical Ionization
CID	Collision Induced Dissociation
E	Electrostatic Sector Potential
EI	Electron Impact Ionization
E_k	Ion Translational Energy
FAB	Fast Atom Bombardment
MS/MS	Tamdem Mass Spectrometry
TEL	Translational Energy Loss
V_{acc}	Accelerating Voltage
V_{cell}	Collision Cell Voltage
ΔV	Translational Energy Loss

List of Figures

List of Tables

Summary

The work contained in this thesis covers two aspects of mass spectrometry, namely chemical ionization (CI) and collision induced dissociation (CID). Chapter 2 deals with an investigation into the CI mass spectra of tetraisopropyl methylenebisphosphonate recorded using mixtures of argon and dimethylamine as the reagent gas. Comparison of the mixed gas spectra with those obtained using the individual gases revealed additional fragmentation in the case of the mixed gases. The conclusion drawn from the study is that the dilution of dimethylamine with argon causes the formation of additional protonating species of lower proton affinity than dimethylamine which can undergo more exothermic proton transfer reactions with the sample. Chapter 3 reports a comprehensive study of the chemical ionization mass spectra of urethanes. Four main classes of fragment ions are found in the spectra and the mechanisms for their formation are postulated. Evidence for these mechanisms is obtained from parallel studies of methyl carbamates and from a CID study. A study of the effects of the collision gas on the CID mass spectra of leucine-enkephalin is presented in chapter 4. The collision gases used were helium, argon, krypton and carbon tetrafluoride The monatomic gases used cause more fragmentation of the peptide ion as the mass of the collision gas is increased. Conversely, when a polyatomic species is used, the CID spectra resemble those acquired using a much less heavy target gas. Two possible explanations are proposed. Either the additional internal energy which would be expected to be transferred to the incident ion is absorbed by vibrational modes of the target molecule, or that the amount of energy transferred during the collision is dependent on the particular atoms of the colliding species rather than their overall masses. The final chapter of this thesis is a report of the development of new linked-scan equations for the detection of fragment ions resulting from CID in the first field-free region of a forward geometry mass spectrometer. These scan laws and terms relating to the size of the translational energy losses are incorporated into the calibration software for use with a commercial mass spectrometer.

Chapter 1

Introduction

1.1. Introduction.

The mass spectrum of a compound is a plot of ion abundances normalized to the most abundant ion as a function of mass to charge ratio (m/z). The simplest form which this can take is a spectrum containing one peak corresponding to the ionized sample molecules. This only provides information about the relative molecular mass (r.m.m.) of the sample. Fragment ions may be formed from this molecular ion by competing, consecutive unimolecular reactions. These ions provide useful structural information about the molecule. The whole spectrum is characteristic of the compound and may be compared with libraries of mass spectra for rapid identification of unknown samples. More complex spectra are obtained from mixtures of compounds since it is difficult to ascertain which peaks in the spectrum result from which component of the mixture. These difficulties can be overcome by using chromatographic techniques, such as gas chromatography (g.c.)[1] and high performance liquid chromatography (HPLC)[2], before admitting the sample to the mass spectrometer. It is possible to perform such separation techniques in an 'on-line' manner where the eluent from the chromatographic instrument enters the mass spectrometer via a suitable interface. This permits rapid analysis of complex mixtures since many mass spectra can be recorded every second. More rapid identification of a single component of a mixture can be achieved by ionizing the entire mixture, selecting a single precursor ion and recording a collision induced dissociation (CID) mass spectrum using a tandem mass spectrometer[3].

1.2 The Mass Spectrometer.

A mass spectrometer has three main components; a source of ions, a means of separating ions according to their mass to charge ratio and an ion detector.

1.2.1. Ion Production.

The most common method employed to ionize samples is electron impact ionization (EI). Volatile samples introduced into the ion source of the mass spectrometer are vaporized and the vapour produced is bombarded by a beam of electrons. The electrons are produced by a hot wire filament and are accelerated through a potential of 70 V into the ion source. As the

electrons collide with the sample molecules, 15 to 20 eV of energy is transferred to the molecule. Since organic molecules require approximately 10 eV for ionization, the remaining energy causes the newly formed cations to fragment in a characteristic[4] manner. Ions formed by EI have an odd number of electrons, i.e. they are radical species. Fragmentation of radical cations usually occurs by expulsion of a radical species leaving an ion with an even number of electrons. This ion may fragment further by loss of closed-shell molecules to form another even electron ion. This is generally referred to as the even electron rule. For certain organic ions, fragmentation is a very favourable process. This may produce a mass spectrum containing no peaks due to molecular ions which is clearly undesirable when molecular weight information is required. This has led to the development of 'soft' ionization techniques such as chemical ionization (CI)[5] and desorption techniques. Chemical ionization mass spectrometry is discussed more fully in Chapter 2. There are many desorption techniques available to the mass spectroscopist; fast atom bombardment[6] (FAB) and secondary ion mass spectrometry[7] (SIMS), field desorption[8] (FD), laser desorption[9] and plasma desorption mass spectrometry[10] (PDMS). The most common of these techniques is FAB in which a beam of xenon atoms is directed towards the sample which is dissolved in an involatile matrix such as glycerol. The effect of the impact of xenon atoms, of typically 8 keV energy, is desorption and ionization though the exact mechanism is uncertain[11]. FAB is now commonly used for ionization of involatile inorganic and biological samples.

1.2.2. Mass Analyzers.

There are four main types of mass analyzer. These are magnetic, quadrupole, time of flight (TOF) and Fourier transform ion cyclotron resonance (FTMS or FT-ICR).

A magnetic field can be used to separate ions of different mass to charge ratios. Ions moving in a magnetic field experience a force mutually perpendicular to their direction of motion and the magnetic field. The ions will travel through the field in a circular path whose radius, r, is given by

$$r = mv_0/Bez \qquad (1.1)$$

where m is the mass of the ion, v_0 is its velocity, z is its multiplicity of charge and B is the magnetic field strength. In addition to this property of a magnetic sector, angularly divergent ion beams entering the magnetic field are refocused to a single point after the magnet[12].

An important feature of a mass spectrometer is its ability to resolve ions of slightly different masses, i.e. mass m from mass (m + δm). The resolving power of a magnetic sector instrument can be increased by reducing the kinetic energy spread of the ions entering the magnetic field. This can be achieved by placing an electrostatic sector, consisting of a pair of concentric cylindrical metal plates with equal but opposite voltages on them, before the magnet. The effect of an electrostatic analyzer (ESA) is to focus ions of the same kinetic energy at a point before the magnetic sector, figure 1.1. The resulting double focusing mass spectrometer is capable of high resolving power. This double focusing property also allows beams of ions of the same mass but of slightly differing energies to be focused at the same point after the magnetic sector of the mass spectrometer as shown in figure 1.1. The resolving power of such instruments can be increased by closing down the source and collector slits at the expense of sensitivity. A similar result can be achieved by placing the ESA after the magnetic sector. Instruments such as this are termed reverse geometry and are commonly used for CID experiments.

The mass to charge ratio of an ion transmitted through a double focussing mass spectrometer is derived below.

Initially, the ions of mass m, are accelerated by a voltage V giving them a velocity v_0 such that

$$\tfrac{1}{2}mv_0^2 = zVe \qquad (1.2)$$

where z is the multiplicity of the charge of the ion.

Eliminating v_0 from equations 1.1 and 1.2 gives

$$m/ze = B^2r^2/2V \qquad (1.3)$$

Hence, a mass spectrum is recorded by scanning B whilst V and r are held constant.

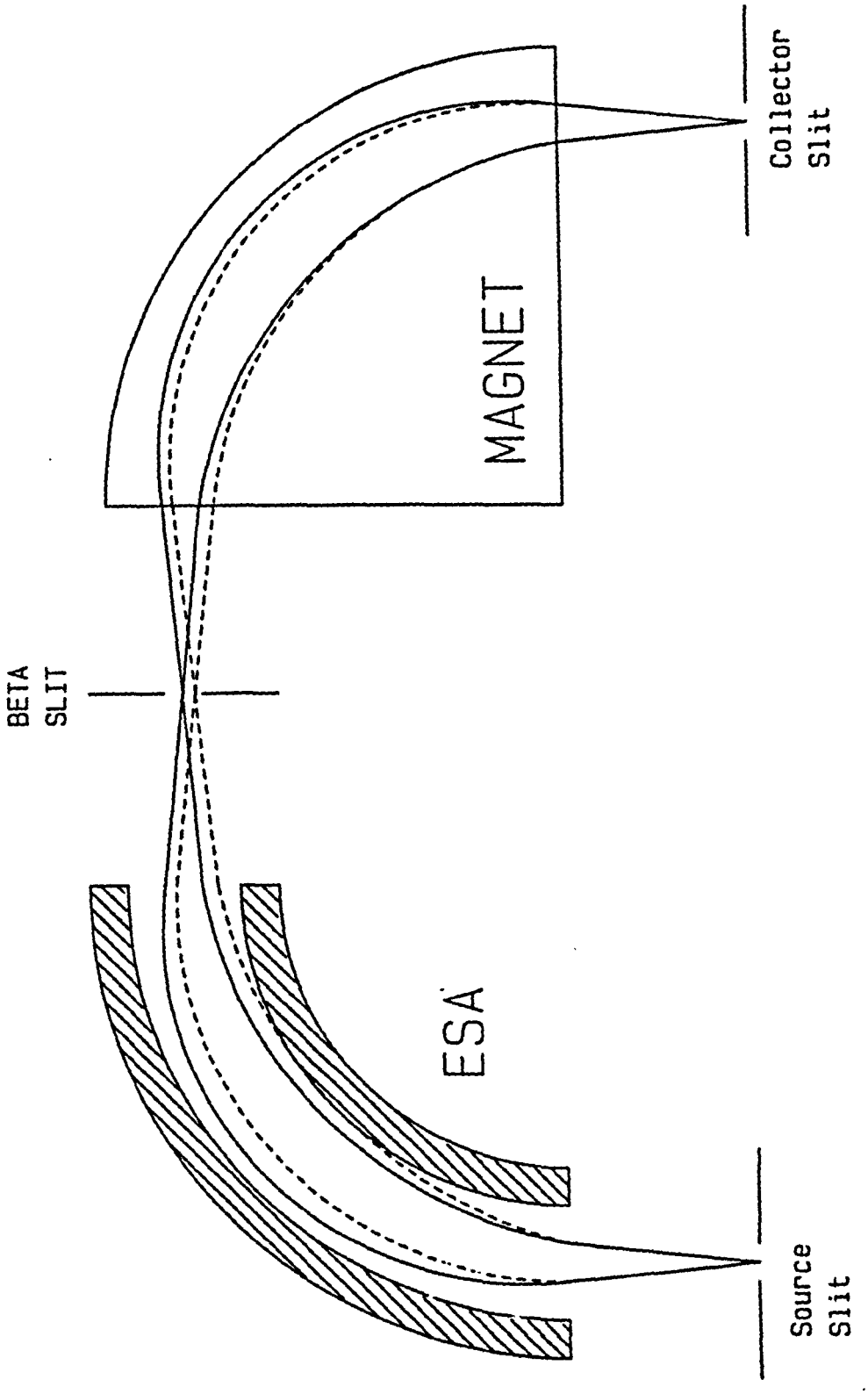

Figure 1.1. Nier-Johnson geometry mass spectrometer illustrating double focusing property.

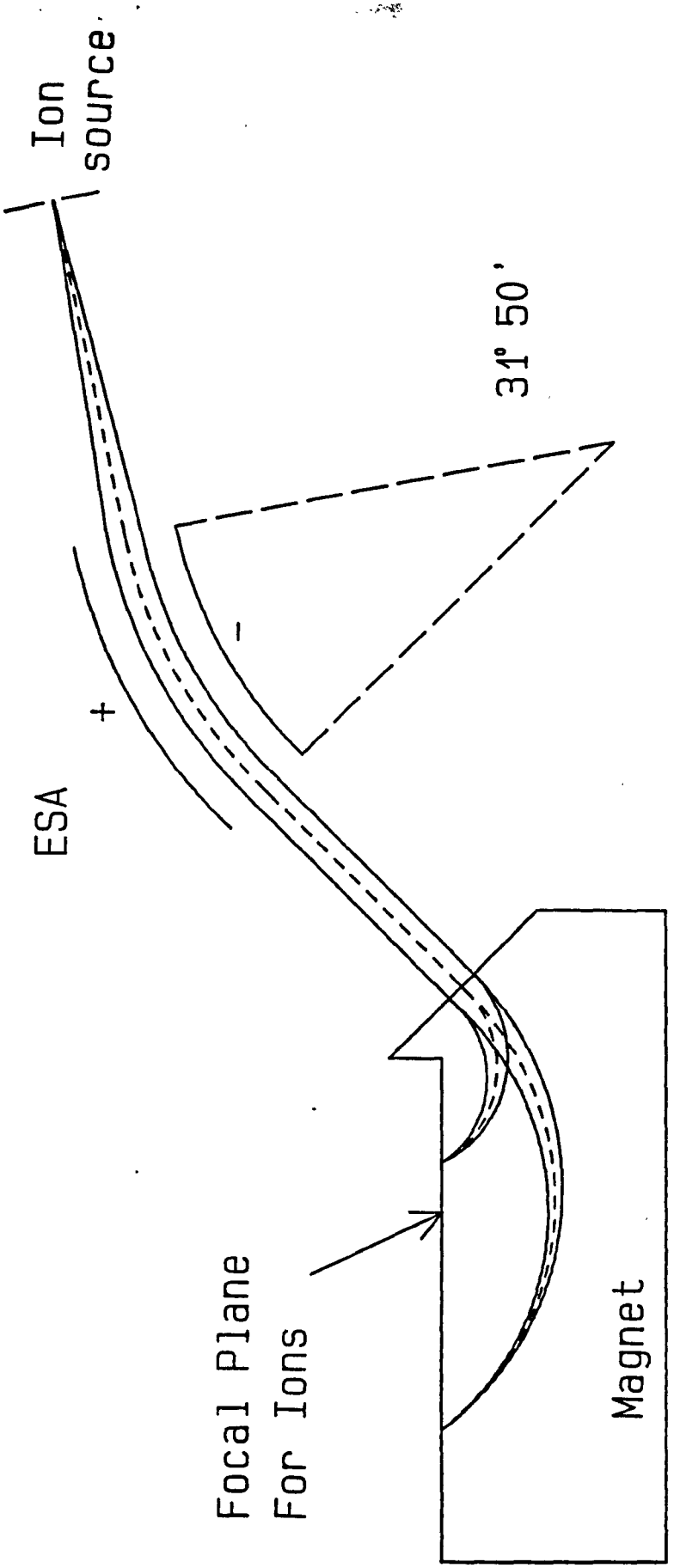

Figure 1.2. Mattauch-Herzog geometry mass spectrometer.

There are two types of mass spectrometer in which the ESA precedes the magnetic sector. The first, developed by Mattauch and Herzog[13], enables ions over a wide range of masses to be detected simultaneously using, for example a photographic plate (figure 1.2). The second type, of Nier-Johnson[14] geometry is the most common for high resolution work is shown in figure 1.1. The instruments used on this study are of this forward, Nier-Johnson geometry.

Of the remaining types of mass analyzer, the quadrupole mass filter[15] is the most common for routine low resolution work. A quadrupole mass filter consists of four parallel, cylindrical or hyperbolic rods to which d.c. and r.f. voltages are applied. By varying the magnitude of these voltages, the mass of an ion which has a stable, cyclical trajectory between the rods, can be selected, all other ions strike the rods and are lost. The advantages of such instruments are that they can be used to acquire mass spectra very rapidly, they are relatively inexpensive and extremely robust and are ideally suited to computer control. However, quadrupole mass spectrometers have limited mass ranges (<4000 Daltons) and resolving powers.

A variation of the quadrupole mass spectrometer is the quadrupole ion storage mass spectrometer (QUISTOR)[16], a three dimensional version of a quadrupole. Ions are formed inside the QUISTOR and held there by d.c. and r.f. fields. After a preset storage time, the ions are ejected by changing the fields inside the QUISTOR cell. More recently such an instrument has been applied to tandem mass spectrometry[17].

The mass to charge ratio of an ion may also be determined by measuring its velocity for a given kinetic energy. Time-of-flight mass spectrometers[18] use this principle. This technique readily lends itself to ionization methods which create pulses of ions. Ionization by laser desorption or by desorption caused by fast, heavy fission fragments such as those of ^{252}Cf are ideally suited. TOF mass spectrometers have limited resolving power but have very high mass range.

Finally, Fourier transform ion cyclotron resonance (FT-ICR or FTMS) mass spectrometers[19] are based on the principle, conceived by Lawrence and Livingstone[20], that ions absorb energy when placed in a radio-frequency field. The ions, if they are also constrained in a magnetic field, will undergo circular motion with a characteristic frequency ω_c which is given by

$$\omega_c = zB/m \qquad (1.4)$$

where z is the charge on the ion, m is its mass and B is the magnetic field. To obtain a mass spectrum using such an instrument, all of the ions inside the ICR cell are coherently excited to larger circular orbits by a 'chirp' of r.f. field. The ions induce an analogue signal in the receiver plates of the cell. This procedure is repeated many times a second and the signal stored in a computer. Once sufficient data have been acquired, Fourier transform and frequency-to-mass conversions are performed producing a mass spectrum. Since all of the ions can be detected at the same time this technique is very sensitive. Its other major advantage is its capability for resolving powers in excess of 1,000,000.

1.2.3. Ion Detection.

The most common device for the detection of ions is the electron multiplier. These devices, either discrete dynode or continuous channel units, have rapid response time and high gain; a gain of 10^6 is typical. A device with higher sensitivity is the post-acceleration detector (PAD), which uses an ion-to-electron conversion dynode and a high voltage to accelerate the secondary electrons produced into the electron multiplier.

The most recent development in ion detection enables ions over a small mass range to be detected simultaneously. These detectors employ charge coupled devices, fibre-optic couplings and photo diode arrays[9]. Used in conjunction with magnetic sector instruments, these devices provide for greater sensitivity since the mass spectrum is recorded in discrete sections which can be enhanced by relatively long integration times (~ 1 s). Using a computer the mass spectrum can be reconstructed.

1.3. Metastable Ions and Collision Induced Dissociation.

There is a finite probability that ions formed in the ion source of a mass spectrometer may fragment before reaching the detector. By considering the amount of time which an ion spends in each part of a mass spectrometer and the rate constants for unimolecular decomposition, it is possible to determine whether such fragmentations will occur. Ions which fragment outside the ion source are known as metastable ions.

An ion may spend between 1 and 5 μs in the ion source of a commercial mass spectrometer[21], however, it is difficult to determine the exact source residence time. Once an ion has left the ion source, the time taken for it to reach the detector can be easily calculated. For an ion of mass 100 Daltons, this is approximately 15 μs in an MS-50 mass spectrometer operating at 8 kV accelerating voltage. Taking into account these values, ions which undergo unimolecular decomposition with a rate constant of 10^6 s^{-1} or greater, will fragment inside the ion source. If the decomposition rate constant is less than 10^5 s^{-1}, the fragmentation will not occur before the ion reaches the detector. So metastable ions will result from unimolecular decompositions with rate constants lying between 10^5 and 10^6 s^{-1} based on these data.

1.3.1. Metastable Ions.

A double focusing mass spectrometer of forward geometry has three field-free regions (FFRs). These are located between the ion source and the ESA, between the ESA and the magnet and between the magnet and the detector. Ions which fragment in the third FFR will appear in the mass spectrum at the same mass to charge ratio as their precursors since they undergo no further mass separation. Ions fragmenting within either of the sectors of the analyzer cannot readily be accounted for in the mass spectrum since their apparent mass will depend upon where in the sector they fragmented. However, it is possible to detect ions which decompose in either the first or second FFR.

Ions formed by metastable decompositions within the second FFR can be observed in a normal mass spectrum as small, broad peaks at non-integral mass to charge ratios[22]. The

mass to charge ratio at which such peaks are observed depends upon the masses of the precursor and fragment ions. This apparent mass, m^*, is given by equation 1.5.

$$m^* = (m_f)^2/m_p \qquad (1.5)$$

The presence of such peaks in a mass spectrum has analytical value, since they can be used to identify precursor-fragment ion pairs. The width of the peak is caused by kinetic energy release on fragmentation[21].

Ions formed by metastable decompositions in the first FFR will not be observed in a normal mass spectrum since their kinetic energy is reduced by the factor m_f/m_p, i.e. they will not pass through the ESA. Detection of these ions is facilitated by linked scanning of the ESA potential and the magnetic field[23]. The relationship between the ESA potential and the magnetic field determines the information contained in the mass spectrum. The most common are shown below.

(i) All fragment ions of a selected precursor ion: B/E = constant.

(ii) All precursor ions of a selected fragment ion: B^2/E = constant.

(iii) All fragment/precursor ions resulting from the loss of a constant neutral: $(B^2/E)((E_0/E) - 1)$ = constant

As with second FFR metastable decompositions, these spectra have significant analytical value in structure determination and a number of techniques for bringing about fragmentation of stable ions in the first FFR of a mass spectrometer have been devised. These include collisions with inert gases[24], collisions with a metal surface[25], photoexcitation[26] and bombardment by electrons[27]. The most commonly used technique for activation of ions, involving collisions with an inert gas, is collision induced dissociation (CID).

1.3.2. Collision Induced Dissociation.

The processes involved in CID can be considered as two distinct events. Firstly, collisions between the incident ions and the inert target gas, causes excitation or activation of the ions

(equation 1.6) and secondly unimolecular decomposition of the activated ions if they have

$$m_p^+ + N \rightarrow m_p^{+*} + N \quad (1.6)$$

gained sufficient internal energy (equation 1.7).

$$m_p^{+*} \rightarrow m_f^+ + m_n \quad (1.7)$$

Other processes which may occur include charge stripping and charge exchange reactions. The latter becomes more important when the target gas has a low ionization potential (IP). For this reason, the most commonly used collision gas is helium since it has a very high IP, 24.5 eV[28]. The mass spectra produced by high energy CID, i.e. those recorded using sector instruments, resemble the e.i. spectra of the same ion. The analytical value of this technique was first noted by Jennings[24] and has become a valuable tool for ion structure determination.

A disadvantage of CID is that it is not possible to determine the amount of energy deposited in the activation step, unlike experiments involving photoexcitation. It is possible, however, to vary the amount of energy transferred to the ion by changing the collision conditions, i.e. the incident ion energy, the collision gas and the pressure of the collision gas.

1.4. References.

1. J.R. Chapman, "Practical Organic Mass Spectrometry", Wiley-Interscience, Chichester, 1985.
2. W.H. McFadden, *J. Chromatogr. Sci.*, **17**, 2 (1979).
3. "Tandem Mass Spectrometry", Ed. F.W. McLafferty, Wiley, New York, 1983.
4. K. Levsen, "Fundamental Aspects of Organic Mass Spectrometry", Verlag Chemie, Weinheim, 1975.
5. M.S.B. Munson and F.H. Field, *J. Am. Chem. Soc.*, **88**, 2621 (1966).
6. M. Barber, R.S. Bordoli, R.D. Sedgwick and L.W. Tetler, *Org. Mass Spectrom.*, **16**, 256 (1981).
7. R.. Honig, *Int. J. Mass Spec. Ion Phys.*, **66**, 31 (1985).
8. H.-R. Schulten, *Int. J. Mass Spec. Ion Phys.*, **32**, 97 (1979).

9. F.A. White and G.M. Wood, "Mass Spectrometry: Applications in Science and Engineering", Wiley-Interscience, New York, 1986.

10. R.D. Macfarlane, *Anal. Chem.*, **55**, 1247A (1983).

11. J.M. Miller, K. Balasanmugam and A. Fulcher, *Org. Mass Spectrom.*, **24**, 497 (1989) and references cited therein.

12. J. Roboz, "Introduction to Mass Spectrometry", Wiley-Interscience, New York, 1968.

13. A.J. Mattauch and R. Herzog, *Z. Physik*, **89**, 786 (1934).

14. E.G. Johnson and A.O. Nier, *Phys. Rev.*, **91**, 10 (1953).

15. "Quadrupole Mass Spectrometry and its Applications", Ed. P.H. Dawson, Elsevier, New York, 1976.

16. E. Fischer, *Z. Phys.*, **156**, 1 (1959).

17. J.N. Louris, R.G. Cooks, J.E.P. Syka, P.E. Kelley, G.C. Stafford Jr. and J.F. Todd, *Anal. Chem.*, **59**, 1677 (1987).

18. W.C. Wiley and I.H. McLaren, *Rev. Sci. Instrum.*, **26**, 1150 (1955).

19. M.B. Commisarow and A.C. Marshall, *Chem. Phys. Lett.*, **25**, 282 (1974).

20. E.O. Lawrence and M.S. Livingstone, *Phys. Rev.*, **37**, 707 (1931).

21. I. Howe, D.H. Williams and R.D. Bowen, "Mass Spectrometry: Principles and Applications", 2nd Edn., McGraw-Hill, London, 1981.

22. J.A. Hipple, R.E. Fox and E.U. Condon, *Phys. Rev.*, **69**, 347 (1946).

23. K.R. Jennings and R.S. Mason in reference 3.

24. K.R. Jennings, *Int. J. Mass Spec. Ion Phys.*, **1**, 227 (1968).

25. R.G. Cooks, D.T.Terwilliger, T. Ast, J.H. Beynon and T. Keough, *J. Am. Chem. Soc.*, **17**,1583 (1975).

26. E.S. Mukhtar, I.W. Griffiths, F.M. Harris and J.H. Beynon, *Int. J. Mass Spec. Ion Phys.*, **37**, 159 (1981).

27. S. Tajima, S. Tobita, K. Ogino and Y. Niwa, *Org. Mass Spectrom.*, **21**, 236 (1986).

28. H.M. Rosenstock, K. Draxl, B.W. Steiner and J.T. Herron, *J. Phys. Chem. Ref. Data*, **6**, supplement 1, I-71 (1977).

Chapter 2

Chemical Ionization Using Mixed Reagent Gases

2.1. Introduction.

Chemical ionization[1] (CI) is a method of producing ions by chemical reactions in the gas phase. A small amount of sample is introduced into the ion source of a mass spectrometer along with a large excess of a reagent gas. Ions formed from the reagent gas react with the sample molecules forming ions characteristic of the sample. The ratio of the partial pressures of the reagent gas and the sample should be in excess of 10^3, (ref. 1) otherwise it is possible to ionize a significant proportion of the sample directly by electron impact[2] which may cause confusion[3]. The total pressure inside the ion source is relatively high (typically >0.5 Torr) so that ion-molecule reactions can occur.

For positive ion chemical ionization mass spectrometry, typical reagent gases used are methane, ammonia and isobutane. These gases form cationic species which are capable of transferring a proton to the sample molecules. The ions formed from these gases which may take part in the proton transfer reactions are shown in table 2.1.

Reagent Gas	Reactive Species
CH_4	CH_5^+
	$C_2H_5^+$
	$C_3H_5^+$
NH_3	NH_4^+
	$(NH_3)_2H^+$
i-C_4H_{10}	$C_3H_7^+$
	$C_4H_9^+$

Table 2.1 Ions formed in reagent gas plasmas. (Data from ref. 4)

The ions formed from the sample will have a mass to charge ratio one Dalton greater than the relative molecular mass of the sample since a proton has been added. A major difference is observed in the fragmentation patterns of the protonated species compared with ions formed

under EI conditions. The protonated ion will have an even number of electrons and consequently is unlikely to undergo fragmentations involving the loss of radical species (see Chapter 1). With chemical ionization, it is possible to control the extent of fragmentation by limiting the amount of energy transferred to the sample ions. The maximum amount of energy transferred to the ions is dependent upon the proton affinities (PAs) of the sample and reagent. The proton affinity of a species is defined as the enthalpy change for the reaction (reaction 2.1).

$$AH^+ \rightarrow A + H^+ \qquad (2.1)$$

i.e. $PA(A) = \Delta H$

So the overall enthalpy change for a chemical ionization reaction (reaction 2.2)

$$AH^+ + B \rightarrow A + BH^+ \qquad (2.2)$$

is given by

$$\Delta H = PA(A) - PA(B)$$

The proton affinity values for the common reagent gases are given in table 2.2.

Reagent Gas	Reactive Species	Conjugate Base	Proton Affinity /kJ mol^{-1}
CH_4	CH_5^+	CH_4	552
	$C_2H_5^+$	C_2H_4	680
NH_3	NH_4^+	NH_3	853.5
i-C_4H_{10}	$C_4H_9^+$	$(CH_3)_2C{=}CH_2$	820

Table 2.2 Proton affinity values for selected reagent gases.

The ability to select the extent of fragmentation of a sample is obviously a great advantage of chemical ionization mass spectrometry.

Other types of gas phase reactions used to form positive ions include charge exchange reactions (reaction 2.3).

$$R^{+\cdot} + M \rightarrow R + M^{+\cdot} \qquad (2.3)$$

Such reactions produce radical cations which will undergo similar fragmentations to those of ions formed by electron bombardment. Unlike with EI, it is possible to control the amount of internal energy supplied to the sample ions. The enthalpy change for the ionization process is given by equation 2.4

$$\Delta H = IE(M) - RE(R^{+\cdot}) \qquad (2.4)$$

where IE(M) is the ionization energy of the sample molecule and $RE(R^{+\cdot})$ is the recombination energy of the reagent ion[2]. The recombination energy of a monatomic ion is the same as the ionization energy of the neutral species. This is not necessarily the case for diatomic and larger species. So, by selection of the reagent ion it is possible to control the extent of fragmentation of the sample ions. Recombination energies for typical reagent ions are given in table 2.3.

Ion	RE/eV
$Ar^{+\cdot}$	15.8
$N_2^{+\cdot}$	15.3
$CO_2^{+\cdot}$	13.8
$CS_2^{+\cdot}$	~10
$C_6H_6^{+\cdot}$	9.2

Table 2.3. Selected recombination energies for radical cations[4]. (1 eV = 96.5 kJ mol^{-1}).

The final type of positive ion formation using chemical ionization methods involves capture of the reagent ion by the sample molecules. In the chemical ionization plasmas of methane and ammonia several species are formed which can form bonds with the sample molecules. For methane, the species $C_2H_5^+$ and $C_3H_5^+$ may form adducts with samples giving peaks in the mass spectrum at m/z [M + 29] and [M + 41] where M is the molecular weight of the sample. These are observed in the methane chemical ionization spectra of urethanes (see Chapter 3). Similarly, a common reaction in ammonia CI is capture of NH_4^+ by samples with

proton affinities close to that of ammonia[5]. These adduct ions have a mass 18 Daltons greater than the molecular weight of the sample.

It is also possible to form negative ions under chemical ionization conditions. Proton abstraction, chloride ion attachment and electron attachment reactions occur with suitable reagent gases. Hydroxyl ions, formed by electron bombardment of N_2O/CH_4 mixtures can be used to remove a proton from a wide range of compounds[4]. Chloride ions are formed by electron ionization of dichloromethane readily attach to species containing hydroxyl, carbonyl and amine groups[2]. The final type of negative ion production uses a high pressure of gas, usually methane, to slow down the electrons to thermal energies. The thermal electrons may then be captured by electrophilic species such as nitro-aromatic compounds[6].

Selective ionization can be achieved under chemical ionization conditions by using a reagent ion which can only react with particular species in a mixture. By using a reagent gas of high proton affinity it is possible to protonate only the most basic components of a mixture. Another example of a chemical reaction in the gas phase which results in selective ionization uses vinyl methyl ether as the reagent gas. This reagent gas not only selectively ionizes alkenes but enables the determination of the position of the double bond in the molecule without the need for derivatisation[7].

2.1.1. Introduction to This Study.

It was noted by Vekey[8] that using dimethylamine, a high proton affinity reagent gas, tetraisopropyl methylene bisphosphonate (TMBP, figure 2.1) could be selectively ionized from an unrefined sample.

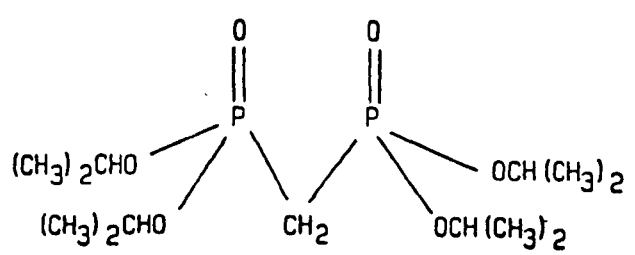

Figure 2.1 The structure of tetraisopropyl methylene bisphosphonate.

It was also noted that when the reagent gas was diluted with nitrogen, fragmentation is observed without the loss of selectivity. This study attempts to provide a satisfactory explanation for these results.

2.2. Experimental.

A sample of TMBP was prepared by the reaction of tri-isopropyl phosphite with dibromomethane (reaction 2.5)[9]. The crude TMBP was not purified so that the selectivity of the ionization could be tested.

$$2[(CH_3)_2CHO]_3P + CH_2Br_2 \rightarrow$$
$$((CH_3)_2CHO)_2OPCH_2PO(OCH(CH_3)_2)_2 + 2(CH_3)_2CHBr \qquad (2.5)$$

All of the mass spectra were recorded using an AEI (Kratos) MS 30 mass spectrometer modified for chemical ionization and equipped with a Mass Spectrometry Services data system. Reagent gases were admitted to the ion source from a 2 dm^3 glass bulb via the reagent gas inlet line (figure 2.2). The pure gases and mixtures of gases were introduced into the bulb using an all glass vacuum line.

The pressure of the reagent gas inside the ion source could not be measured, but the pressure of the gas in the inlet line was measured using an Edwards High Vacuum capsule dial gauge. The reagent gas pressures were varied between 100 and 700 mBar. The temperature of the ion source was varied between 50° and 250°C allowing 30 minutes for this temperature to be stabilized. The ionizing electrons were accelerated into the ion source with an energy of 100 eV using the electron current setting 3 (500 μA emission current).

2.3. Results and Discussion.

The chemical ionization mass spectra of crude and pure samples of TMBP were recorded using ammonia, dimethylamine, argon and mixtures of argon and dimethylamine. The electron impact mass spectra were also recorded for comparison.

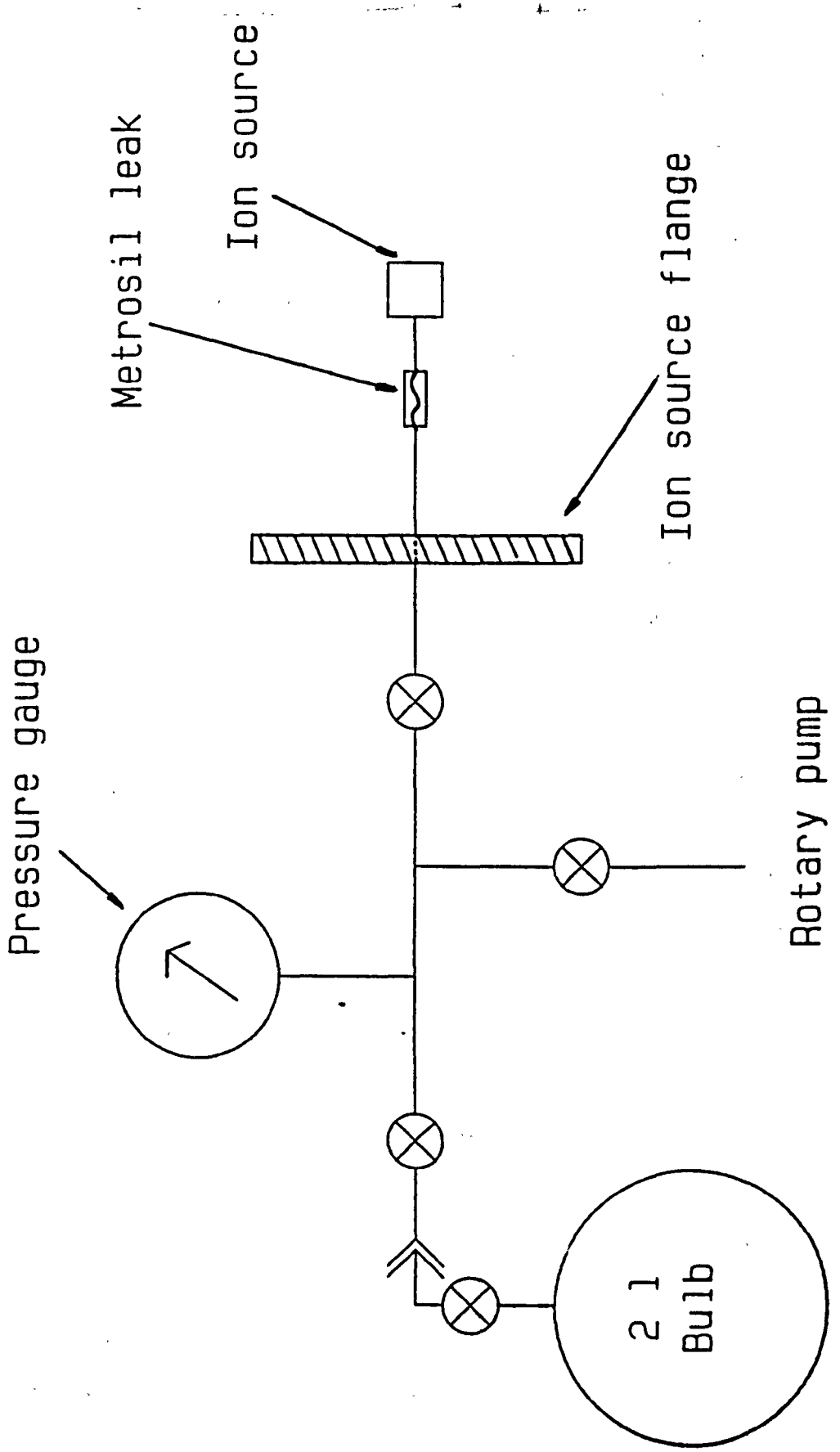

Figure 2.2. Reagent gas inlet system for the MS 30 mass spectrometer.

2.3.1. Ammonia Chemical Ionization.

The ammonia chemical ionization mass spectrum of pure TMBP is shown in figure 2.3. The spectrum contains peaks due to the protonated molecular ion of TMBP and several fragment ions due to successive losses of propene molecules. The fragmentation scheme is shown in figure 2.4. The ammonia CI spectrum of the crude sample is shown for comparison (figure 2.5). TMBP can be seen as a minor component of the mixture, being characterized by the peaks at m/z 345, 303 and 261. The nature of the impurities is not important, but they are probably residual reagents from the synthesis procedure.

2.3.2. Dimethylamine Chemical Ionization.

In order to perhaps selectively ionize the TMBP in the mixture, a reagent gas of high proton affinity was employed. The gas chosen was dimethylamine with a proton affinity of 923 kJ mol^{-1}, 69 kJ mol^{-1} higher than ammonia[10].

The CI spectra of both the crude and pure samples contain only two significant peaks, both of which are due to ionized TMBP. Figure 2.6 shows the spectrum of the impure compound. The peak at m/z 345 is due to protonated TMBP and the peak at m/z 390 is due to the ion formed by capture of the reagent ion, $(CH_3)_2NH_2^+$, by the sample molecules. It is therefore clear that none of the contaminants are ionized when dimethylamine is used as the reagent gas. Using this method, only the molecular weight of the sample can be determined.

2.3.3. Electron Impact and Charge Transfer Spectra.

The spectra of TMBP recorded using EI, nitrogen and argon charge transfer are shown in figure 2.7. All three spectra of the pure compound contain no molecular ion of TMBP.

2.3.4. Ionization Using Mixtures of Gases.

An example of the spectra obtained using mixtures of argon and dimethylamine is shown in figure 2.8. The spectrum was recorded using a 9:1 mixture of argon and dimethylamine at an ion source temperature of 200°C. It should be noted that the spectrum is not the same as that

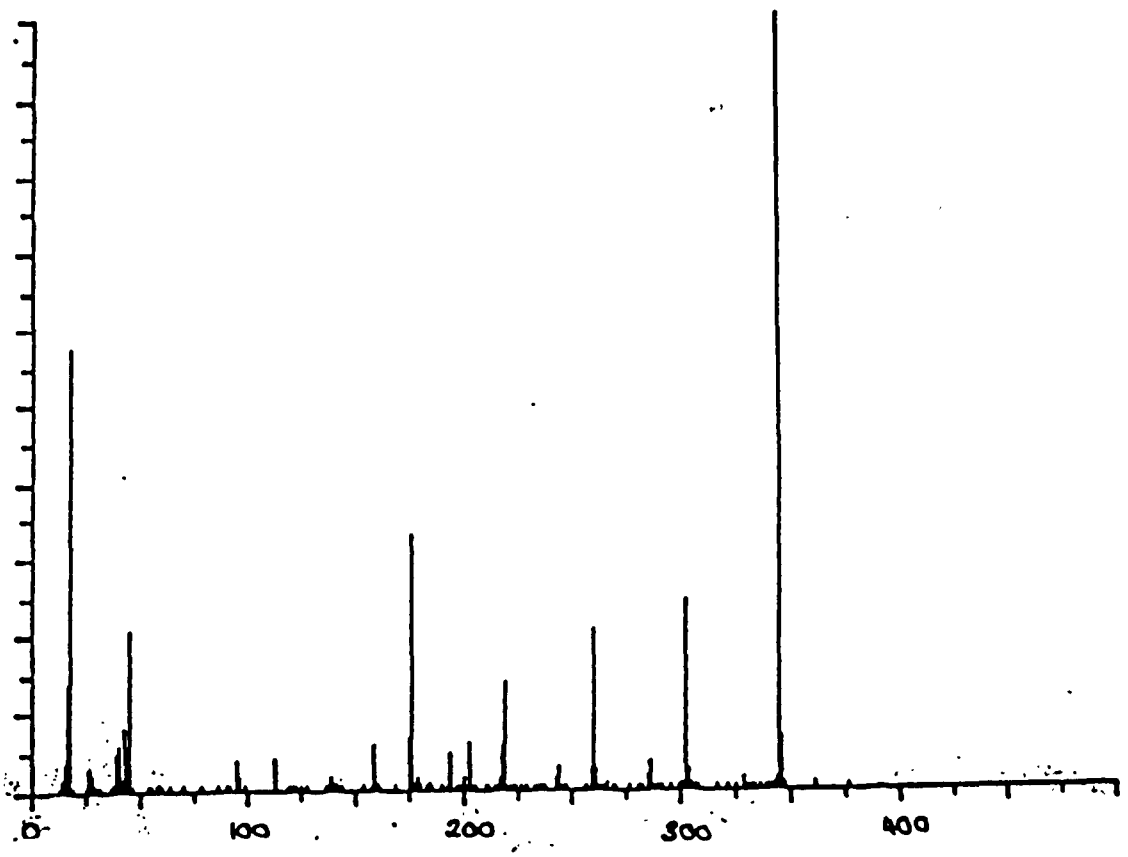

Figure 2.3. Ammonia CI mass spectrum of pure TMBP.

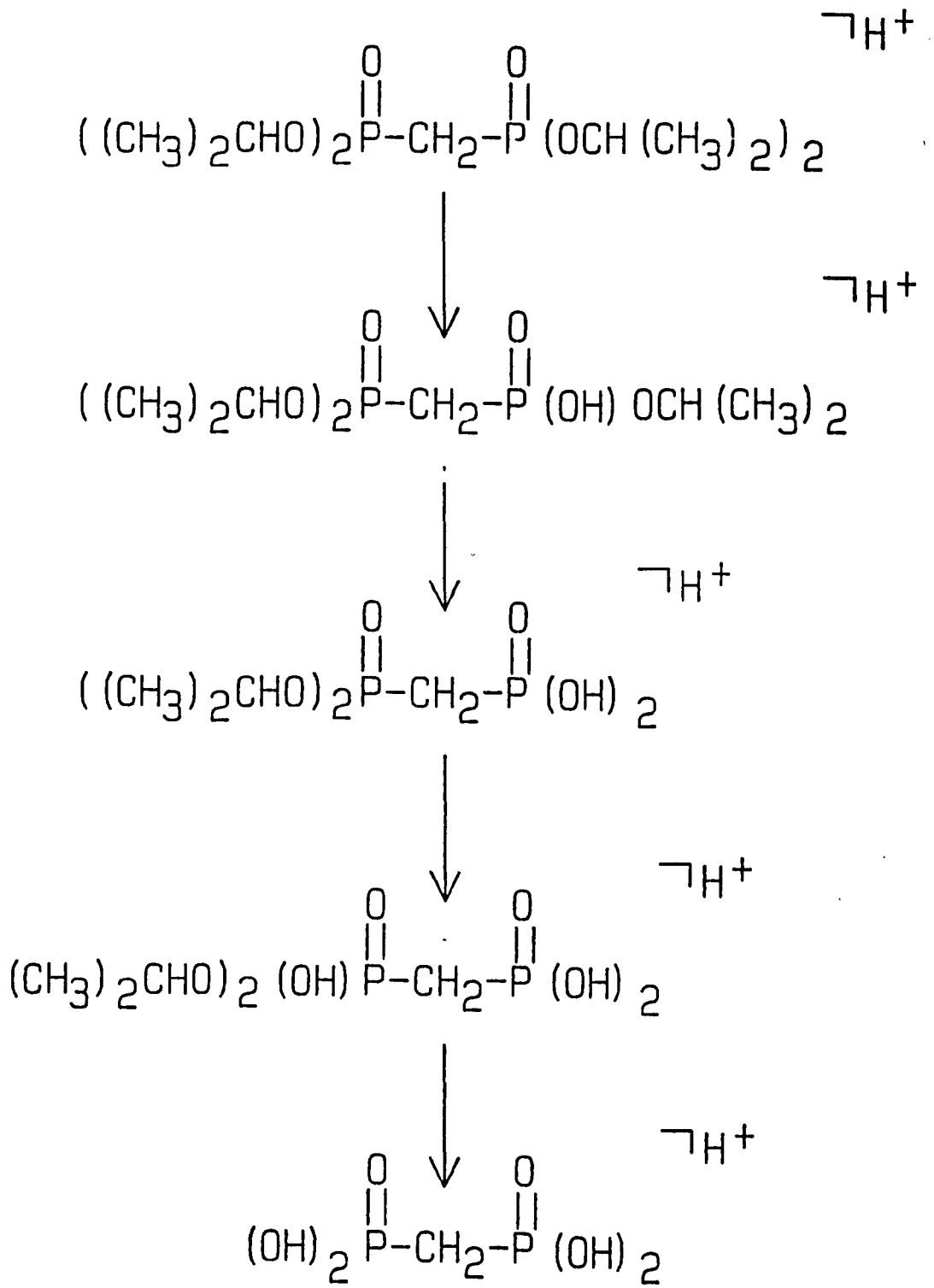

Figure 2.4. Fragmentation scheme for ammonia CI of TMBP.

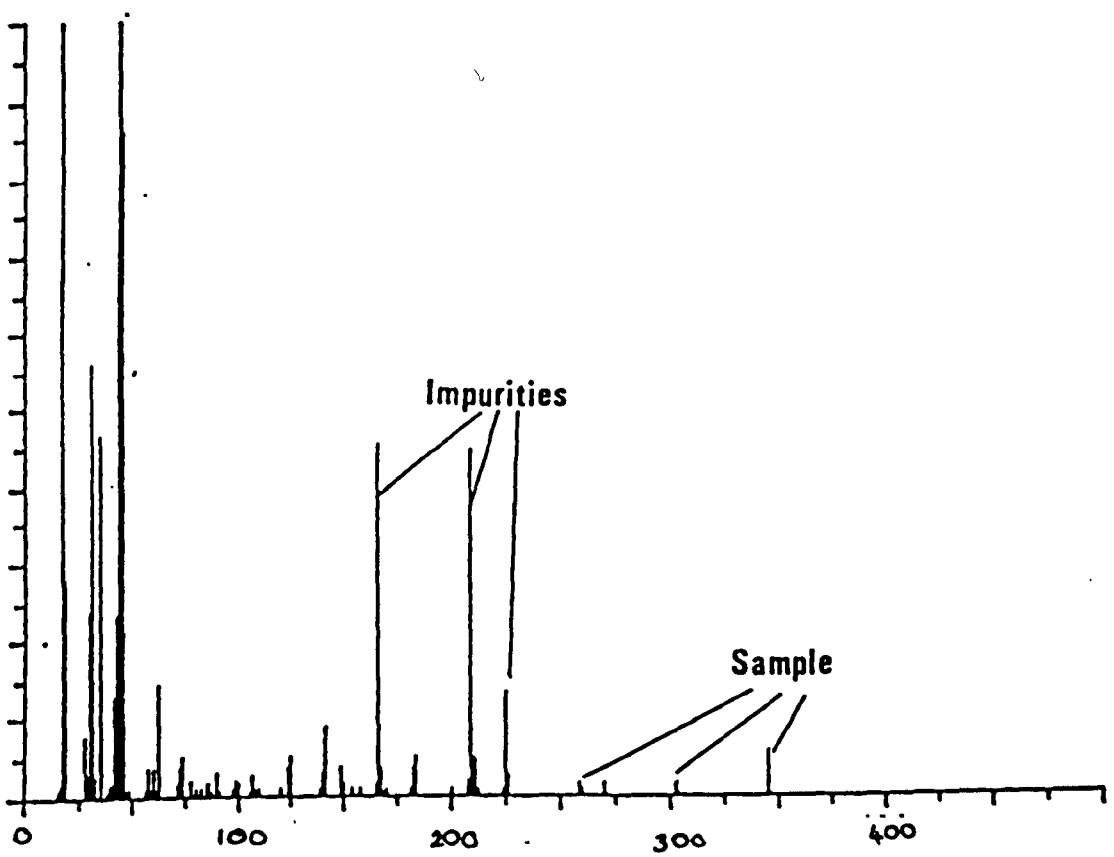

Figure 2.5. Ammonia CI mass spectrum of crude TMBP.

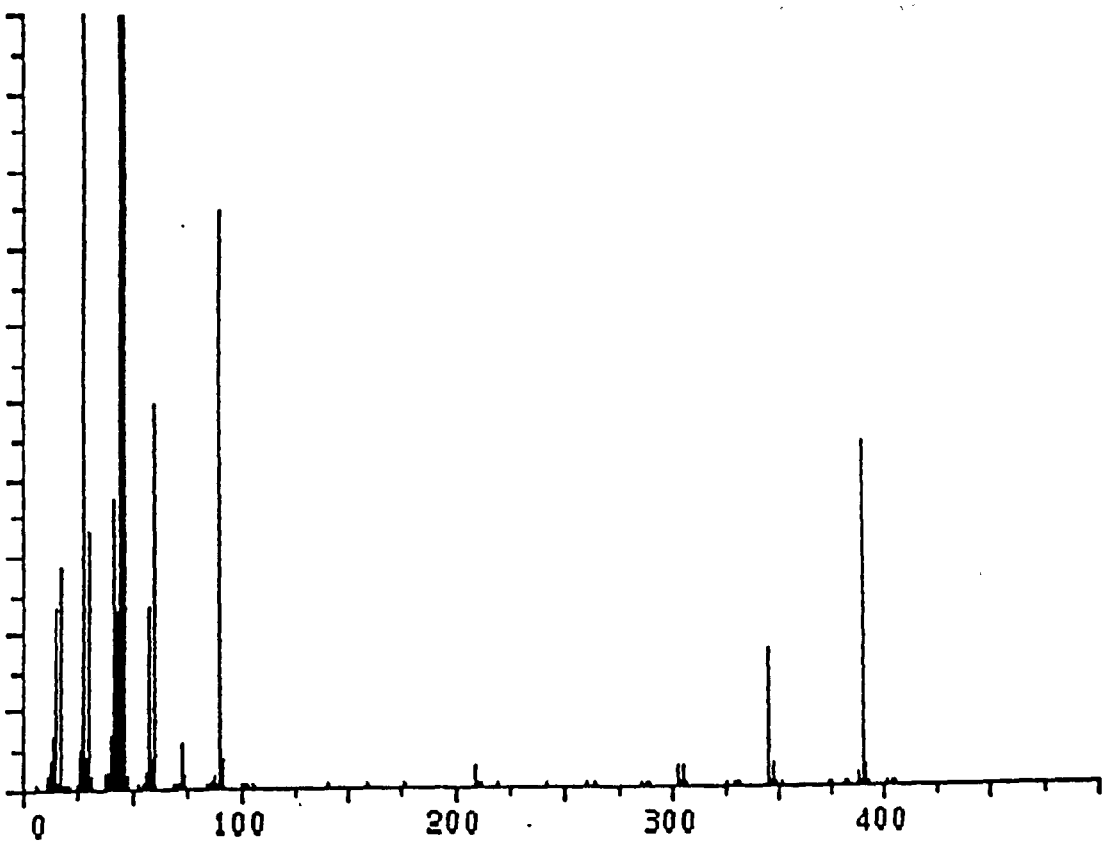

Figure 2.6. Dimethylamine CI mass spectrum of crude TMBP.

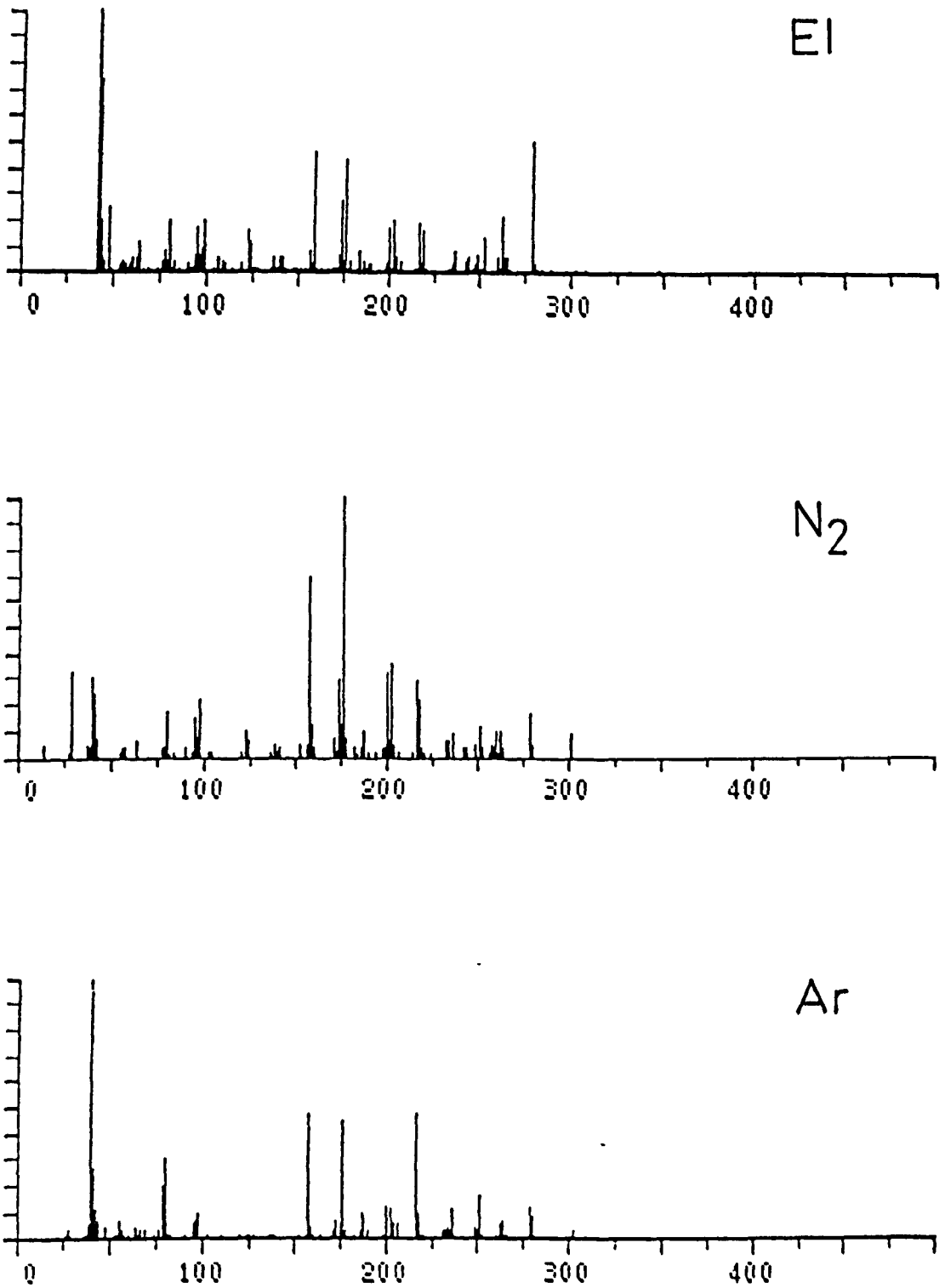

Figure 2.7. Electron impact, nitrogen and argon charge transfer mass spectra of TMBP.

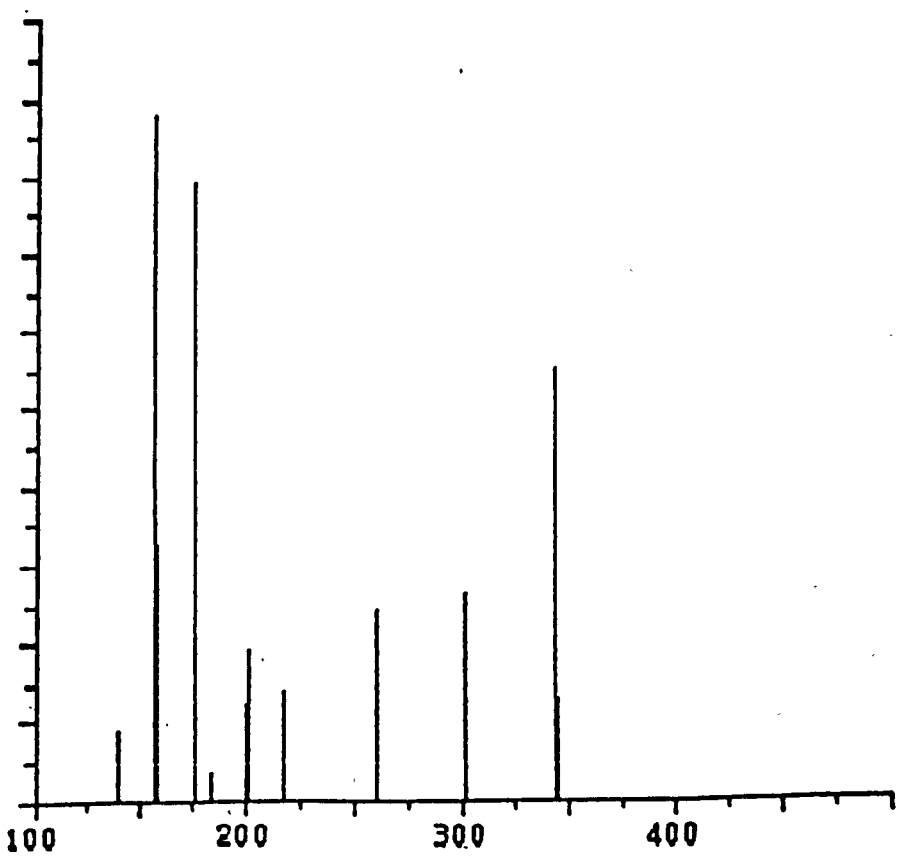

Figure 2.8. Argon/dimethylamine (9:1) CI mass spectrum of pure TMBP at 200°C.

which would be obtained by simple superposition of the spectra recorded using argon and dimethylamine alone, as is the case when mixtures of argon and water are used[11]. This observation prompted further studies of the ionization process.

2.3.4.1. Effects of Gas Mixture Composition.

The chemical ionization mass spectra of TMBP, recorded using mixtures of argon and dimethylamine in the ratios 1:1, 4:1 and 9:1 are shown in figure 2.9. The overall trend in these spectra is that as the fraction of argon in the mixture is increased, the extent of fragmentation is also increased and the abundance of the adduct ion, m/z 390, decreases. The increase in fragmentation can simply be explained by the increase in the amount of argon present since charge transfer ionization from argon is assumed to be the source of the fragment ions. Similarly the decrease in the abundance of the adduct ion is explained by the reduction in concentration of the dimethylamine.

2.3.4.2. Effects of Ion Source Temperature.

The effects of increasing the ion source temperature on the argon/dimethylamine CI spectra of TMBP are illustrated by figures 2.10a to 2.10d. The most dramatic effect is the change in the relative abundances of the fragment ions. At higher temperatures the extent of fragmentation is much greater than at lower temperatures. Whether or not this is due entirely to the increased thermal energy of the ions is not certain, but by consideration of the abundances of the reagent ions it is possible to suggest an alternative source of internal energy.

2.3.4.3. Ions formed from the reagent gases.

Two spectra, shown in figures 2.11a and 2.11b, were recorded to show the ions formed in the reagent gas plasma.

At low temperature (figure 2.11a), the dominant ion is that at m/z 46 corresponding to protonated dimethylamine. The minor reagent ions at m/z 44, 28 and 18 are due to fragmentation of either protonated dimethylamine or the dimethylamine radical cation. The

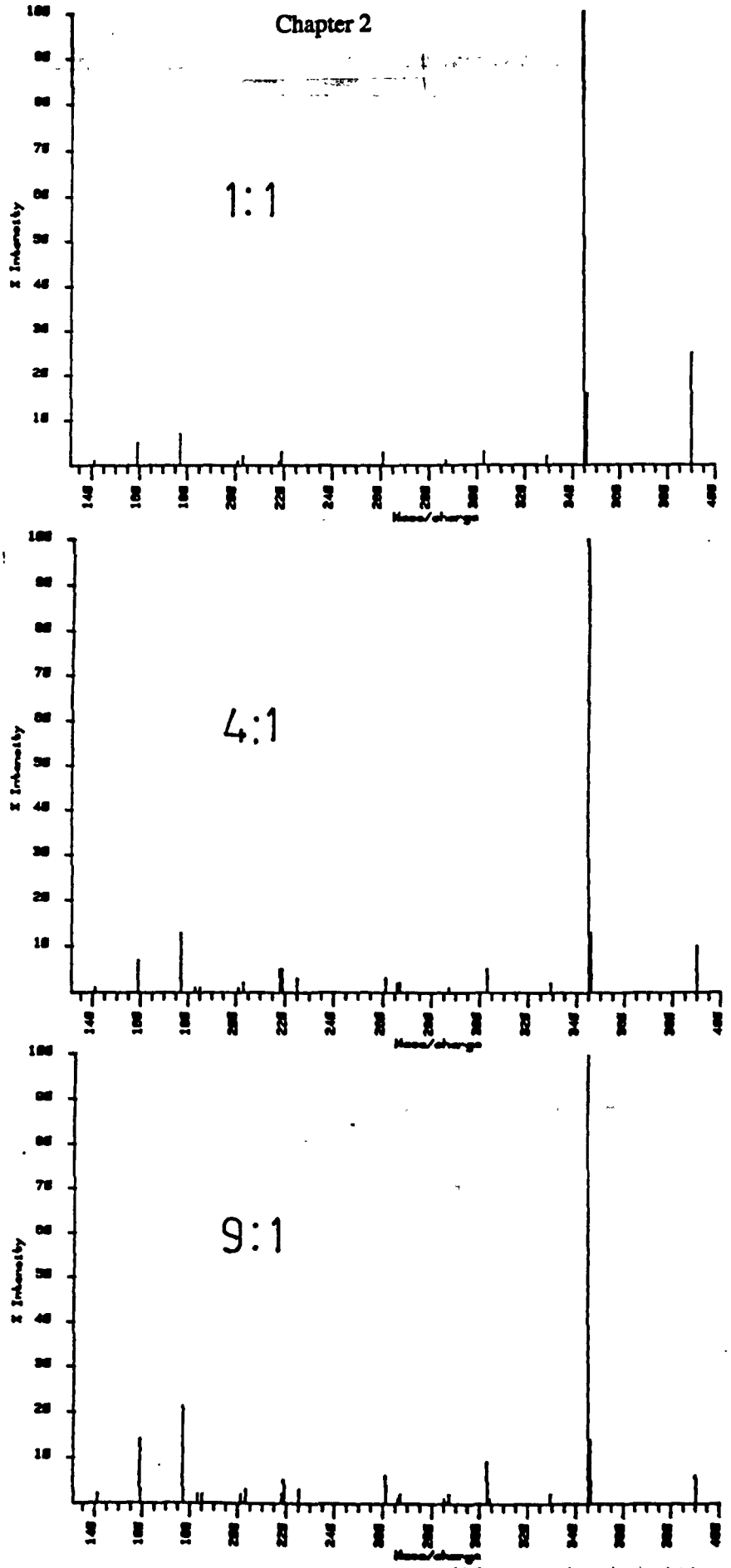

Figure 2.9. The effects of reagent gas composition on the argon/dimethylamine chemical ionization mass spectrum of TMBP.

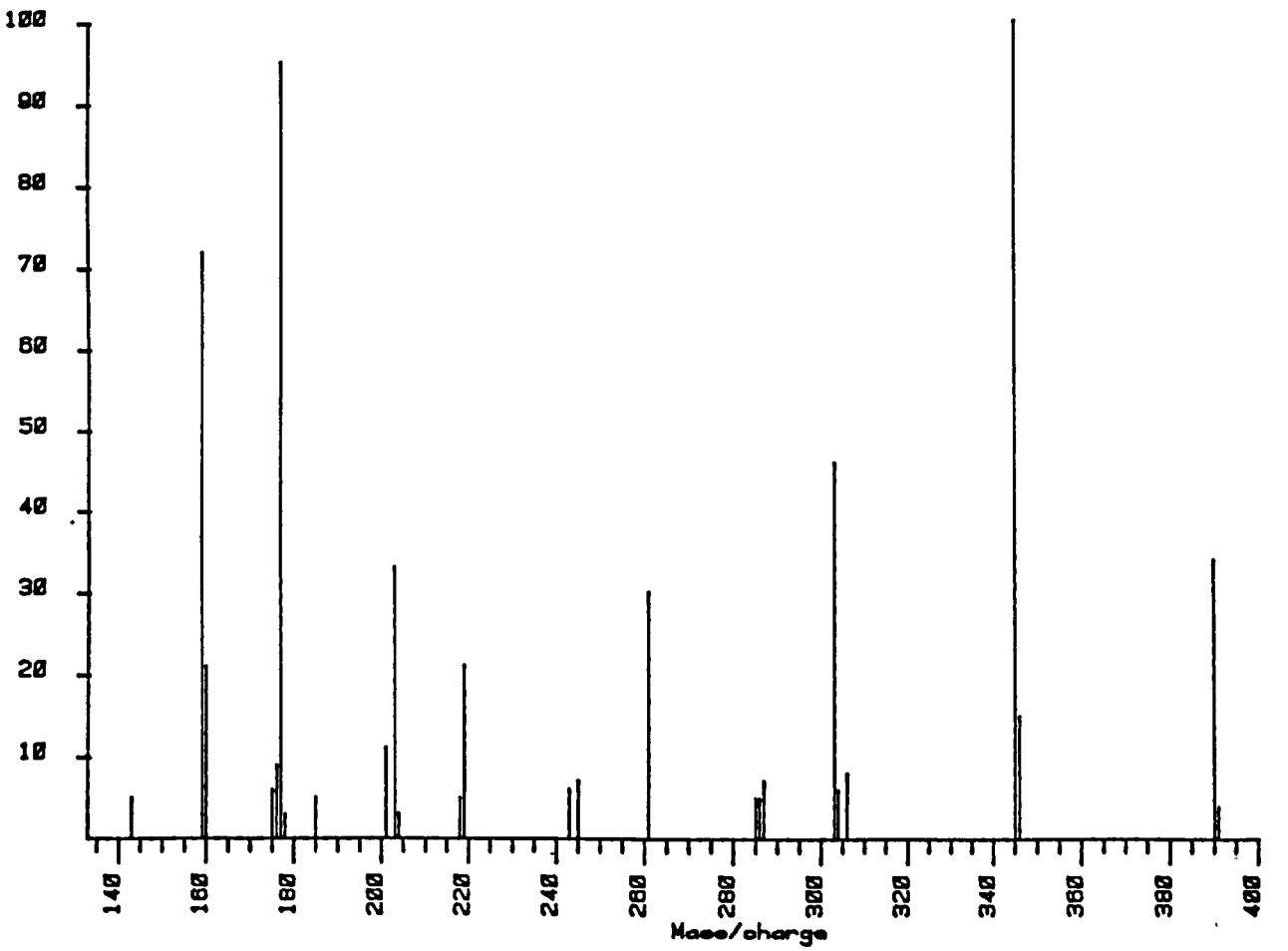

Figure 2.10a. Argon/dimethylamine CI mass spectrum of TMBP at 50°C.

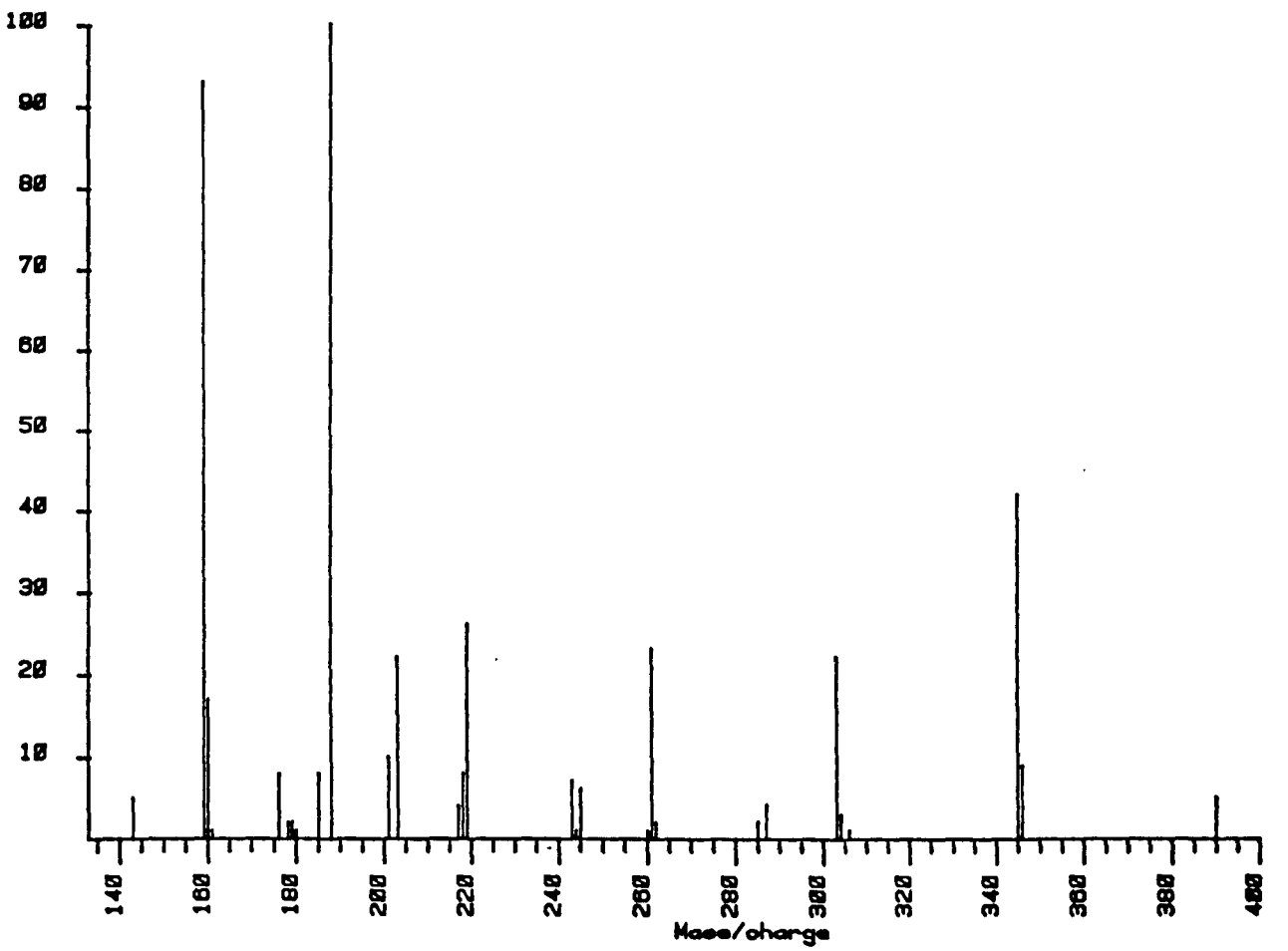

Figure 2.10b. Argon/dimethylamine CI mass spectrum of TMBP at 100°C.

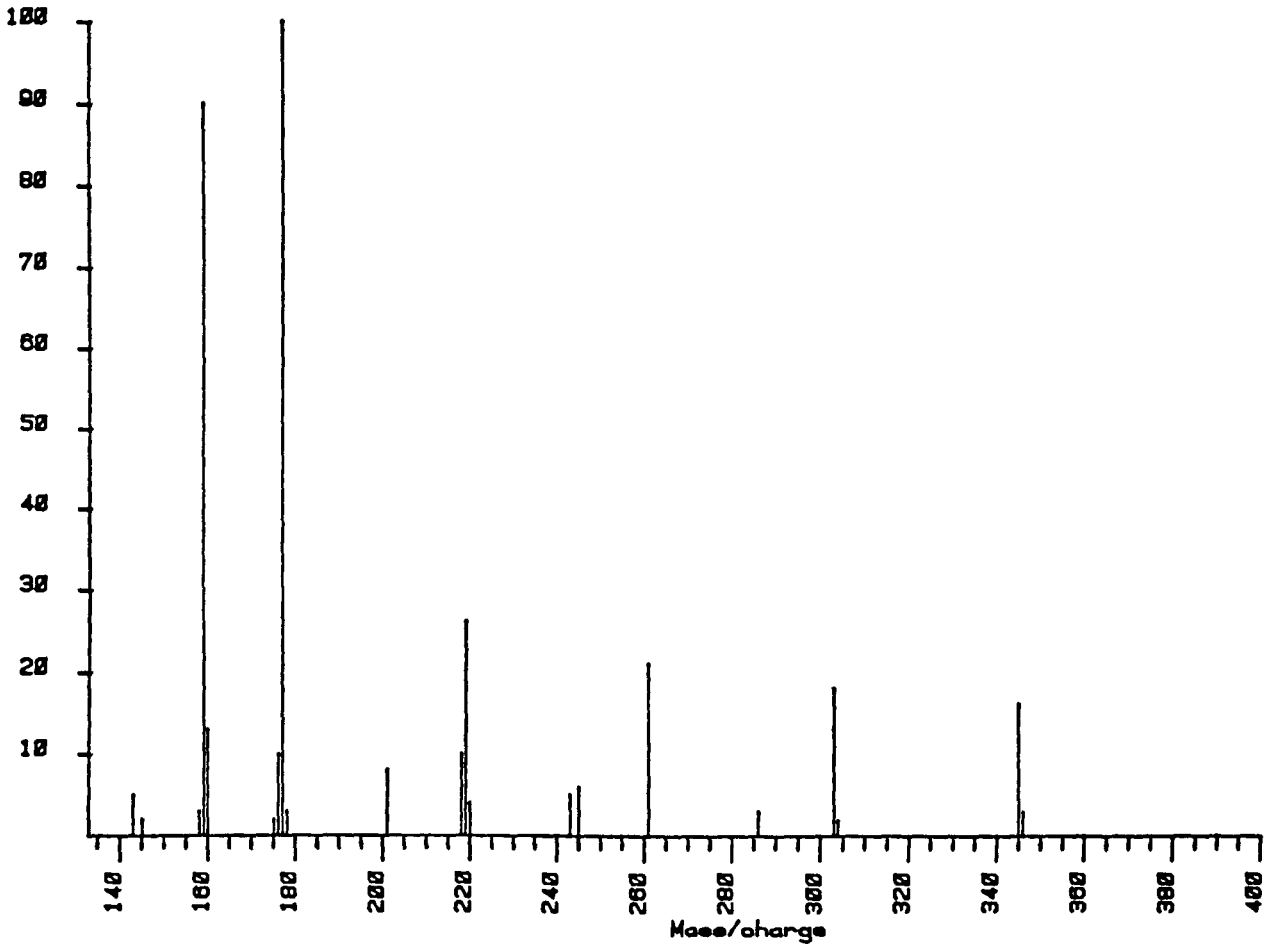

Figure 2.10c. Argon/dimethylamine CI mass spectrum of TMBP at 150°C.

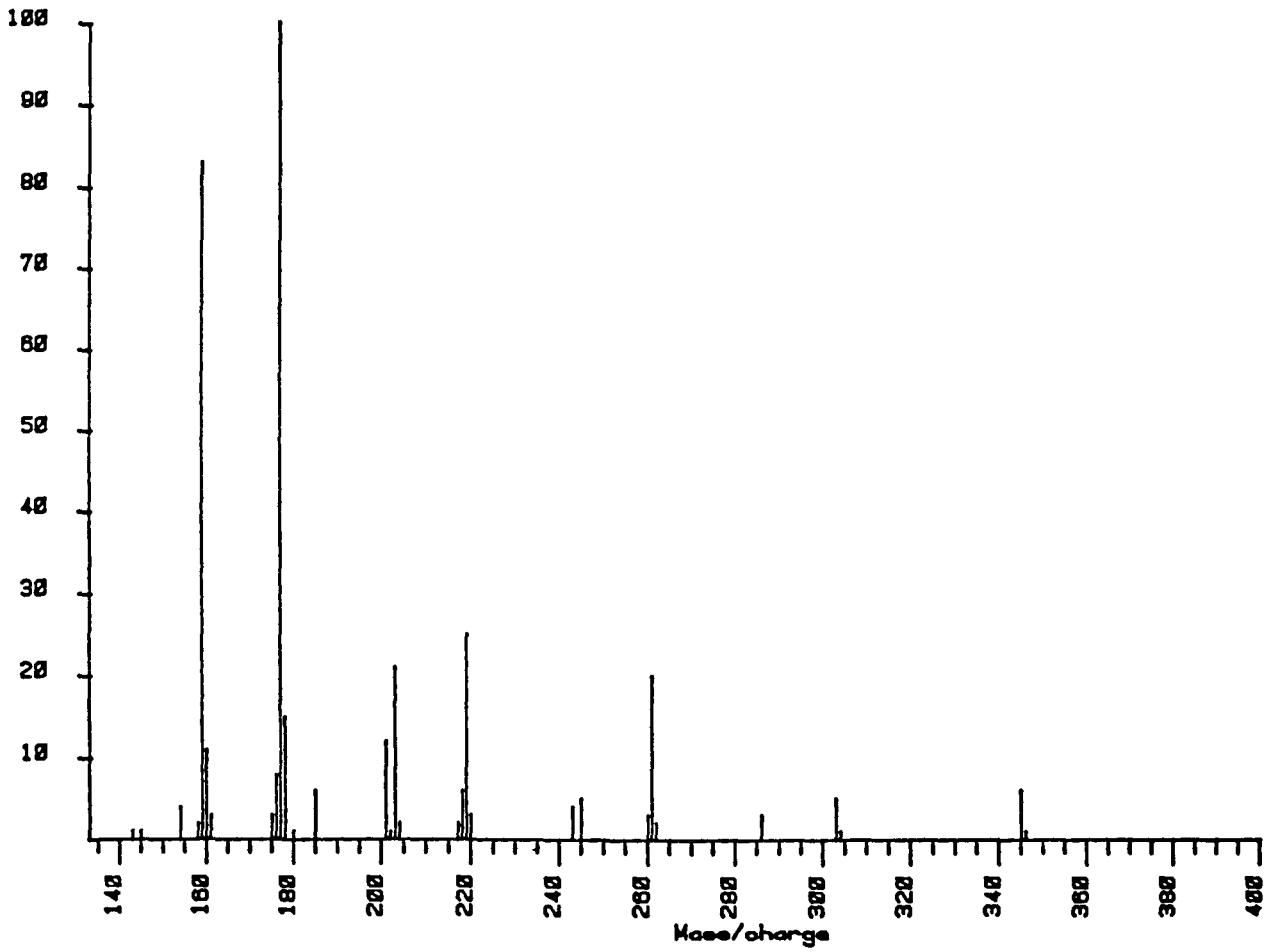

Figure 2.10d. Argon/dimethylamine CI mass spectrum of TMBP at 200°C.

ion at m/z 40 is the argon radical cation. On the basis of the relative abundances of these ions one would expect the mixed gas chemical ionization mass spectrum of TMBP to resemble closely that of the spectrum obtained using pure dimethylamine. The fragmentation observed in the mixed gas spectrum of TMBP, figure 2.10a, must therefore be due to the additional ions present. The large relative abundance of the fragment ions reflects the high abundance of the reagent ions which cause fragmentation compared with the abundance of the protonated dimethylamine ions.

At higher temperature, the relative abundance of the m/z 46 ion decreases with respect to the other reagent ions. This is reflected in the mixed gas spectra of TMBP at higher temperatures, figure 2.10d, in which the protonated molecular ion of TMBP is of very low abundance.

By considering the nature of these additional reagent ions, it is possible to suggest that they are responsible for the extra high mass fragment ions observed in the mixed gas spectra. Structures of the ions at m/z 44, 28 and 18 are suggested in table 2.4. These ions may be formed by direct fragmentation of the dimethylamine ions formed by charge exchange with the argon present or by other bimolecular gas phase reactions.

Ion m/z	Reactive Species
46	$(CH_3)_2NH_2^+$
44	$\overbrace{CH_2CH_2NH_2}^{+}$
28	$HCNH^+$
18	NH_4^+

Table 2.4. Possible structures for the reagent ions resulting from dimethylamine in argon/dimethylamine mixtures.

By considering the proton affinities of the neutrals resulting from these protonated ions, figure 2.12, it is possible to suggest that the additional fragmentation observed results from

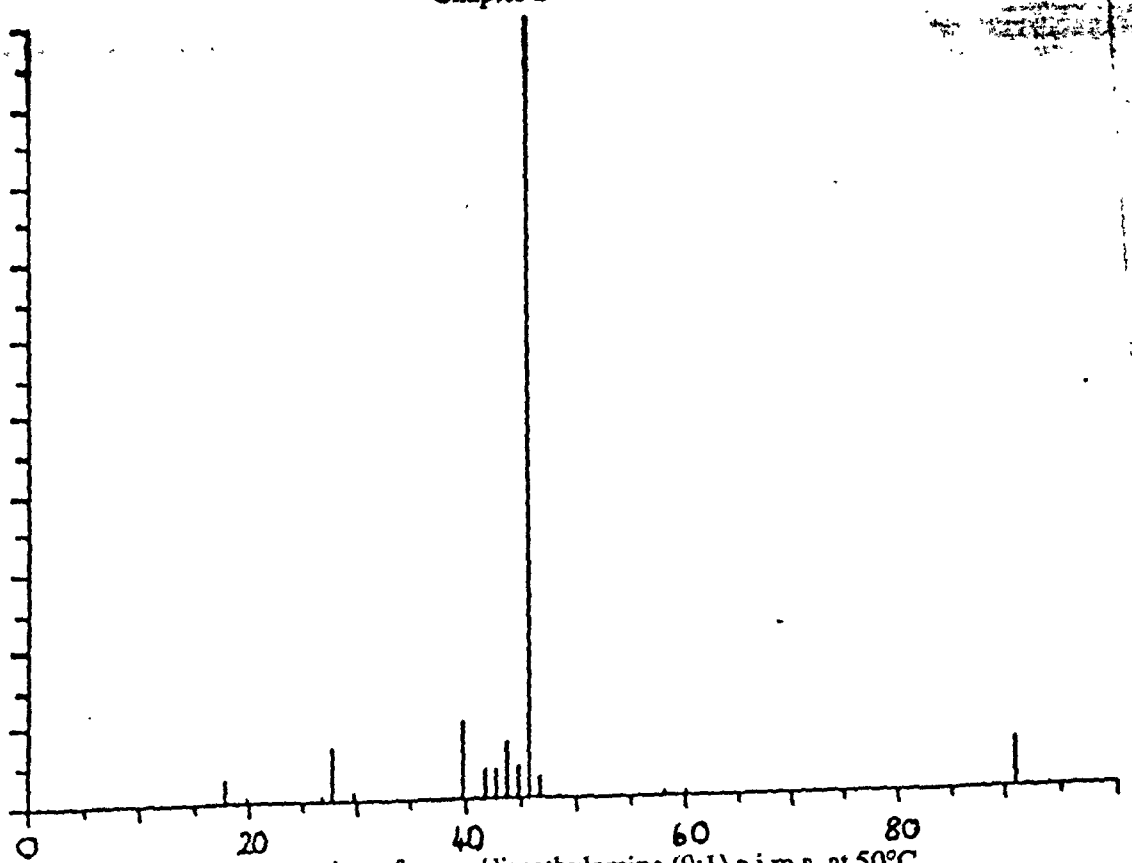

Figure 2.11a. Low mass region of argon/dimethylamine (9:1) c.i.m.s. at 50°C.

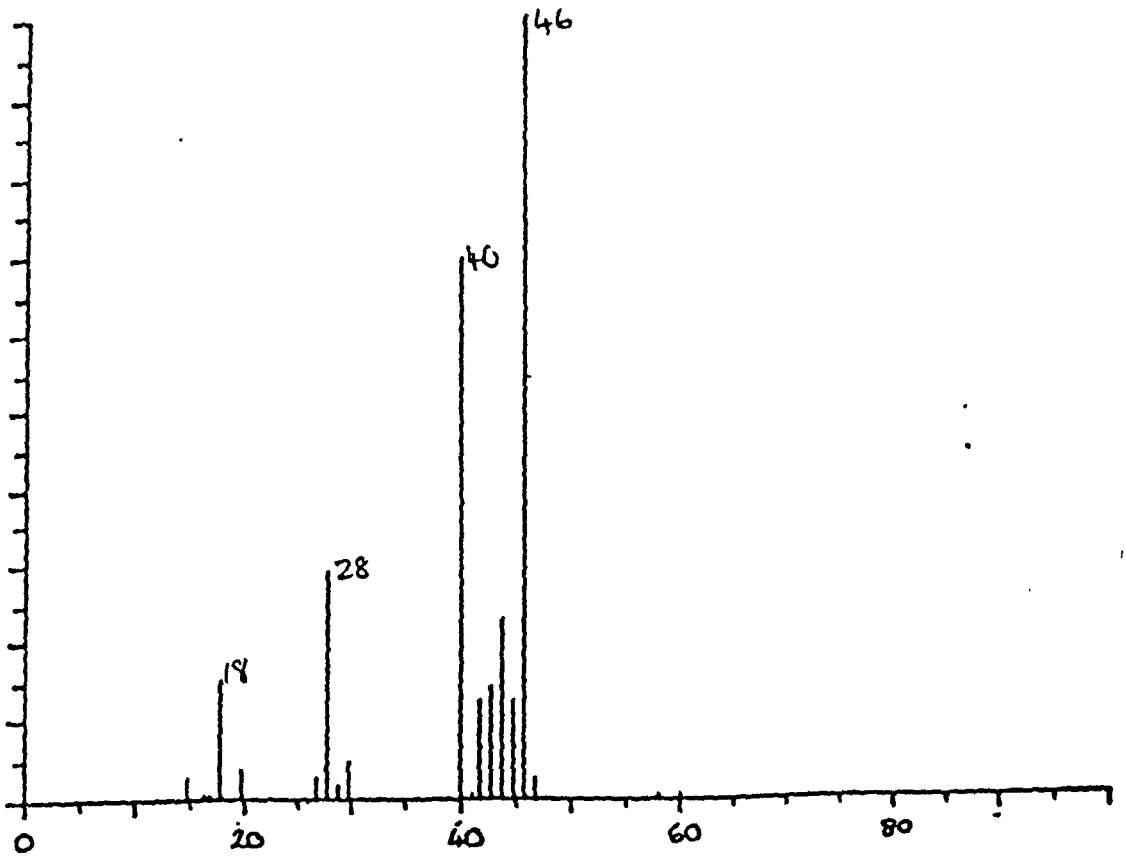

Figure 2.11b. Low mass region of argon/dimethylamine (9:1) c.i.m.s. at 200°C.

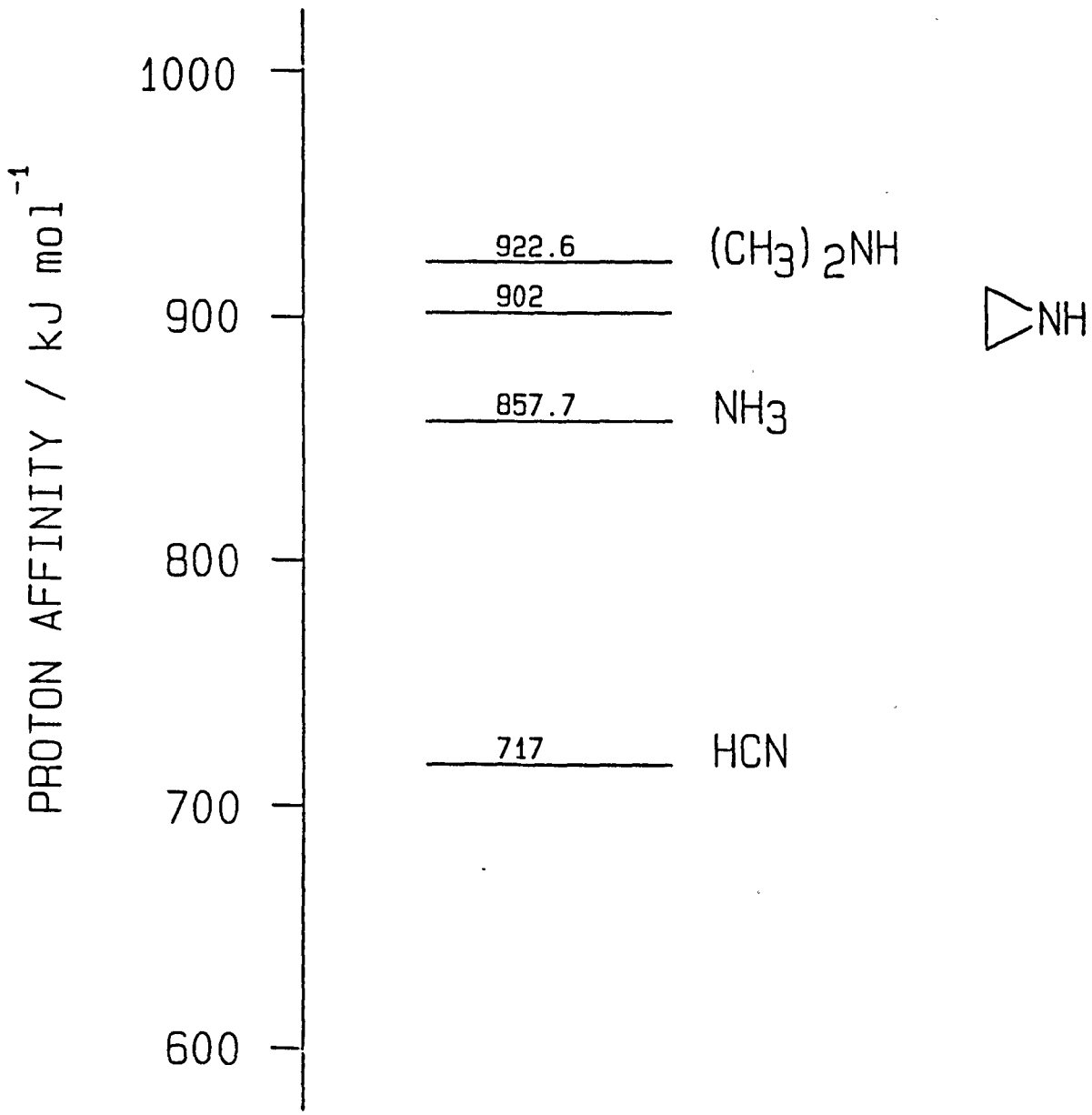

Figure 2.12. Relative proton affinity ladder for the species in the mixed reagent gas plasma.

more exothermic protonation by the minor reagent ions.

2.4. Conclusion.

The application of mixed reagent gases to chemical ionization mass spectrometry can be used to achieve both molecular weight and structural information. When this is attempted it must be noted that if the protonating reagent ion is able to form stable fragment ions corresponding to lower proton affinity neutrals, this may lead to additional fragmentation. Such problems were not incurred by Hunt and Ryan[11] since using water as the protonating reagent does not allow additional protonating species to be formed.

A further set of mixed reagent gases which may form additional protonating species contains isobutane as the protic reagent and either argon or nitrogen as the source of charge transfer species.

2.5. References.

1. M.S.B. Munson and F.H. Field, *J. Am. Chem. Soc.*, **88**, 2621 (1966).
2. A.G. Harrison, "Chemical Ionization Mass Spectrometry", C.R.C. Press, Boca Raton, Florida, 1983.
3. S.J. Hazell, R.D. Bowen and K.R. Jennings, *Org. Mass Spectrom.*, **23**, 597 (1988).
4. J.R. Chapman, "Practical Organic Mass Spectrometry", Wiley-Interscience, Chichester, 1986.
5. I. Howe, D.H. Williams and R.D. Bowen, "Mass Spectrometry, Principles and Applications", 2nd, Edn McGraw-Hill, London, 1981.
6. D.L. Newton, M.D. Erickson, K.B. Tomer, E.D. Pellizzari and P. Gentry, *Environ. Sci. Technol.*, **16**, 206 (1982).
7. A.J. Ferrer-Correia, K.R. Jennings and D.K. Sen Sharma, *Org. Mass Spectrom.*, **11**, 867 (1976).
8. Personal communication to Prof. K.R.Jennings.
9. U.S. Patent 3,251,907 (1966).

10. S.G. Lias, J.F. Liebman and R.D. Levin, *J. Phys. Chem. Ref. Data*, **13**, 695 (1984).

11. D.F. Hunt and R.F. Ryan III, *Anal. Chem.*, **44**, 1306 (1972).

Chapter 3

Chemical Ionization Mass Spectra of Urethanes

3.1. Introduction.

Relatively little attention has been given to the mass spectra of urethanes. Early work described the fragmentation patterns of a small selection of urethanes under the conditions of 70 eV electron impact ionization[1] and ^2H labelling experiments to elucidate the fragmentation pathways of two urethanes, $C_2H_5NHCO_2C_2H_5$ and $PhNHCO_2C_2H_5$ [2]. More recently, the chemical ionization mass spectra (c.i.m.s.) of a number of urethanes of pesticidal activity were reported[3,4].

The use of 12.1 eV, 75°C electron impact ionization of the homologous series of urethanes $RNHCO_2C_2H_5$ and $R_2NCO_2C_2H_5$ has established the analytical value of such low energy spectra[5]. In the light of these results a systematic survey of the methane chemical ionization mass spectra of these urethanes was carried out.

3.2. Synthesis of the Urethanes.

Many of the urethanes were readily available, having either been synthesized by Dr. R.D. Bowen or being commercially available (Aldrich). It was necessary to synthesize two of the urethanes, $t\text{-}C_4H_9NHCO_2C_2H_5$ and $Ph(CH_3)CHNHCO_2C_2H_5$ to complete the study. The synthesis involves the condensation of the parent amine with the appropriate chloroformate ester at -50 to -20°C in pyridine/dichloromethane solution (equation 3.1).

$$RR'NH + ClCO_2R'' \xrightarrow[\text{dichloromethane}]{\text{pyridine}} RR'NCO_2R'' \qquad (3.1)$$

The crude urethanes were then extracted into dichloromethane and, after aqueous workup, were purified by fractional distillation and recrystallisation from hexane respectively.

Two ^2H-labelled urethanes were synthesized in order to aid the determination of the fragmentation mechanisms of the protonated urethanes. The syntheses are outlined in equations 3.2 and 3.3.

$$(CH_3)_3CNHCO_2C_2H_5 \xrightarrow{\text{(i) } NaH,(CH_3)_2SO \text{ (ii) } CD_3I} (CH_3)_3C(CD_3)NCO_2C_2H_5 \qquad (3.2)$$

$$(CH_3CH_2)_2CO \xrightarrow[Bu_4N^+Br^-]{NaOD/D_2O} (CH_3CD_2)_2CO \xrightarrow[D_2O,\,\Delta]{ND_2OD/K_2CO_3} (CH_3CD_2)_2C{=}NOD$$

(ii) repeat

$$LiAlH_4 \xrightarrow[Et_2O]{} (CH_3CD_2)_2CHNH_2 \xrightarrow[pyridine/CH_2Cl_2\ -30°C]{ClCO_2CH_2CH_3} (CH_3CD_2)_2CHNHCO_2C_2H_5 \qquad (3.3)$$

3.3. Chemical Ionization Mass Spectra.

The chemical ionization mass spectra of 35 urethanes of general structure $RNHCO_2C_2H_5$ [R = H, C_nH_{2n+1} (n = 1-8), $CH_2CH{=}CH_2$, cyclo-C_6H_{11}, $(CH_3CD_2)_2CH$, Ph, $PhCH_2CH_2$ and $Ph(CH_3)CH$] and $RR'NHCO_2C_2H_5$ [R = R' = C_nH_{2n+1} (n = 1-4) and R=$(CH_3)_3C$, R' = CD_3] were recorded using methane as reagent gas. The spectra are presented in tabular form in tables 3.1 to 3.6 with the exception of the butyl urethanes which are represented graphically as figure 3.1.

3.3.1. Experimental.

The chemical ionization mass spectra of the urethanes were recorded using a Kratos MS-80 mass spectrometer and DS-90 data system. The instrument was operated at an accelerating voltage of 4 kV using a combined EI/CI ion source. The pressure of the reagent gas could not be measured directly but spectra were recorded when the source housing pressure was 10^{-5} Torr. The reagent gas was ionized using 100 eV electrons. Samples were admitted to the methane plasma using a direct insertion probe. The probe tip was cooled by a flow of chilled air when necessary for the more volatile urethanes.

1		2		3		4		5		
R = H		R = CH_3		R = C_2H_5		R = n-C_3H_7		R = i-C_3H_7		Assignment
m/z	RI[a]	m/z	RI[a]	m/z	RI[a]	m/z	RI[a]	m/z	RI[a]	
						160	4	160	4	$[M+C_2H_5]^+$
91	4	105	5	119	7	133	7	133	8	
90	100	104	100	118	100	132	100	132	100	MH^+
89	1	103	5	117	<4	131	4	131	<1	$M^{+\cdot}$
						130	5	130	3	$[M-H]^+$
						118	8			
				102	7			116	21	$[MH-CH_4]^+$
						105	2	105	2	
62	9	76	84	90	60	104	45	104	52	$[MH-C_2H_4]^+$
				88	15	102	16			$[MH-C_2H_6]^+$
						90	8	90	7	$C_3H_8NO_2^+$
44	3	58	23	72	20	86	9	86	9	$[MH-C_2H_5OH]^+$
						62	7	62	5	

[a] Intensities normalized to a value of 100 units for the base peak excluding peaks due to reagent ions.

Table 3.1. Methane c.i.m.s. of $RNHCO_2C_2H_5$ ($R=C_nH_{2n+1}$; n=0 - 3).

R										
n-C_6H_{13}		n-C_7H_{15}		n-C_8H_{17}		CH_2=$CHCH_2$		c-C_6H_{11}		Assignment
m/z	RI[a]	m/z	RI[a]	m/z	RI[a]	m/z	RI[a]	m/z	RI[a]	
214	2	228	2	242	2			212	1	$[M+C_3H_5]+$
202	8	216	14	230	12	158	<3	200	7	$[M+C_2H_5]+$
175	10	189	13	203	13	131	6	173	14	
174	100	188	100	202	100	130	76	172	100	MH+
173	4	187	6	201	7	129	10	171	6	M+.
172	8	186	16	200	21			170	9	$[MH-H_2]+$
158	6	172	2	186	3					$[MH-CH_4]+$
146	19	160	10	174	8	102	100	144	10	$[MH-C_2H_4]+$
144	3	158	4	172	5	100	14	142	3	$[MH-C_2H_6]+$
130	1	144	2	158	2	86	11	128	8	$[MH-C_3H_8]+$
128	6	142	9	156	7	84	16	126	4	$[MH-C_2H_5OH]+$
		130	1	144	2					$[MH-C_4H_{10}]+$
102	24	116	1	130	1			100	1	$[MH-C_5H_{12}]+$
		103	2	113	1					
		102	23							$[MH-C_6H_{14}]+$
				103	3					
				102	28					$[MH-C_7H_{16}]+$
		99	2							$C_7H_{15}+$
90	4	90	6	90	9			90	13	$C_3H_8NO_2+$
85	5	85	1							$C_6H_{13}+$
83	1	83	1	83	1			83	6	$C_6H_{11}+$

[a] Intensities normalized to a value of 100 units for the base peak excluding peaks due to reagent ions.

Table 3.2. Methane c.i.m.s. of $RNHCO_2C_2H_5$ compounds.

	RI[a]								
m/z	A[b]	B[b]	C[b]	D[b]	E[b]	F[b]	G[b]	H[b]	Assignment
188	5	9	10	7	13	7	9		$[M+C_2H_5]+$
161	8	9	9	9	13	12	9	3	
160	100	100	100	100	100	100	100	35	MH+
159	4	3	4	1	1	<2	1	<1	M+.
158	5	4	6	3	5	5	6	2	$[MH-H_2]+$
144		3	2	6	4		6	6	$[MH-CH_4]+$
132	31	21	20	22	20	25	24		$[MH-C_2H_4]+$
130	2	1	3	1	2	71	2	39	$[MH-C_2H_6]+$
116	2	2	1	1	38		33	1	$[MH-C_3H_8]+$
114	8	8	8	5	9	9	5	2	$[MH-C_2H_5OH]+$
104			2	5	1		5	1	
103	2	3	2	8					
102	22	19	20	8	1	3	3	1	$[MH-C_4H_{10}]+$
90	4	8	5	4	13	18	15	100	$C_3H_8NO_2+$
71	6	10	14	6	15	20	22	29	$C_5H_{11}+$

a Intensities normalized to a value of 100 units for the base peak excluding peaks due to reagent ions.

b Structures are given in table 3.3a.

Table 3.3. Methane c.i.m.s. of $C_5H_{11}NHCO_2C_2H_5$ compounds.

A	n-pentyl	$CH_3CH_2CH_2CH_2CH_2NHCO_2C_2H_5$
B	i-pentyl	$(CH_3)_2CHCH_2CH_2NHCO_2C_2H_5$
C	2-methyl-1-butyl	$CH_3CH_2(CH_3)CHCH_2NHCO_2C_2H_5$
D	neo-pentyl	$(CH_3)_3CCH_2NHCO_2C_2H_5$
E	2-pentyl	$CH_3CH_2CH_2(CH_3)CHNHCO_2C_2H_5$
F	3-pentyl	$(CH_3CH_2)_2CHNHCO_2C_2H_5$
G	3-methyl-2-butyl	$(CH_3)_2CH(CH_3)CHNHCO_2C_2H_5$
H	t-pentyl	$CH_3CH_2(CH_3)_2CNHCO_2C_2H_5$

Table 3.3a. Structures of pentyl urethanes for table 3.3.

R								
Ph		$PhCH_2$[b]		$PhCH_2CH_2$		$Ph(CH_3)CH$[b]		
m/z	RI[a]	m/z	RI[a]	m/z	RI[a]	m/z	RI[a]	Assignment
				234	1			$[M+C_3H_5]+$
194	4	208	4	222	3			$[M+C_2H_5]+$
167	11			195	14			
166	100	80	100	194	100	194	91	MH+
165	10	179	0	193	2	193	0	M+.
		178	5	192	1	192	2	
						180	19	
						178	15	$[MH-CH_4]+$
138	21	152	18	166	2	166	2	$[MH-C_2H_4]+$
120	4	134	3	148	6			$[MH-C_2H_5OH]+$
						116	20	[MH-PhH]+
				106	2			
		105	5	105	27	105	99	$C_8H_9^+$
		102	58	102	8			$C_4H_8NO_2^+$
		91	45	91	2			$C_7H_7^+$
						90	100	$C_3H_8NO_2^+$

a Intensities normalized to a value of 100 units for the base peak excluding peaks due to reagent ions.

b The residual e.i. component in these spectra remained large in these spectra even at low sample pressures and was removed by a subtraction procedure.

Table 3.4. Methane c.i.m.s. of aromatic $RNHCO_2C_2H_5$.

R								
CH_3		C_2H_5		n-C_3H_7		i-C_3H_7		
m/z	RIa	m/z	RIa	m/z	RIa	m/z	RIa	Assignment
		186	3	214	2	214	3	$[M+C_3H_5]^+$
146	3	174	11	202	9	202	14	$[M+C_2H_5]^+$
119	5	147	13	175	12	175	12	
118	100	146	100	174	100	174	100	MH^+
117	6	145	4	173	3	173	3	$M^{+\cdot}$
116	5	144	7	172	7	172	5	$[MH-H_2]^+$
		130	14	158	3	158	22	$[MH-CH_4]^+$
90	59	118	33	146	14	146	9	$[MH-C_2H_4]^+$
		116	3	144	22	144	1	$[MH-C_2H_6]^+$
						132	7	$[MH-C_3H_6]^+$
				130	1	130	2	$[MH-C_3H_8]^+$
72	15	100	24	128	23	128	16	$[MH-C_2H_5OH]^+$

a Intensities normalized to a value of 100 units for the base peak excluding peaks due to reagent ions.

Table 3.5. Methane c.i.m.s. of $R_2NCO_2C_2H_5$ compounds.

	RI[a]			
m/z	n-C_4H_9	i-C_4H_9	s-C_4H_9	Assignment
242	2	2	3	$[M+C_3H_5]^+$
230	10	11	21	$[M+C_2H_5]^+$
203	13	12	20	
202	100	100	100	MH^+
201	5	4	4	$M^{+\cdot}$
200	11	11	11	$[MH-H_2]^+$
186	3	11	16	$[MH-CH_4]^+$
174	8	6	6	$[MH-C_2H_4]^+$
172	3	1	69	$[MH-C_2H_6]^+$
158	38	30		$[MH-C_3H_8]^+$
156	15	15	23	$[MH-C_2H_5OH]^+$
146	1	6	16	$[MH-C_4H_8]^+$
144			4	$[MH-C_4H_{10}]^+$

a Intensities normalized to a value of 100 units for the base peak excluding peaks due to reagent ions.

Table 3.6. Methane c.i.m.s. of $(C_4H_9)_2NCO_2C_2H_5$ compounds.

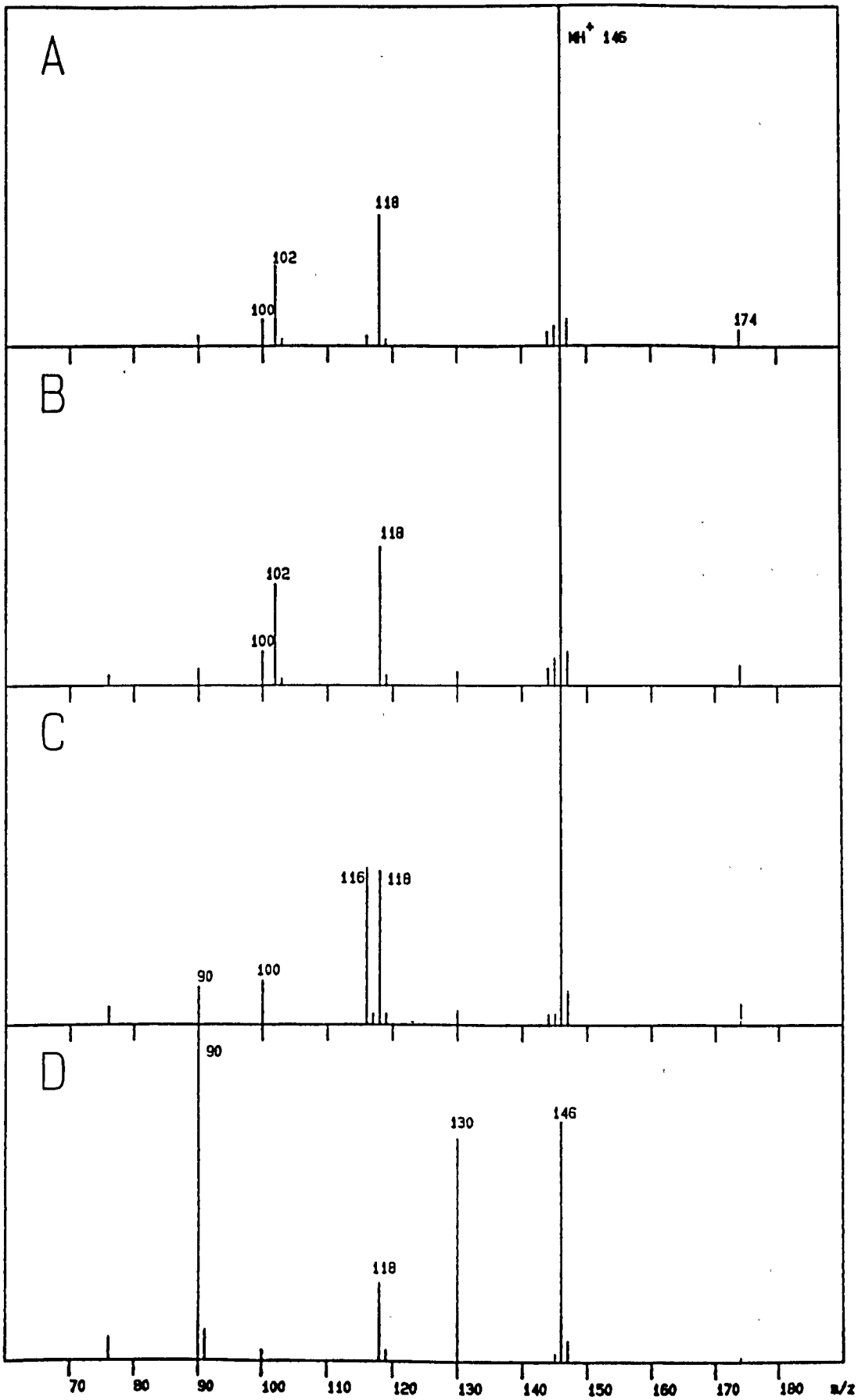

Figure 3.1. Methane c.i.m.s. of $C_4H_9NHCO_2C_2H_5$ compounds; A: n-$C_4H_9NHCO_2C_2H_5$, B: $(CH_3)_2CHCH_2NHCO_2C_2H_5$, C: $CH_3CH_2(CH_3)CHNHCO_2C_2H_5$ and D: $(CH_3)_3CNHCO_2C_2H_5$.

3.3.2. MH^+ and Related Ions.

All of the 35 urethanes give spectra containing abundant MH^+ ions formed by proton transfer from species in the methane plasma. In most of the cases this is the base peak in the spectra. Other ions present in the spectra are formed by ionization involving the capture of $C_2H_5^+$ or $C_3H_5^+$ by the urethanes. These ions, $[M+29]^+$ and $[M+41]^+$, become more abundant as the homologous series of urethanes is ascended. Despite the low abundance of these ions they are useful in the confirmation of the relative molecular mass of the urethanes.

3.3.3. Fragment Ions.

Accompanying the directly ionized species there are four main classes of fragment ions. The analytical use of these fragment ions and mechanisms whereby they are formed are discussed below.

3.3.3.1. Elimination of Ethene: $[MH\text{-}C_2H_4]^+$.

Elimination of ethene from the protonated molecular ion gives a peak in the spectra 28 Daltons below MH^+. The abundance of this ion decreases on ascending the homologous series of urethanes $RNHCO_2C_2H_5$ with the exception of the parent urethane, $H_2NCO_2C_2H_5$, which has an unusually small peak due to ethene expulsion. A similar trend is observed for the disubstituted species. This is taken as good evidence that this fragment ion is formed from the O-ethyl function. Further evidence for this is found in the spectra of two methyl carbamates, $n\text{-}C_5H_{11}NHCO_2CH_3$ and $(CH_3)_3CCH_2NHCO_2CH_3$, in which little ethene elimination is observed; m/z 118 in each case is less than 2%.

Since it is proposed that ethene elimination occurs from the O-ethyl function, two plausible mechanisms are postulated. The first, shown in figure 3.2a, requires that a fraction of the ions are formed by protonation on the O-ethyl oxygen atom or that proton transfer to the O-ethyl group precedes fragmentation. This appears quite reasonable in the light of the mechanisms shown for water loss from protonated carboxylic acids as reported by Middlemiss and Harrison[6]. The second involves ethene elimination remote from the site of the charge, figure

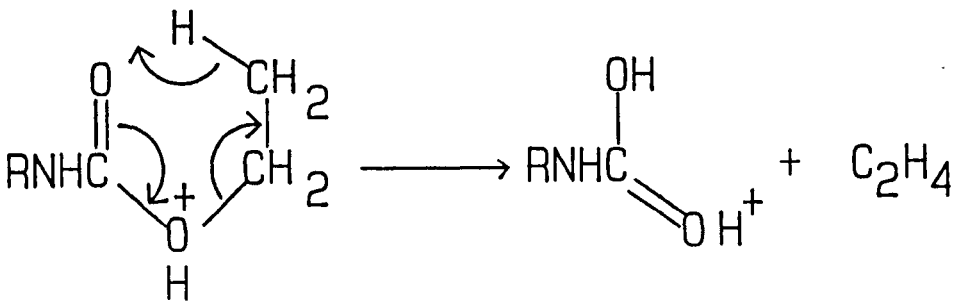

Figure 3.2a. Mechanism for ethene elimination from protonated urethanes.

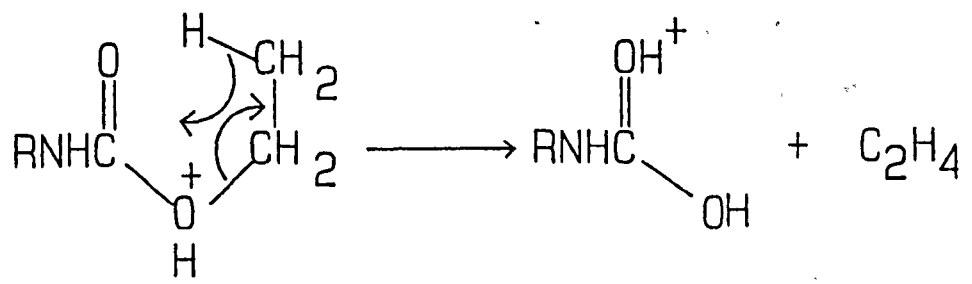

Figure 3.2b. Alternative mechanism for ethene elimination from protonated urethanes.

3.2b. There is evidence that alkene expulsion from closed-shell ions via ion-molecule complexes and/or species containing incipient cations[7,8,9], but this mechanism seems less likely.

3.3.3.2. Elimination of Ethanol: $[MH-C_2H_5OH]^+$.

Loss of ethanol from the protonated molecular ion produces a peak in the spectra 46 daltons below MH+. The abundance of this ion is usually slightly lower than $[MH-C_2H_4]^+$, but varies in a similar manner for the singly alkylated urethanes. For the disubstituted species, $R_2NCO_2C_2H_5$, the abundance of this ion decreases less rapidly than $[MH-C_2H_4]^+$ becoming the larger peak in the spectra of $(C_3H_7)_2NCO_2C_2H_5$ and $(C_4H_9)_2NCO_2C_2H_5$.

As with ethene elimination, ethanol loss is associated with the O-ethyl group because of its general occurrence throughout the set of urethanes studied. Evidence to support this is found in the spectra of the methyl carbamates, $n\text{-}C_5H_{11}NHCO_2CH_3$ and $(CH_3)_3CCH_2NHCO_2CH_3$ which contain ions at m/z 114 corresponding to methanol loss from MH+ but no ions due to ethanol loss at m/z 102.

Two possible mechanisms are postulated for this reaction. The first is a simple cleavage of the ethoxy protonated isomer, figure 3.3a, the second involves a 1,2-elimination from the carbonyl protonated isomer, figure 3.3b. The first of these seems the more likely considering the similarity to the behaviour of protonated carboxylic acids[6]. The ethoxy protonated isomer may be formed during ionization or by internal proton transfer from the carboxyl group. A two-step mechanism involving the successive loss of ethene and water was discounted because methanol loss is observed in the spectra of methyl carbamates and on energetic grounds.

3.3.3.3. Elimination of Alkane Molecules.

The presence of these ions establishes the nature of the alkyl group, R, in the saturated urethanes, $RNHCO_2C_2H_5$. The mechanism for this fragmentation involves the formal

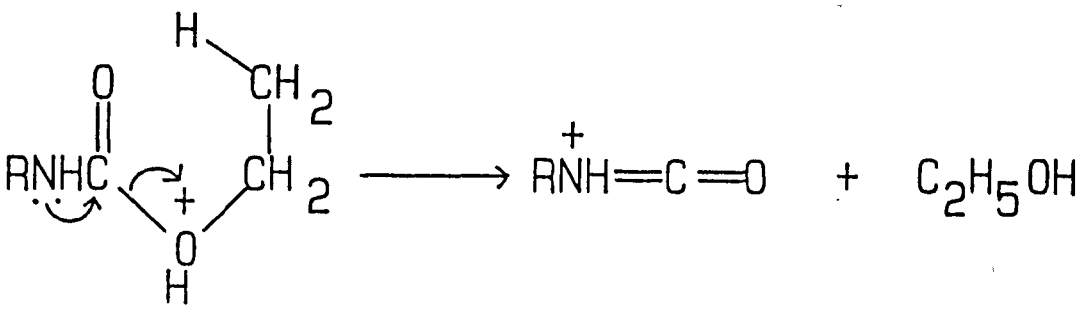

Figure 3.3a. Mechanism for ethanol elimination from protonated urethanes.

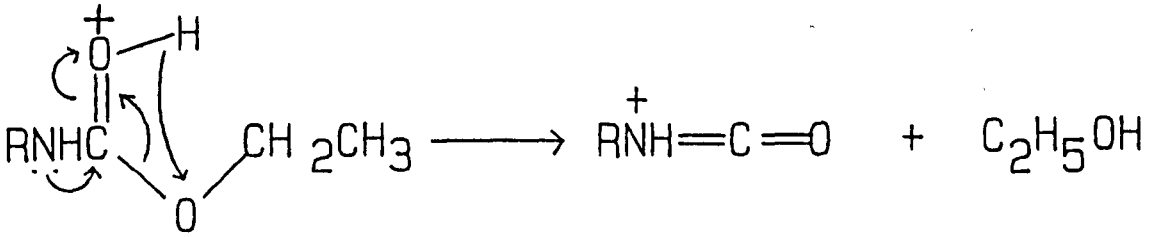

Figure 3.3b. Alternative mechanism for ethanol elimination from protonated urethanes.

cleavage of the bond joining the α- and β-carbon atoms of the alkyl group and a hydrogen transfer from the nitrogen atom, figure 3.4. This mechanism, although very simple, produces very stable delocalised allylic cations and provides a good working model for analytical purposes. Thus for the isomeric butyl urethanes, $C_4H_9NHCO_2C_2H_5$, the n- and iso- isomers form ions of m/z 102 due to elimination of propane. The sec- isomer forms two ions, m/z 116 and m/z 130 due to loss of ethane and methane respectively. The t- isomer produces only one fragment ion, in this class, at m/z 130 corresponding to methane loss. These are illustrated in figure 3.5. This allows the t- and sec- isomers to be clearly distinguished from the other isomers. The n- and iso-butyl urethanes cannot be differentiated between since they only differ beyond the α-carbon atom. Smaller peaks due to cleavage of the bond joining the β- and γ-carbon atoms are also observed. The spectrum of n-$C_4H_9NHCO_2C_2H_5$ contains a larger peak at m/z 116 $[MH-C_2H_6]^+$ (relative intensity 3%) and a smaller peak at m/z 130 $[MH-CH_4]^+$ (relative intensity 3%) than the spectrum of i-$C_4H_9NHCO_2C_2H_5$ (relative intensities 11% and 1% respectively). These ions, being of low abundance, are less reliable for analytical purposes, than those due to α-β cleavage.

Recent work[10] has shown that alkane loss from ions in the gas phase is not as unusual as was once thought. Indeed, $[MH\text{-alkane}]^+$ peaks have also been observed in the spectra of saturated alkylamines from which urethanes are derived[11].

The formation of these $[MH\text{-alkane}]^+$ ions could be confused with $[M\text{-alkyl}]^+$ ions resulting from residual EI Similarly, the $[MH-C_2H_5OH]^+$ might also be $[M-C_2H_5O]^+$ artefacts from residual EI The latter can be discounted since loss of $C_2H_5O\cdot$ from $M^{+\cdot}$ is not of great importance in either 70 eV[1,2] or 12.1 eV[5] EI spectra. However, the low energy EI spectra of urethanes do contain intense $[M\text{-alkyl}]^+$ peaks[5] and therefore the $[MH\text{-alkane}]^+$ peaks reported in tables 3.1 to 3.6 may be due in some part to a residual EI component. This is supported by the presence of several peaks in the CI spectra of neo-pentyl urethane. The ions, m/z 102, 103 and 104, corresponding to $[MH-C_4H_8]^+$,$[MH-C_4H_7]^+$ and $[MH-C_4H_6]^+$ respectively are also to be found in the 12.1 eV EI spectra[5]. It is highly unlikely that all of

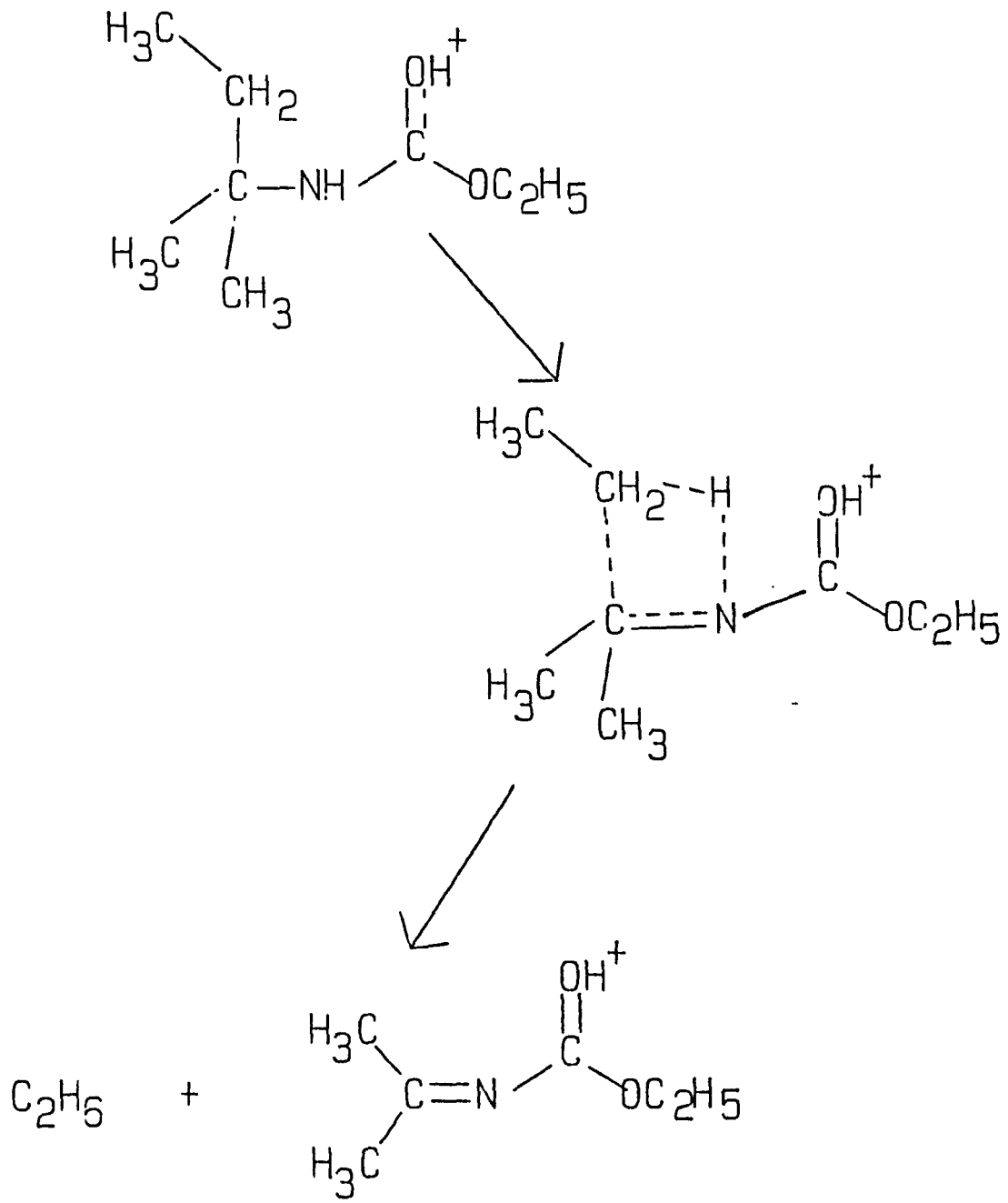

Figure 3.4. Mechanism for alkane loss from protonated urethanes.

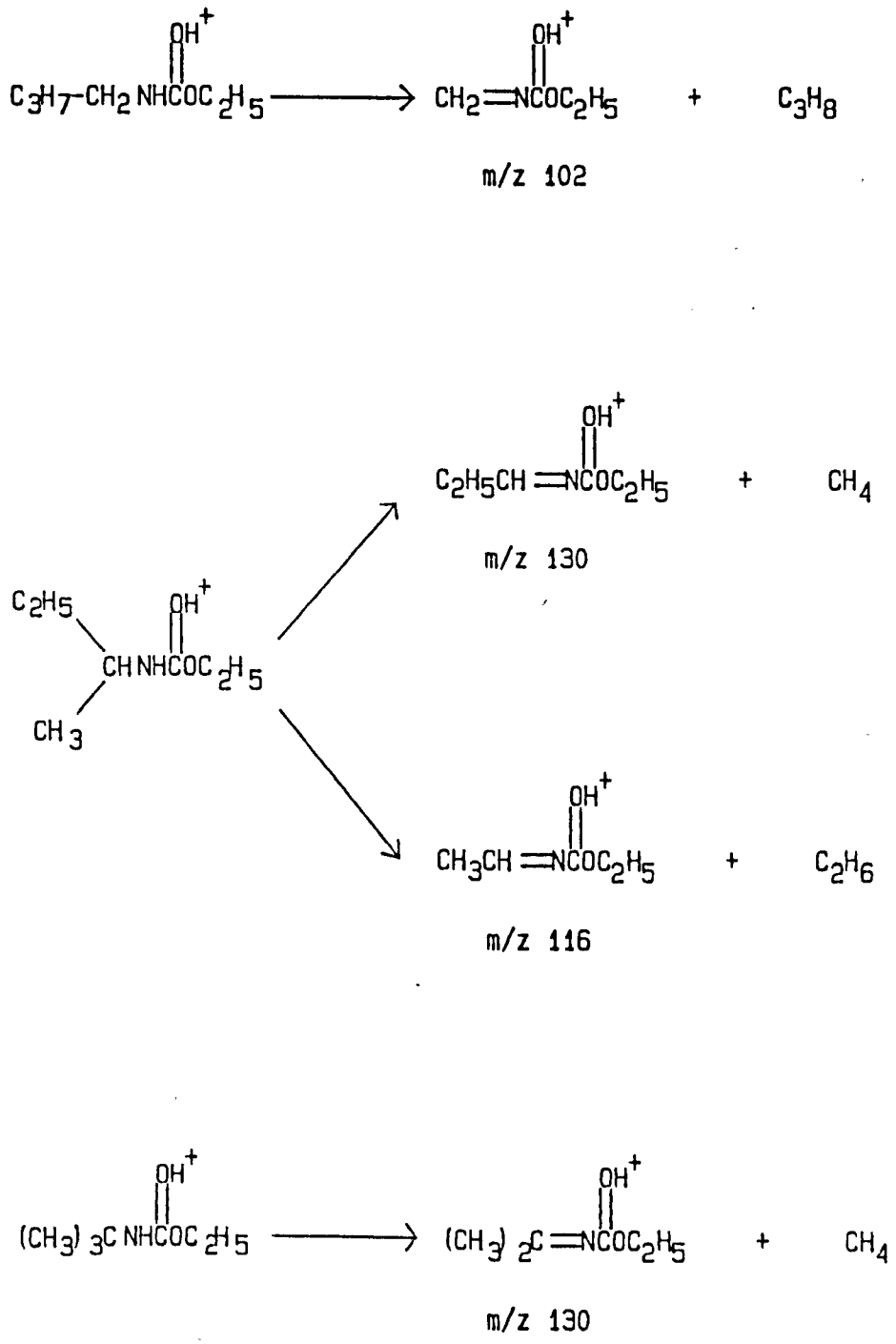

Figure 3.5. Alkane losses in the methane c.i.m.s. of the isomeric butyl urethanes.

these ions arise from decomposition of MH^+ especially the ion at m/z 103 whose formation would constitute a violation[12] of the even-electron rule[13]. This, however, does not detract from the analytical use of these fragment ions.

3.3.3.4. Elimination of Alkene Molecules.

The fourth main class of fragment ions in the spectra contains ions formed by expulsion of an alkene, C_nH_{2n}, derived by hydrogen abstraction from the principal alkyl group ($R=C_nH_{2n+1}$) in $RNHCO_2C_2H_5$. This yields a fragment ion of m/z 90, which is almost certainly protonated O-ethylcarbamic acid (urethane). The abundance of this ion increases slowly and irregularly on ascending the homologous series of urethanes, $n\text{-}C_nH_{2n+1}NHCO_2C_2H_5$. There is, however good correlation between the abundance of this ion and the structure of the principal alkyl group for $RNHCO_2C_2H_5$ compounds. When R is primary, the ion at m/z 90 has low abundance (8% or less). When R is secondary, this rises to between 11% and 18%, with the exception of $iso\text{-}C_3H_7NHCO_2C_2H_5$ where m/z 90 is only 7%, but when R is tertiary, m/z 90 is the base peak in the spectrum. Since this fragmentation is favoured by increased branching at the α-carbon atom of R, a mechanism involving the build up of charge at this centre is postulated, figure 3.6. This explanation is also supported by the spectrum of $Ph(CH_3)CHNHCO_2C_2H_5$, which contains a very large peak at m/z 90, reflecting the high stability of the incipient $PhCHCH_3$ cation.

The mechanism involves the stretching of the C-N σ-bond producing a partial positive charge on the α-carbon atom. Proton transfer from the incipient cation then results in the expulsion of an alkene and formation of the $C_3H_8NO_2^+$ ion. The involvement of such ion-molecule complexes in fragmentation mechanisms has previously been proposed[7,8].

3.3.3.5. Minor Fragment Ions.

Two other, less significant, classes of fragment ions are observed. Firstly, formation of R^+ ions from MH^+ is observed in the spectra of the larger urethanes. These peaks are larger when a favourable fragment ion is produced. This is clearly illustrated in the spectrum of

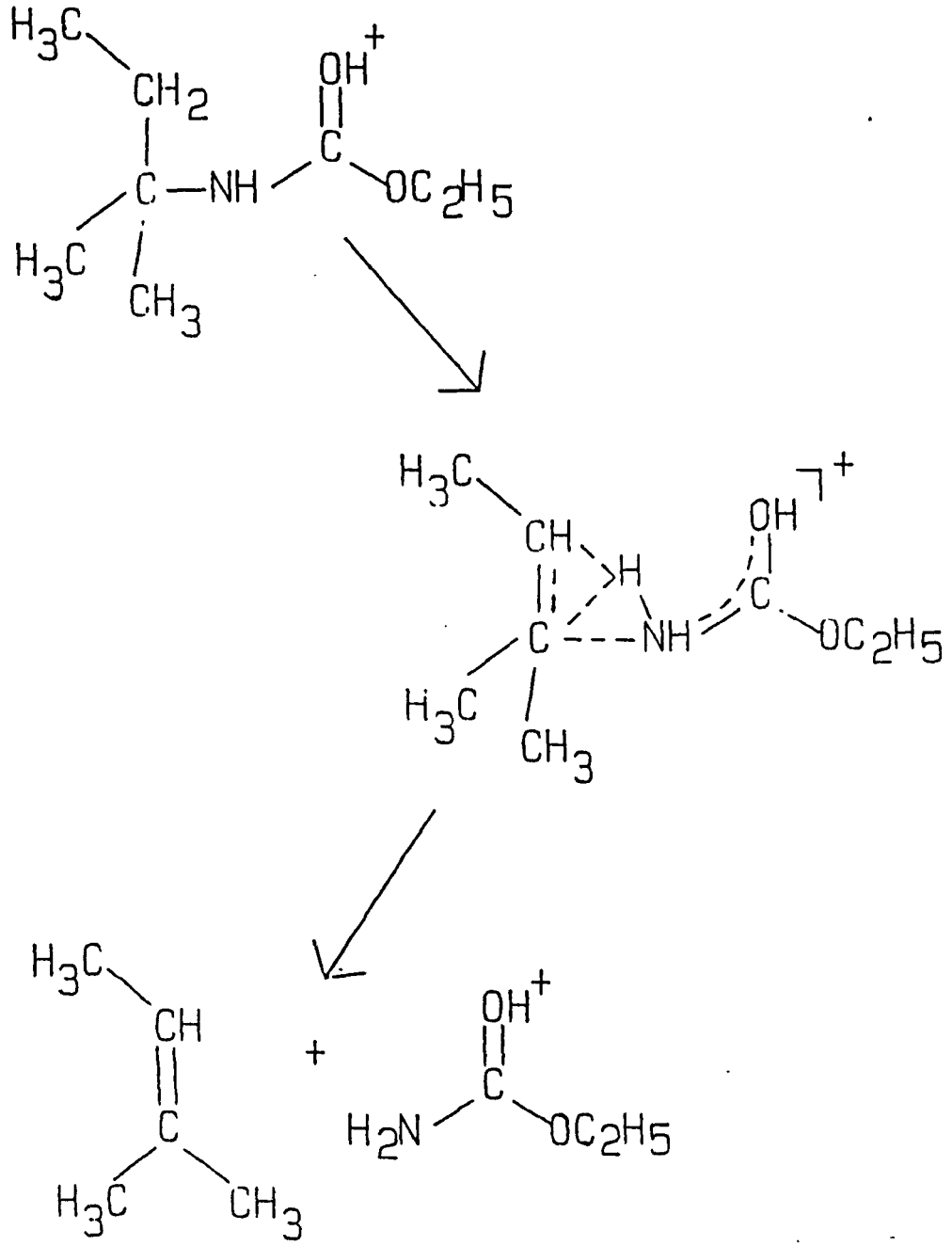

Figure 3.6. Mechanism for alkene loss from protonated urethanes.

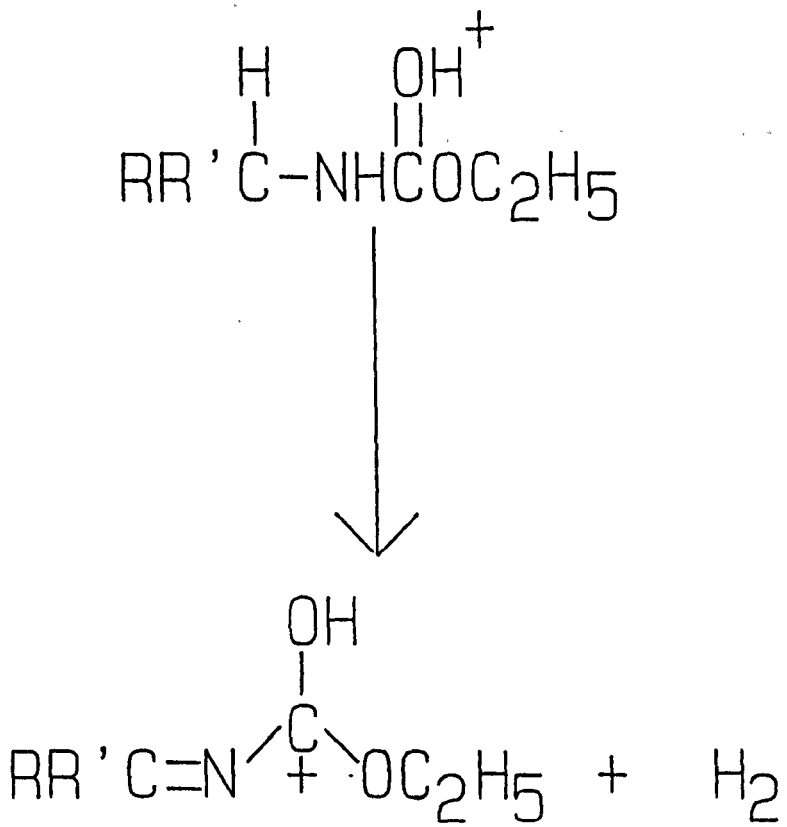

Figure 3.7. Mechanism for H_2 elimination for protonated urethanes.

$PhCH_2NHCO_2C_2H_5$, in which a large peak at m/z 91 is observed corresponding to the stable $C_7H_7^+$ cation. The analytical value of these peaks is limited.

Secondly, $[MH-H_2]^+$ ions are found in many of the spectra. These ions are more abundant for the larger urethanes but they are of negligible abundance in the spectra of urethanes in which no hydrogen atoms are attached to the α-carbon atom. For this reason a simple mechanism involving H_2 elimination across the C_α-N bond producing allylic delocalised fragment ions, figure 3.7. This, however, cannot be the complete mechanism since this mode of fragmentation is also observed in the di-substituted species where there are no hydrogen atoms attached to the nitrogen. In addition, it is known that $[MH-H_2]^+$ ions often arise by hydride abstraction from M, rather than by H_2 elimination from MH^+ [14].

3.4. Collision Induced Dissociation Study.

The mechanism proposed for the elimination of alkene molecules from protonated urethanes, figure 3.6, results in the formation of the ion m/z 90, which has the same structure as the protonated molecular ion of ethyl carbamic acid (urethane), $H_2NCO_2C_2H_5$. In order to verify this, the collision induced dissociation (CID) mass spectra of the ion at m/z 90 were recorded for protonated urethane and protonated t-pentyl urethane. The t-pentyl urethane was selected for the comparison since it gives a highly abundant fragment ion at m/z 90 (table 3.3).

3.4.1. Experimental.

The CID mass spectra were recorded using a Kratos Analytical, Concept II HH four sector mass spectrometer at an accelerating voltage of 8 kV. The samples were ionized using methane chemical ionization with ion source conditions as close as possible to those for the previous work. The precursor ions were selected using the first analyzer of the instrument and were transmitted into the collision cell which was electrically floated to 2 kV above ground potential. The helium collision gas was admitted to the cell until 15% attenuation was attained. The CID spectra were recorded using the second analyzer.

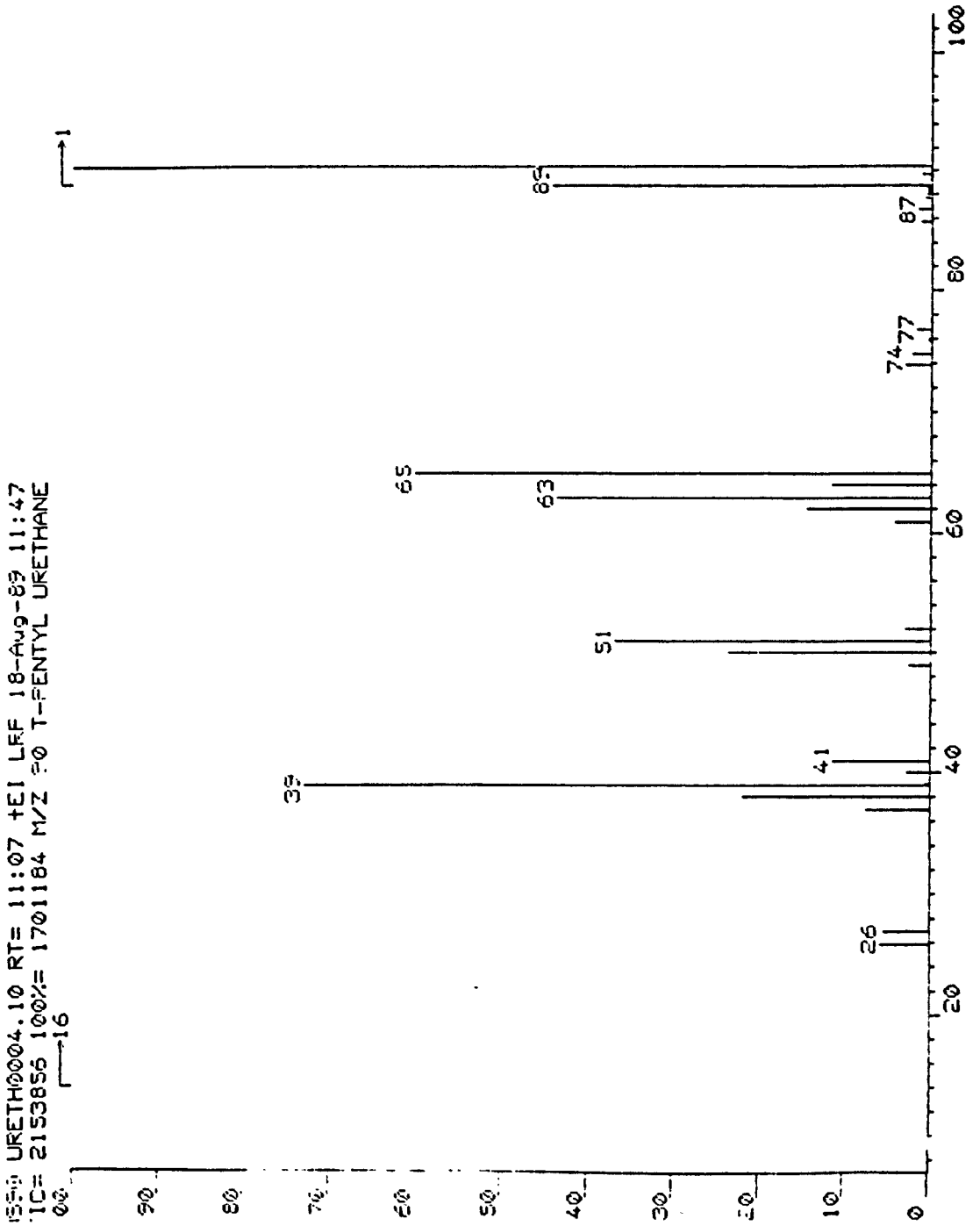

Figure 3.8. CID mass spectrum of m/z 90 from the methane c.i.m.s of $H_2NCO_2C_2H_5$.

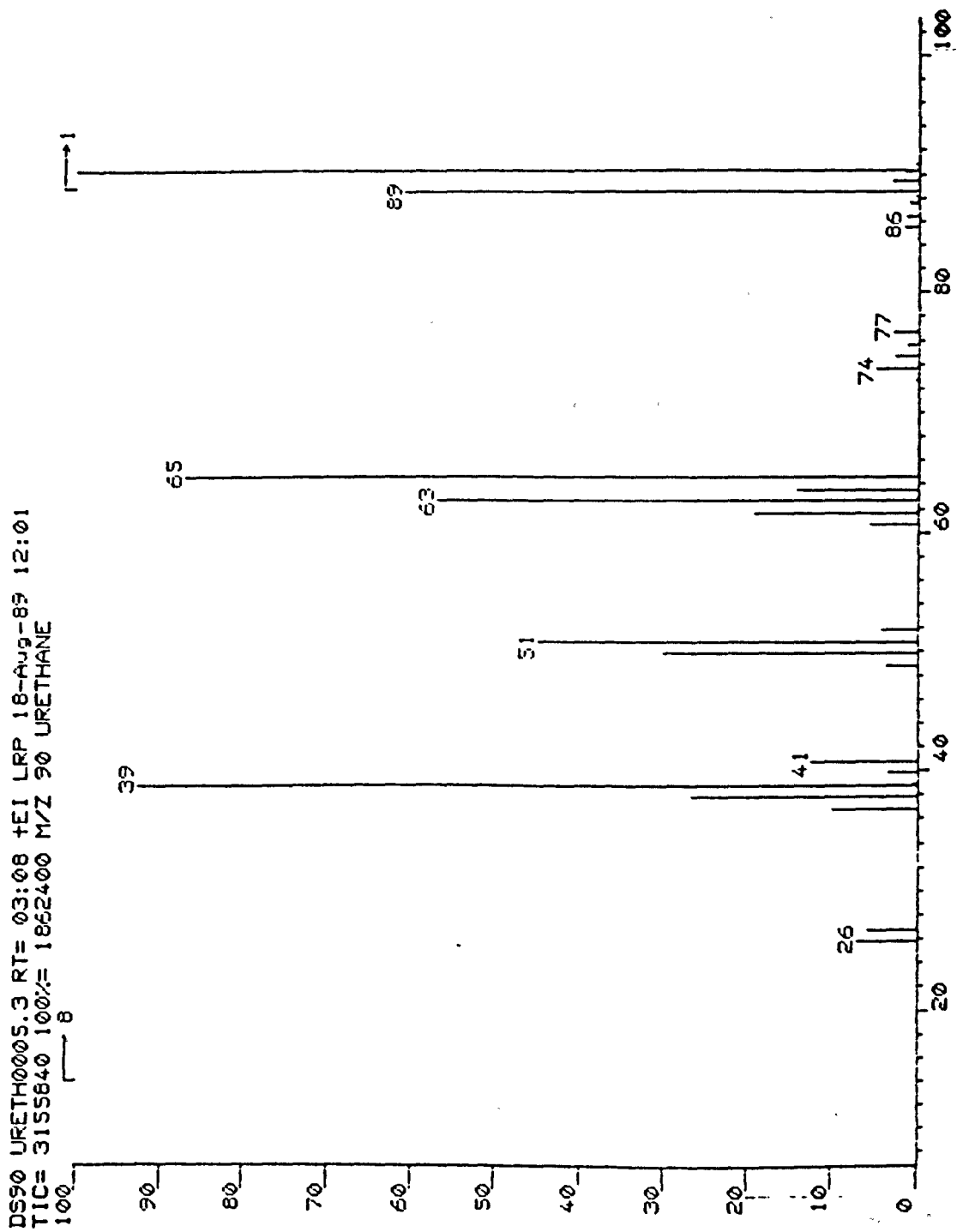

Figure 3.9. CID mass spectrum of m/z 90 from the methane c.i.m.s of t-$C_5H_{11}NCO_2C_2H_5$.

3.4.2. Results.

The CID spectra are presented in figures 3.8 and 3.9. It should be noted that the relative intensities of the peaks in the spectra are multiplied by 16 and 8 respectively to make comparison of the spectra easier.

3.4.3. Discussion.

It can be clearly seen that the CID spectra obtained are very similar to each other. This suggests that the ion at m/z 90 in the methane chemical ionization mass spectra of both of the urethanes, have the same structure. The expected structure of the ion formed by chemical ionization of urethane is shown in figure 3.10. This structure would be due to protonation at the most basic site of the molecule.

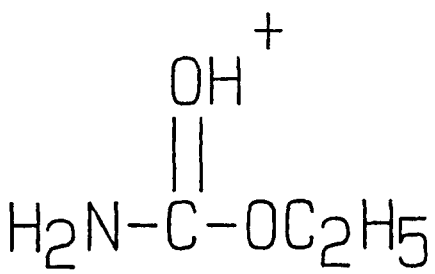

Figure 3.10. Expected structure of protonated O-ethyl carbamic acid.

3.5. Conclusion.

Methane chemical ionization mass spectrometry is applicable to the elucidation of the structures of urethanes of general formula $RR'NCO_2C_2H_5$. All of the spectra contain intense $[MH]^+$ peaks. The presence of the $CO_2C_2H_5$ group is revealed by $[MH\text{-}C_2H_4]^+$ and $[MH\text{-}C_2H_5OH]^+$ peaks. Structural information about the R groups attached to the nitrogen atom is available from peaks due to alkane and alkene losses. The structure of the ion resulting from elimination of an alkene molecule from the mono-alkylated urethanes was shown to be that formed by the postulated mechanism.

3.6. References.

1. C.P. Lewis, *Anal. Chem.*, **36**, 1582 (1964).
2. C.P. Lewis, *Anal. Chem.*, **36**, 176 (1964).
3. E.G. Sigmund and J.J. Stamp, *Org. Mass Spectrom.*, **21**, 161 (1986).
4. J.J. Stamp, E.G. Sigmund, T. Cairns and K.K. Chan, *Anal. Chem.*, **58**, 873 (1986).
5. R.D. Bowen and A. Maccoll, *Org. Mass Spectrom.*, **24**, 113 (1989).
6. N.E. Middlemiss and A.G. Harrison, *Can. J. Chem.*, **57**, 2827 (1979); and references cited therein.
7. R.D. Bowen and D.H. Williams, *J. Am. Chem. Soc.*, **102**, 2752 (1980).
8. T.H. Morton, *Tetrahedron*, **38**, 3195 (1982).
9. D.J. McAdoo, *Mass Spectrom. Rev.*, **7**, 363 (1988).
10. S. Hammerum, K.F. Donchi and P.J. Derrick, *Int. J. Mass Spectrom. Ion Proc.*, **47**, 347 (1983).
11. E.J. Reiner, R.A. Poirier, M.R. Peterson, I.G. Csizmadia and A.G. Harrison, *Can. J. Chem.*, **64**, 162 (1986).
12. For a review of the even electron rule, see: M. Karni and A. Mandelbaum, *Org. Mass Spectrom.*, **15**, 53 (1980).
13. L. Friedman and F.A. Long, *J. Am. Chem, Soc.*, **75**, 2832 (1952).
14. A.G. Harrison, 'Chemical Ionization Mass Spectrometry', C.R.C. Press, Boca Raton, Florida, 1983.

Chapter 4

Collision Induced Dissociation Mass Spectrometry: An Investigation of Collision Gases

4.1. Introduction.

Collisional activation (CA) of organic ions and the recording of collision induced dissociation (CID) mass spectra were first reported by Jennings in 1968[1]. Much work involving the collisional activation of ions, as applied to many types of problems, has been reported since then. Three of the main applications of CID are

(1) mixture analysis, especially the targeting of specific components in complex mixtures, e.g. identification of toxins in water,

(2) the determination of ion structures in a similar way to which EI mass spectra are used to determine the structure of organic molecules,

(3) the study of fragmentation mechanisms by comparison of the CID spectra of an ion formed by fragmentation and that of an ion of known structure.

An example of the final application is shown in chapter 3.

The collision gas of choice for CID experiments of small organic molecules is helium because of its small size and high ionization potential. A small target atom is favourable since the scattering of the incident ions by collisions with the target atom is minimized. Also, additional ion loss processes, such as charge exchange, can be reduced by using a target gas with a high ionization potential.

The early work involving CID was limited in mass range because of the limitations of the available ionization techniques. With the advent of techniques such as fast atom bombardment (FAB)[2], these mass limits were removed enabling the study of larger, biologically active molecules. It is now accepted that small, unknown peptides (molecular mass ~ 500 Daltons) can be unambiguously sequenced by CID mass spectrometry[3]. For peptides of higher mass the determination of amino acid sequence becomes much more difficult for two reasons. The first is due to the complexity of the CID spectra produced. The major fragment ions formed by CA of peptide ions result from cleavage of bonds in the backbone of the peptide with retention of the charge on either fragment. Such fragmentations

can produce six series of fragment ions[4]. Additional fragment ions, formed by cleavages of the side chains of the peptides, have been identified recently[5]. Consequently, a CID mass spectrum containing all of these fragment ions will be very complex. Secondly, when peptides of even higher mass are studied, the abundance of fragment ions decreases because the internal energy gained by the peptide ion is distributed between a large number of vibrational degrees of freedom so that the energy in a single vibrational mode is insufficient to cause breakage of that bond. Attempts to overcome this problem have led to the use of collision gases other than helium in an attempt to increase the amount of internal energy transferred to the large ions.

4.1.1. The Effects of Different Collision Gases on The CID Mass Spectra of Large Ions.

A theoretical approach to this problem was made by Uggerud and Derrick[6]. By considering the collisions between incident ions and target atoms as impulsive collisions, they concluded that helium should be the best collision gas for large peptides. The argument used suggests that the efficiency of energy transfer to the large peptide ion is maximized when helium is the target gas. Their argument is summarised below.

The maximum energy available for conversion to internal energy is the centre of mass energy, E_{com}, given by equation 4.1:

$$E_{com} = E_i m_g/(m_g+m_i) \qquad (4.1)$$

where m_g is the mass of the collision gas, m_i is the mass of the incident ion and E_i is the kinetic energy of the incident ion. The energy transferred to the ion, Q, is related to the maximum energy by an efficiency factor, χ, according to equation 4.2:

$$Q = \chi E_{com} \qquad (4.2)$$

The efficiency factor itself is related to the masses of the colliding species such that

$$\chi = 4m_g m_a/(m_g + m_a) \qquad (4.3)$$

where m_a is the mass of the specific atom of the ion involved in the collision. By considering which atom of the peptide ion will take part in the collision, χ values for helium and argon collisions were calculated (table 4.1).

Peptide Atom mass	Collision Gas He	Ar
1 (H)	0.32	0.05
7.2*	0.46	0.26
12 (C)	0.38	0.35

* The average mass of an atom in a peptide.

Table 4.1. Energy transfer efficiency values of atoms of a peptide ion involved in impulsive collisions with argon and helium.

Based upon these values, and assuming that the target gas atoms are more likely to undergo collisions with the hydrogen atoms of the ion since they are to be found on the "outside" of a peptide, it was suggested that helium should be the most efficient collision gas.

Two investigations of the effects of different collision gases on the CID mass spectra of peptides have been reported recently. Work by Carr *et al*[7] showed, for peptides up to mass 2000 Daltons, that argon can be used to produce qualitatively better CID spectra than helium using an electrically floated collision cell. The collision cell voltage for these experiments was half of the accelerating voltage. With peptides of masses greater that 2000 Daltons, the ion loss processes were shown to outweigh the advantages of the heavier collision gas. In these cases the best results were obtained using helium as the target gas.

A more detailed study by Curtis *et al*[8] reported the performances of two "light" collision gases, hydrogen and helium, and three "heavy" gases, nitrogen, argon and xenon. For peptides of masses between 500 and 1500 Daltons, the heavy gases produced abundant low mass fragment ions and the light gases produced abundant high mass fragment ions. It was reported that a 1:1 mixture of hydrogen and xenon could be used to good effect, giving rise to abundant fragment ions throughout the fragment ion spectrum. For peptides of masses in the range 1500 to 2500 Daltons, only the heavier gases were useful in CID experiments. If

peptides of even higher mass are studied, the use of heavy collision gases at lower pressures than normal (~30% ion beam attenuation rather than the more general 60-70% attenuation used in this work) satisfactory results could be obtained.

Despite these conlusions, satisfactory results are still obtained using helium as the collision gas for peptides of varying masses[4,9].

4.1.2. Introduction to This Work.

This work is a result of the apparent confusion over which is the "best" gas to use for CID mass spectrometry of peptides. The CID mass spectra of a small neuro-peptide, leucine-enkephalin, under controlled conditions are reported and discussed. The collision gases employed in this study are helium, argon, carbon tetrafluoride and krypton. Control of the collision gas pressures is attempted using a specially designed inlet system

4.2. Control of Collision Gas Pressure.

Since it is the aim of this work to compare the efficiency of several gases used for CID, it is necessary to be able to maintain and reproduce constant gas pressures within the collision region of the mass spectrometer. The CID mass spectra reported in this work were recorded using a Kratos Analytical MS-50 mass spectrometer and a DS 90 data system. The collision region of this instrument lies between the source slit and the z-restrictor, figure 4.1. Gases can be admitted to this region through a ¼"o.d. stainless steel tube attached to a flexible metal hose which is also connected to a small oil vapour diffusion pump for differential pumping of the collision region. In order to be able to control the pressure of gas admitted to this line, a glass inlet system was constructed, figure 4.2. The inlet system consists of two glass bulbs of the same volume (2 dm^3) attached to a glass manifold via teflon keyed taps. The use of two bulbs is necessary to facilitate rapid changeover of collision gases so that two gases may be used in a single run, thereby reducing the the effect of all other factors that may affect the CID spectra which are being recorded. Attached to the manifold are four side arms. Two of these, connected to a gas cylinder and a rotary pump, can be isolated using teflon keyed taps.

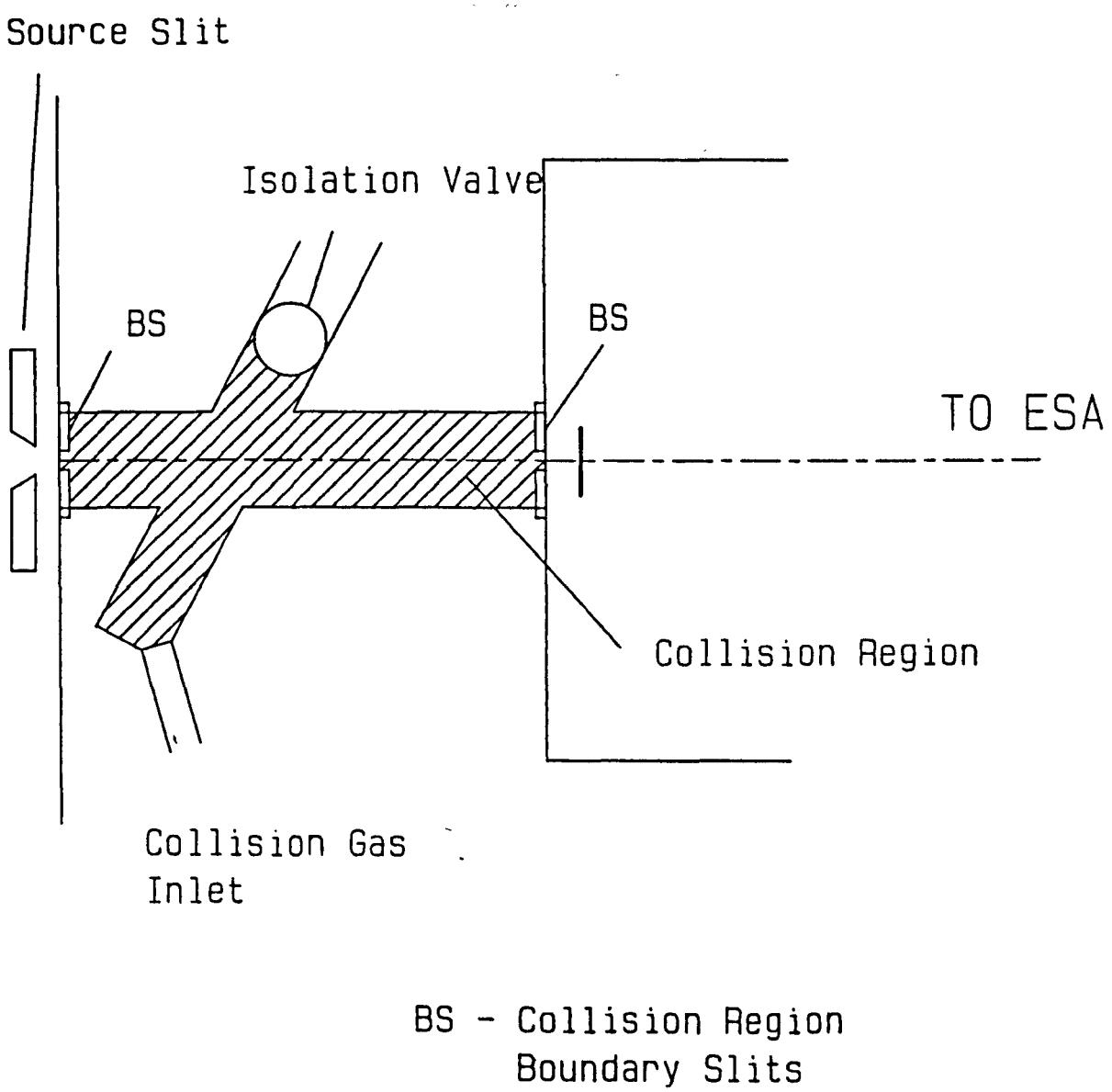

Figure 4.1. Collision region of the Kratos Analytical MS-50 mass spectrometer.

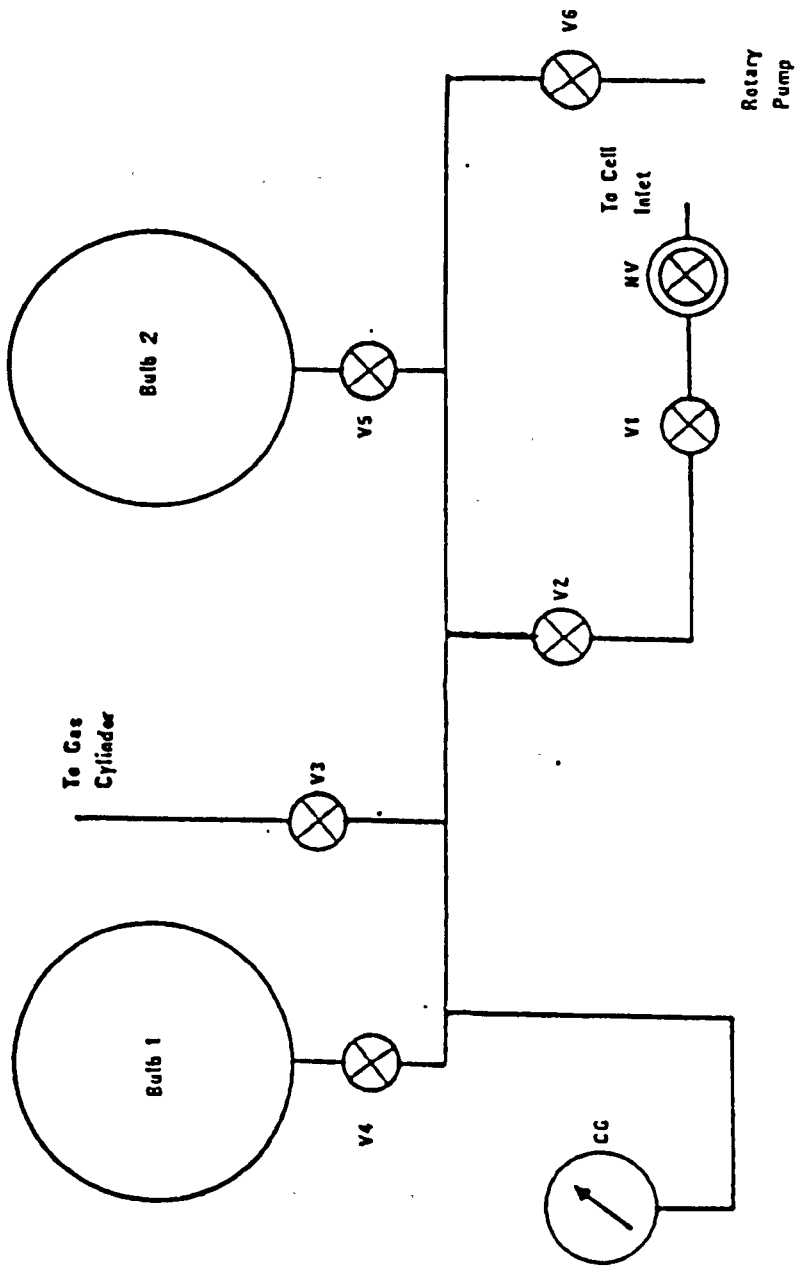

Figure 4.2. Inlet system used for admitting gases to the MS-50 collision region.

Another side arm is connected directly to a mechanical pressure gauge (Edwards High Vacuum CG3, 0 - 125 mBar capsule dial gauge). The final side arm is connected to the MS-50 collision gas inlet line via an on/off tap and a fine micrometer needle valve. The dead volume between these two taps was minimized to enable rapid pump-out of this section during gas changeovers.

4.2.1. Operation of the Inlet System.

In order to be able to reproduce CID experiments easily, a standard procedure for filling the inlet system was devised. First the entire inlet system is evacuated by opening taps V2, V4, V5 and V6. Both of the bulbs are then isolated by closing V4 and V5, and a gas cylinder is attached to the line connected to V3. This line is evacuated by opening V3. After closing the tap, V6, to the rotary pump, the manifold is filled with gas from the cylinder to a pressure of ~125 mBar. This gas is then pumped away to purge the inlet system. Gas is now admitted to the required bulb by opening the appropriate tap (V4 or V5) allowing gas into the inlet system to the required pressure and closing the tap. The manifold is then evacuated and the second bulb can be filled using the same procedure. When both bulbs contain the required gases, the manifold is evacuated and the inlet system is ready for use.

Gas is admitted to the collision region by allowing gas from one of the bulbs into the manifold and opening V1. Control of the gas pressure in the collision region is achieved using the needle valve.

4.2.2. Determination of the Optimum Pressure of Gas in the Inlet System.

Accurate control of the pressure in the collision region can only be achieved if the flow of gas through the needle valve does not change rapidly as the needle valve is opened. This requires the pressure difference across the needle valve to be small. However, if the pressure in the inlet system is low, it may be possible for this pressure to change drastically during the course of a single experiment. Clearly this is undesirable for these experiments.

To determine a suitable pressure, the variation of the attenuation of an ion beam was measured as a function of needle valve reading for three pressures of helium in the inlet system. The pressures investigated were 50, 75 and 100 mBar. The ion used for this experiment was $Cs_3I_2^+$ at m/z 653, obtained by FAB ionization of caesium iodide. The results are shown in figure 4.3. Using these results it was decided that the most appropriate pressure to use was 50 mBar since at this pressure, the rate of change of beam attenuation with needle valve reading is not very large and that the pressure in the inlet system does not change over the time period required to perform a set of CID experiments.

4.2.3. Reproducibility of Setting the Gas Pressure in the Collision Region.

A major requirement of the CID experiments to be carried out, is that the pressure in the collision region of the mass spectrometer must be able to be reproduced exactly. With no means of measuring the pressure in this region, it must be assumed that by setting the needle valve to the a particular position, a certain pressure can be obtained. An experiment was carried out to see if this could be assumed.

4.2.3.1. Experimental.

The inlet system was filled with helium to a pressure of 50 mBar. The variation of precursor ion abundance with needle valve reading was recorded using the same procedure as the previous experiment. This was repeated three times, having re-filled the inlet system between each experiment. The results are shown in figure 4.4.

4.2.3.2. Results.

It can clearly be seen from the results that by setting the needle valve to a particular position cannot be used to select a known pressure in the collision region with a reasonable degree of accuracy. It was therefore decided that spectra which were to be compared had to be recorded without having changed the needle valve setting. The needle valve was set to give the required attenuation of the precursor ion beam using helium at the start of each set of experiments, and not altered until the set of experiments was completed.

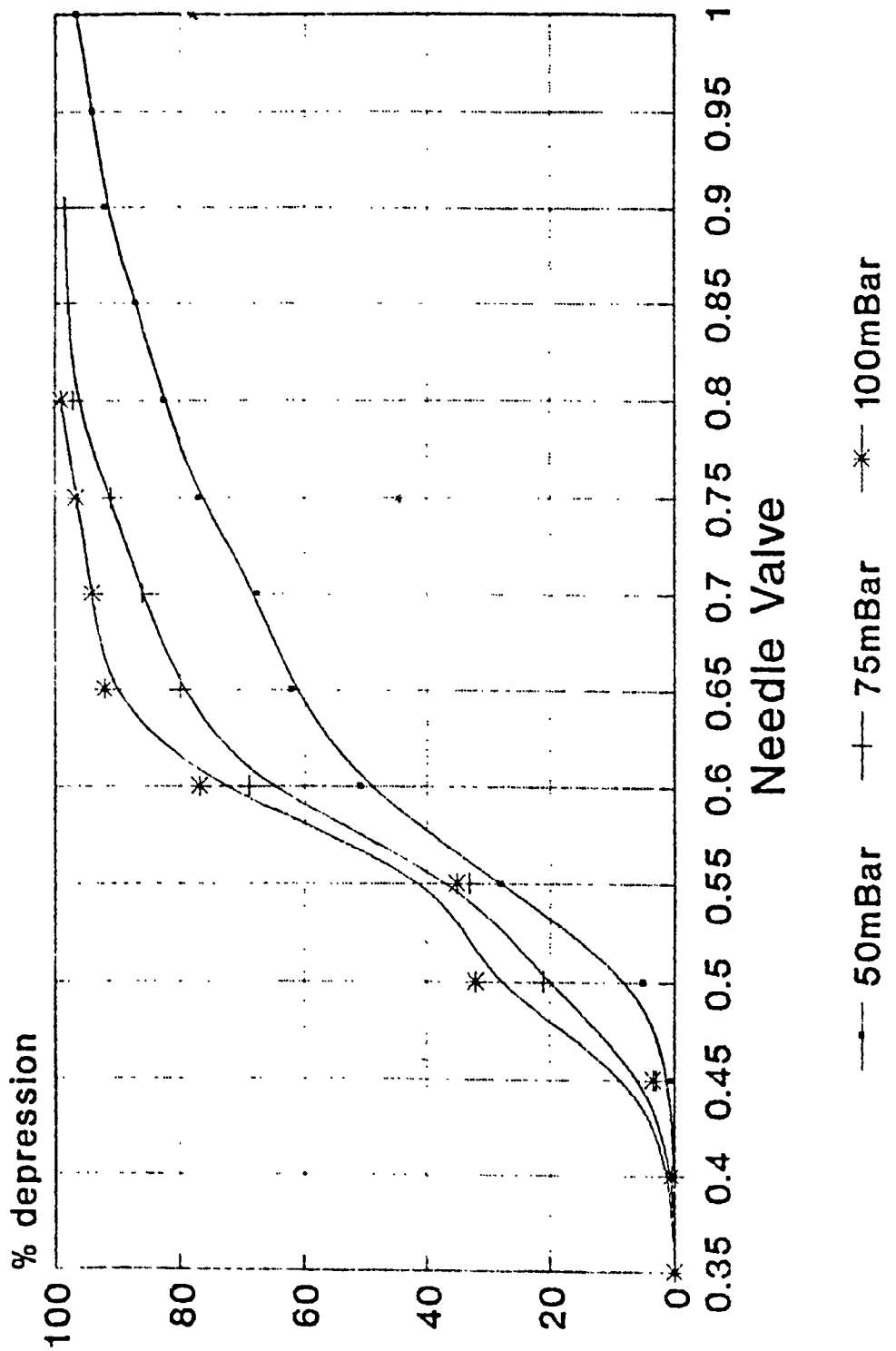

Figure 4.3. Attenuation of the ion beam at m/z 653 ($Cs_3I_2^+$) as a function of needle valve setting for three pressures of helium.

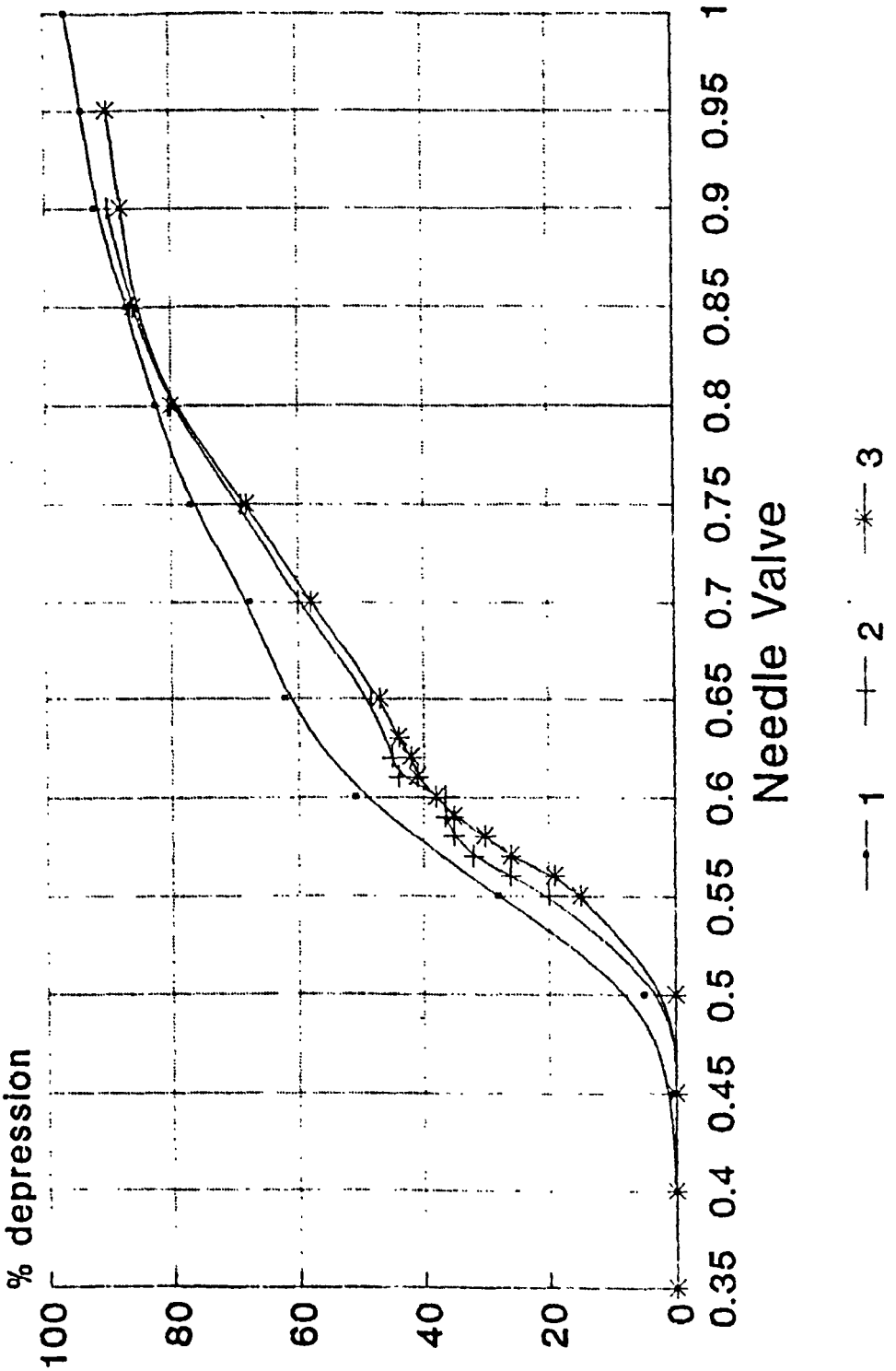

Figure 4.4. Reproducibility of the attenuation of the ion beam at m/z 653 ($Cs_3I_2^+$) as a function of needle valve setting for three pressures of helium.

4.3. CID Mass Spectra of Leucine-Enkephalin.

The CID mass spectra of the protonated molecular ion of leucine-enkephalin at m/z 556 were recorded using helium, argon, krypton and carbon tetrafluoride as collision gases. For all of the spectra discussed in this section, the precursor ion attenuation was set to 50% using helium before the required collision gas was used.

4.3.1. CID Spectra Recorded Using Helium.

The CID mass spectrum of m/z 556 ions obtained by FAB ionization of ~2 nmol of leucine-enkephalin from a glycerol matrix is shown in figure 4.5. Fragment ions at lower mass could not be detected because of the lower limit of the metastable calibration.

To examine the ability to control the collision gas pressure, a second series of spectra were recorded using helium as the collision gas, having followed the same procedure to set up the experiment. Figure 4.6 shows a representative spectrum from that run.

The two sets of spectra obtained are reasonably similar, though no comparison of the absolute abundances of the fragment ions can be made. However, since the relative abundances of the fragment ions have a reasonable correlation, it is suggested that the same pressure of helium in the collision region was obtained in both experiments.

4.3.2. Comparison of Helium and Argon CID Spectra.

The CID spectra recorded using helium and argon under the same conditions are shown in figure 4.7. The spectra contain peaks due to the same fragment ions, but in the case where argon was used as the collision gas, the relative abundances of the fragment ions with respect to the precursor ion are slightly reduced. It would appear therefore, that argon and helium are almost equally suited for the recording of CID mass spectra of peptides of this size. It should be noted that although the attenuation of the precursor ion beam with helium was 50%, the measured attenuation for argon using the same conditions was approximately 60%. The additional losses of ions is probably caused by increased scattering by the argon target gas.

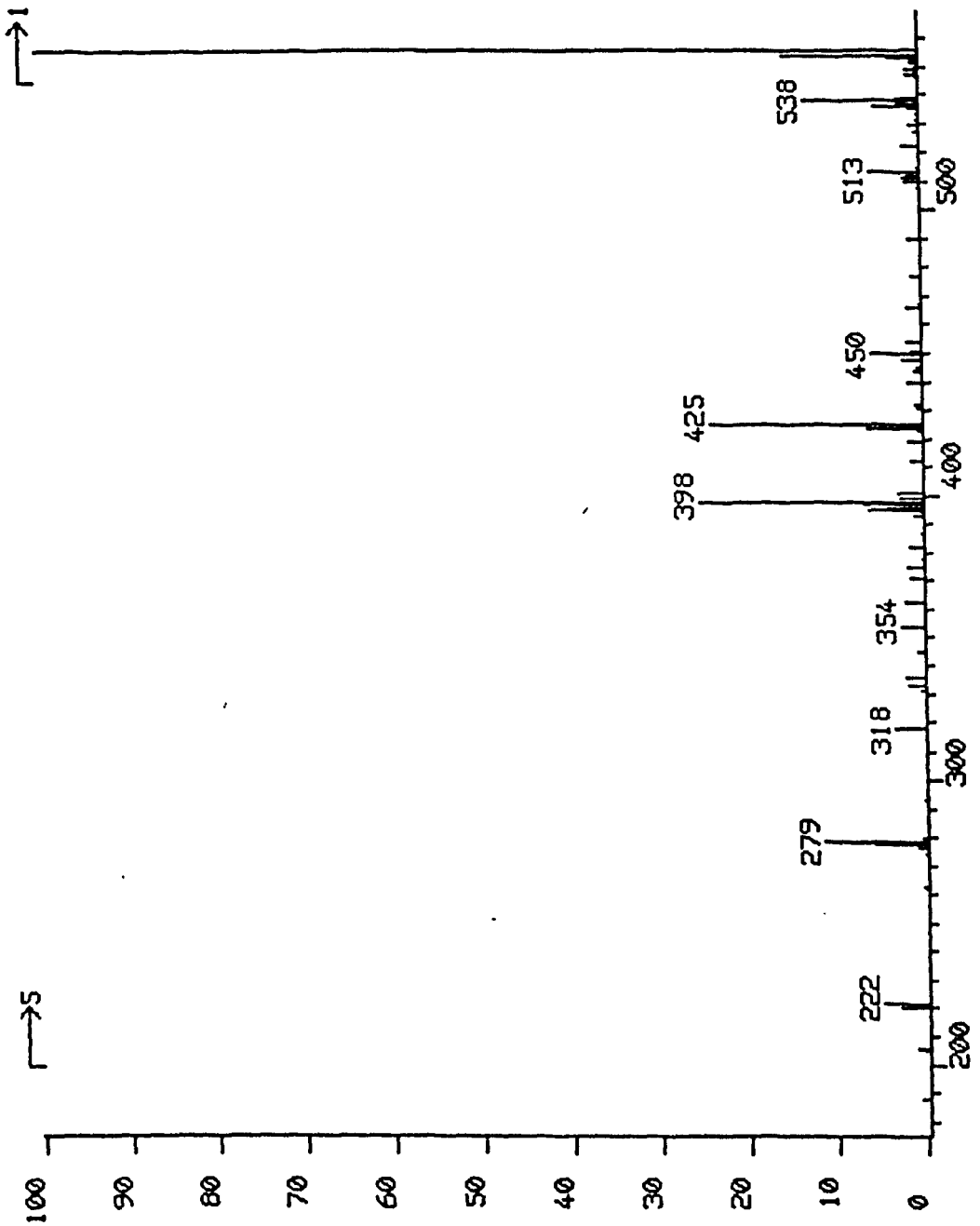

Figure 4.5. CID mass spectrum of leucine-enkephalin recorded using helium as the collision gas.

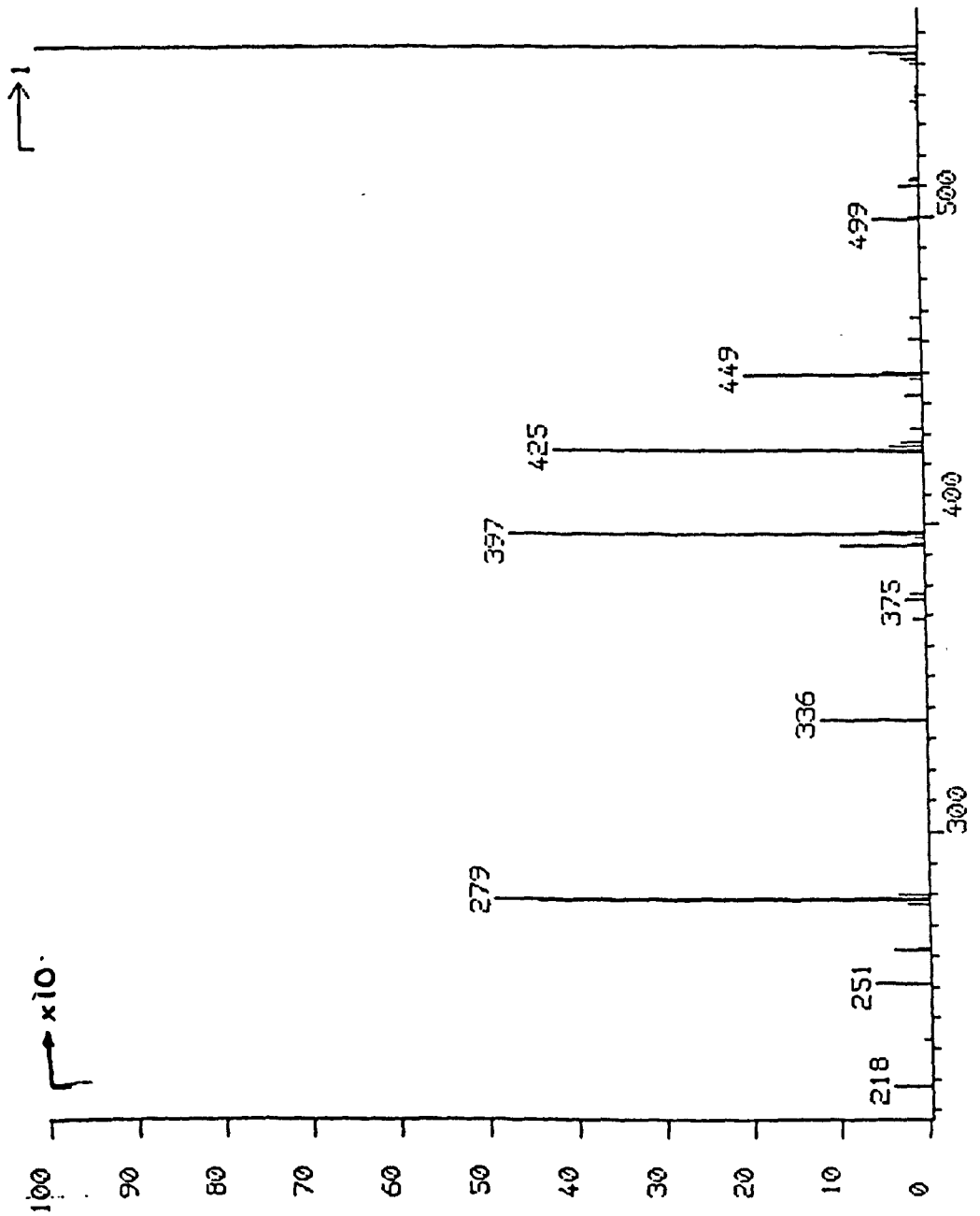

Figure 4.6. A second CID mass spectrum of leucine-enkephalin recorded using helium as the collision gas to check the performance of the inlet system.

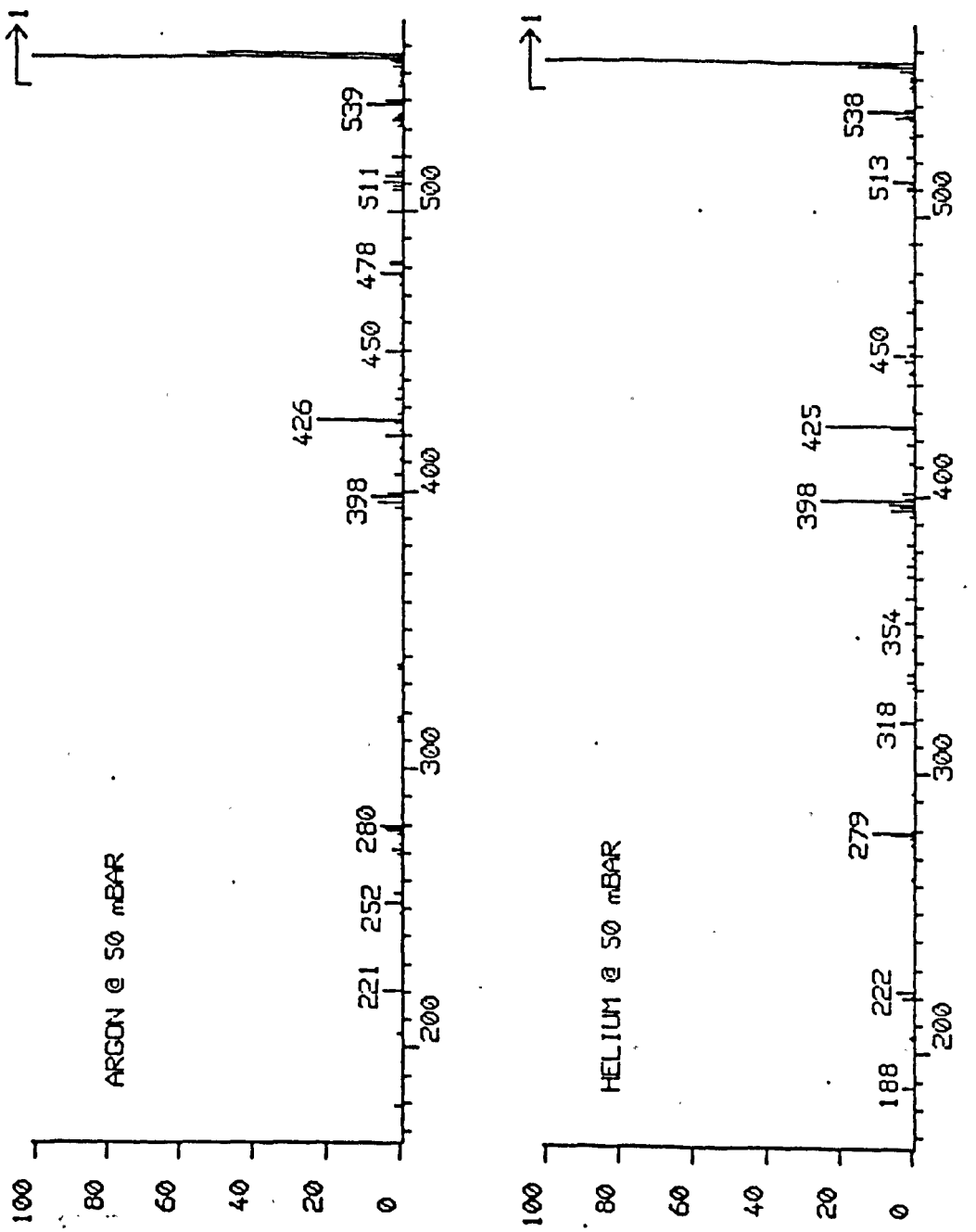

Figure 4.7. A comparison of the CID mass spectra of leucine-enkephalin recorded using helium and argon.

4.3.3. Comparison of Helium and Carbon Tetrafluoride.

The CID spectra recorded using helium and carbon tetrafluoride under the same conditions are shown in figure 4.8. Since carbon tetrafluoride is a much more massive species than helium, it is reasonable to expect that the CID mass spectra recorded using these gases would be very different. The results obtained show that this is indeed not the case, but that the spectra recorded using these collision gases are very similar.

A possible explanation for this discrepancy is that unlike the common collision gases such as helium and argon, carbon tetrafluoride is a polyatomic species, and can therefore also undergo collisional activation in CID experiments. In this way, the additional energy that would be expected to be transferred to the incident ion, could simply be partitioned between the ion and the target molecule. A further explanation, based upon the suggestions of Uggerud and Derrick[6], is that the most likely atoms to be involved in the collision are hydrogen and fluorine. In this way, the efficiency of energy transfer is not reduced significantly.

4.3.4. Comparison of Krypton and Carbon Tetrafluoride

The relative molecular masses of krypton and carbon tetrafluoride are very similar, 84 and 88 respectively. It could therefore be expected that similar CID mass spectra could be obtained using these collision gases. The spectra recorded using krypton and carbon tetrafluoride are shown in figure 4.9. The recorded spectra, however, are different. In the krypton CID spectrum, the fragment ions at lower mass are more abundant than in the carbon tetrafluoride spectrum. This would be expected if carbon tetrafluoride were behaving as a collision gas of lower mass, as described above, since less collisional activation occurs with lower mass collision gases.

4.4. Discussion.

It appears, in general, that the mass of the collision gas does indeed have an effect on the CID mass spectra of leucine-enkephalin. With the inert gases, helium, argon and krypton, as the mass of the collision gas is increased the abundances of the low mass fragment ions in the

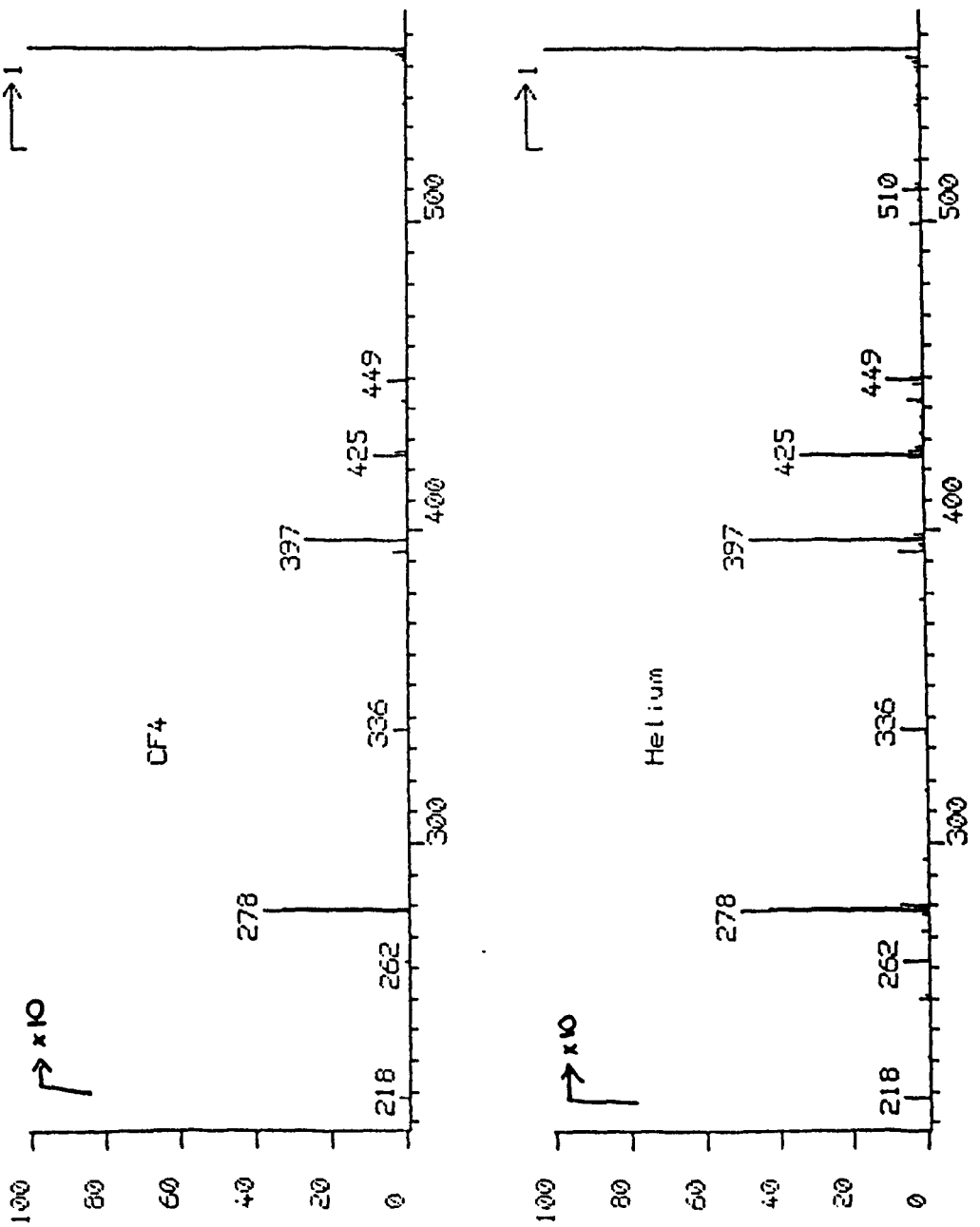

Figure 4.8. A comparison of the CID mass spectra of leucine-enkephalin recorded using helium and carbon tetrafluoride.

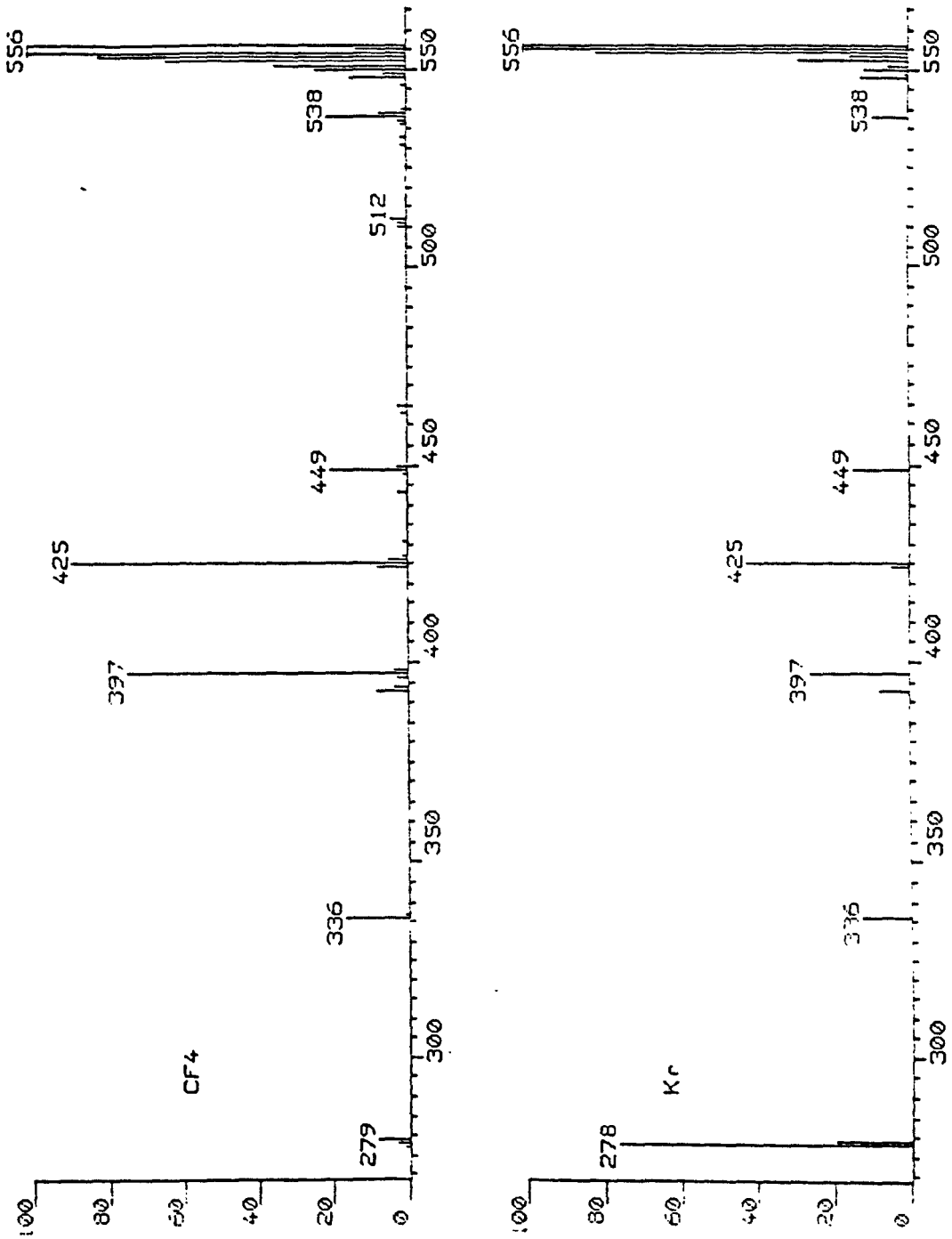

Figure 4.9 A comparison of the CID mass spectra of leucine-enkephalin recorded using carbon tetrafluoride and krypton.

CID spectrum of leucine-enkephalin are also increased. This is reflects the increase in energy transfer to the peptide ion as the mass of the collision gas is increased. However, an exception to this general observation are the CID spectra obtained using a polyatomic collision gas. The spectrum recorded using carbon tetrafluoride as a collision gas, does not have particularly abundant low mass fragment ions. A possible explanation for this deviation follows the arguments of Uggerud and Derrick[6].

If the efficiency of the energy transfer during collisional activation is dependent upon the mass of the actual atom of the ion which is involved in the collision, then logically, the mass of the atom of a polyatomic collision gas involved in the collision will have a similar effect. Using equation 4.3, the energy transfer efficiencies for collisions involving the carbon and fluorine atom of carbon tetrafluoride and the atoms of the peptide were calculated. These values, $\chi/2$, are shown in table 4.2.

Peptide Atom mass	Collision Gas Atom C	F
1 (H)	0.14	0.10
7.2*	0.47	0.40
12 (C)	0.50	0.47

* The average mass of an atom in a peptide.

Table 4.2. Energy transfer efficiencies for the atoms of carbon tetrafluoride in collision with the atoms of a peptide ion.

Comparing these values with those in table 4.1, it can be seen that the efficiencies calculated for collisions with the average atom are very similar for helium and both carbon and fluorine. This suggests that the CID spectra obtained using helium and carbon tetrafluoride should indeed be similar. A similar conclusion can be drawn qualitatively by simply considering the masses of the fluorine and carbon atoms rather than the overall mass of the collision gas, when predicting the extent of fragmentation.

4.5. Conclusions

The results obtained for the CID of leucine-enkephalin clearly indicate that the extent of fragmentation is dependent on the mass of the collision gas, provide that the collision species is monatomic. When polyatomic species are used for collisional activation, the extent of fragmentation appears to be dependent on the masses of the atoms of the molecule rather than its overall mass. Further work is require to determine whether these conclusions are valid for peptides of higher mass.

4.6. References.

1. K.R. Jennings, *Int. J. Mass Spec. Ion. Phys.*, **1**, 227 (1968).
2. M. Barber, R.S. Bordoli, R.D Sedgwick and L.W. Tetler, *Org. Mass Spec.*, **16**, 256 (1981).
3 M.M. Sheil and P.J. Derrick, *Org. Mass Spec.*, **23**, 429 (1988).
4. P. Roepstorff and J. Fohlman, *Biomed Mass Spectrom.*, **11**, (1984).
5. R.S. Johnson, S.A. Martin and K. Biemann, *Int. J. Mass Spec. Ion. Proc.*, **86**. 137 (1988).
6. E. Uggerud and P.J. Derrick, *Z. Naturforsch.*, **44a**, 245 (1989).
7. S.A. Carr, B.N. Green, M.E. Hemling, G.D. Roberts, R.J. Anderegg and R. Vickers, 35th A.S.M.S. Conference on Mass Spectrometry and Allied Topics, Denver, CO, U.S.A. (1987).
8. J.M. Curtis, L.S. Rong, R.. Milberg and K.L. Reinhart, 35th A.S.M.S. Conference on Mass Spectrometry and Allied Topics, San Fransisco, CA, U.S.A. (1988)
9. R.S. Johnson, S.A. Martin, K. Biemann, J.T. Stults and J.T. Watson, *Anal. Chem.*, **59**, 2621 (1987).

Chapter 5

Scan Laws For Use With An Electrically Floated Gas Collision Cell

5.1. Introduction.

Determination of the structure of peptides and other biomolecules is possible using tandem mass spectrometry (MS/MS). It is necessary for the excitation process used, usually collisional activation, to provide sufficient energy to cause substantial fragmentation of the intact precursor ions, so that structural assignments can be made. Peptides of relative molecular mass 500 can be unambiguously sequenced using the currently available techniques and instrumentation but when larger molecules are considered, very few structurally significant peaks are observed[1]. This can be attributed mainly to the inadequate excitation of the precursor ions, because of the large number of atoms present giving many degrees of vibrational freedom in which the internal energy gained can be divided. The amount of energy transferred to the precursor ion should therefore be increased when more fragmentation is required. It is possible to do this in two ways. Derrick and co-workers, using a specialized mass spectrometer[2], increased the collisional activation of peptides by increasing the kinetic energy of the incident ion beam to values up to 15000 eV. Clearly this technique is not applicable to commercial mass spectrometers where the maximum accelerating voltage is typically 8000 V. The other possibility is increase the number of collisions between the target gas and the precursor ions either by electrically floating the gas collision cell or by increasing the target gas pressure.

5.1.1. The Effects of Floating a Gas Collision Cell.

The advantages of an electrically floated collision cell are twofold. Firstly, since the ions are retarded by the voltage on the cell as they approach, the ions will travel more slowly through the cell and consequently will be able to undergo more collisions with the target gas. This allows a greater increase in internal energy and hence more fragmentation can occur. In the absence of lasers and high intensity beams of electrons which can be used to significantly increase the internal energy of such molecules, this is a viable method is to increase the internal energy uptake of ions in a CID experiment.

Secondly, the acceleration of the ions out of the collision cell increases the detection efficiency of low mass fragment ions. The kinetic energy of a fragment ion leaving the collision cell is lower than that of the precursor ion. As the mass of this ion becomes smaller, its kinetic energy decreases. Detection of these slow moving ions is much less sensitive than for faster moving ions so that fragment ions of low mass will appear to be less abundant than they actually are. Raising the voltage on the collision cell increases the kinetic energy of the fragment ions. This can be clearly seen from equation 5.5. Therefore the recorded abundances of these ions will reflect more closely their actual abundances.

Additionally ,losses of low mass fragment ions caused by scattering during the collision event can be reduced by placing a series of focusing lenses after the floated collision cell. The scattered ions can be refocused into the ESA so that the ion losses due to scattering are minimized.

5.1.2. Translational Energy Losses; The Derrick Effect.

Derrick and co-workers[1,2,3], have reported significant kinetic energy losses, some greater than 1000 eV, for the fragment ions of peptides. The energy shifts were measured using mass-analyzed ion kinetic energy spectrometry[4] (MIKES), by calculating the difference between the ESA potential at which the fragment ions were transmitted and the potential at which transmission of the expected fragment ions should occur. This, however, assumes that the fragment ions formed by CID are in fact those predicted by considering fragmentations of the backbone of the peptide[3].

Such assumptions were not necessary in the work by Guevremont and Boyd[5], who used a reverse geometry instrument fitted with a quadrupole mass filter after the ESA. The quadrupole was used to determine the actual mass of the fragment ions transmitted by the ESA by rapidly scanning the quadrupole mass filter during the MIKES scan and accumulating the data in a multichannel analyzer. The energy losses measured in this way were smaller by some 50% than those measured by Derrick and co-workers.

The effect of such energy losses on the tandem mass spectra of large molecules using forward geometry instruments is that conventional linked scanning techniques will cause low mass fragment ions to follow trajectories which are not on the ion optical axis of the ESA. As a result of this it is possible that the transmission of energy depleted ions will be reduced since the ions may strike the inner ESA plate as shown in figure 5.1. Little change in the recorded mass for these ions will be observed because of the double-focusing properties of the instrument. The addition of energy loss correction terms in the linked-scan laws for such instruments is the aim of this work.

5.2. Derivation of Scan Laws.

The scan laws for an electrically floated collision cell have previously been derived by Boyd[6]. It is the intention of this chapter to add to these scan laws terms related to translation energy losses of the ions. These new scan laws are derived in full below.

5.2.1. General Equations.

The linked-scan equations for a mass spectrometer of forward geometry which has a first field-free region collision cell which can be electrically floated are derived. Additional terms related to the reduction of ion kinetic energies due to collisions with the target gas, the *Derrick Effect*, are included. The precise nature of these terms is discussed later. The processes of collision induced dissociation in a floated collision cell are represented schematically in figure 5.2.

Initially, the precursor ion m_p^+, has kinetic energy due to acceleration from the ion source which is at a voltage V_{acc}, given by

$$E_k = zV_{acc} = \tfrac{1}{2}m_p v^2 \qquad (5.1)$$

As this precursor ion enters the collision cell it is retarded by the voltage on the cell. Its kinetic energy is reduced to

$$E_k' = \tfrac{1}{2}m_p v_1^2 = zV_{acc} - zV_{cell} \qquad (5.2)$$

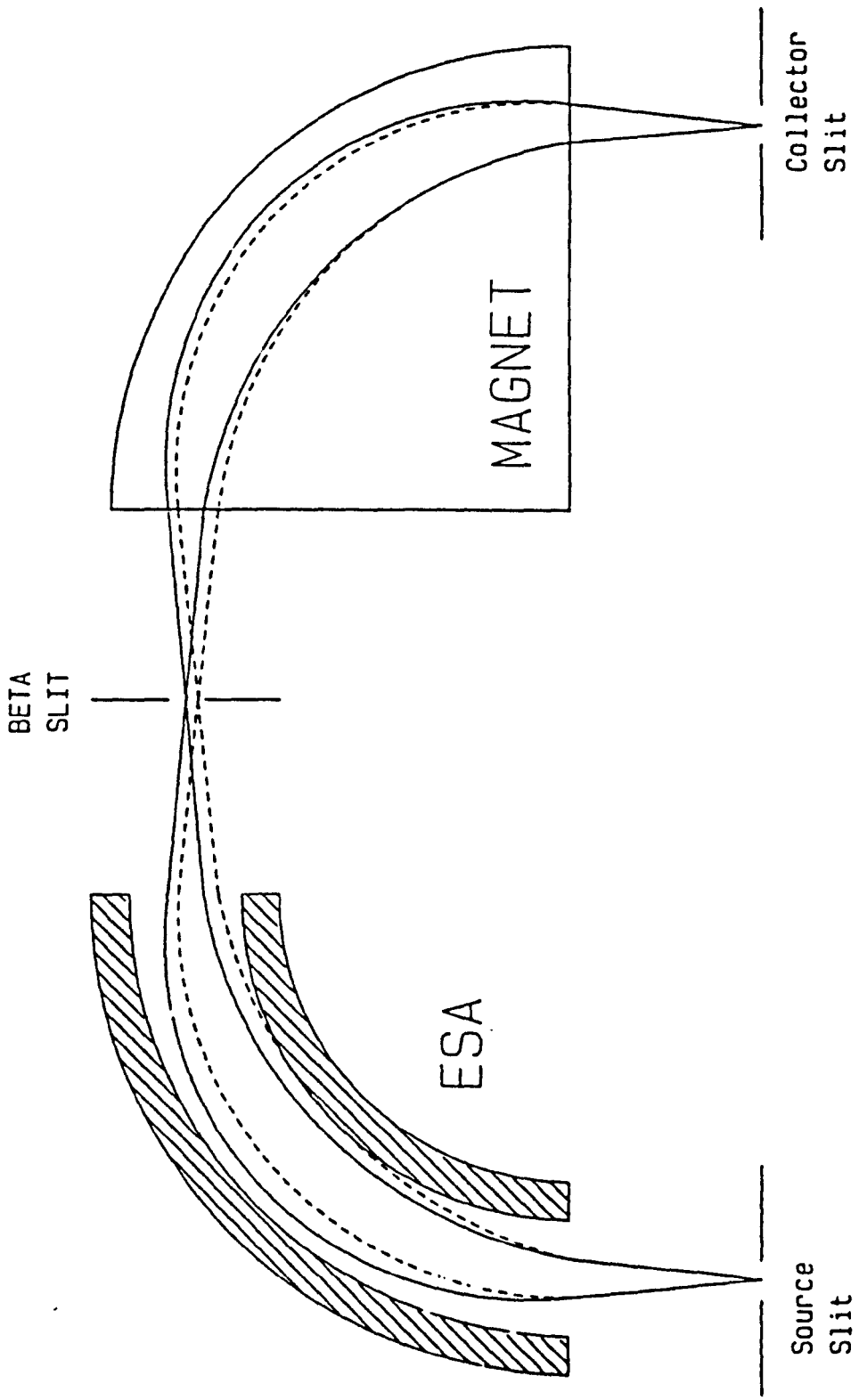

Figure 5.1. The trajectories of ions of normal and low kinetic energy, through a double focusing mass spectrometer.

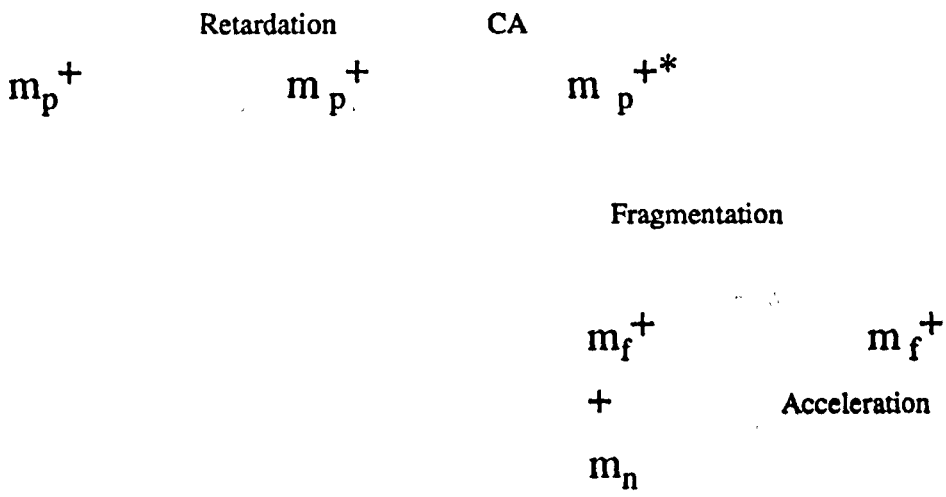

Figure 5.2. Collision induced dissociation in a floated collision cell.

The precursor ion is further retarded by collisions with gas molecules in the collision cell and its kinetic energy is reduced by $z\Delta V$

$$E_k'' = m_p v_2 = zV_{acc} - zV_{cell} - z\Delta V \quad (5.3)$$

On fragmentation, the kinetic energy of the precursor ion will be partitioned between the ion and the neutral molecule formed. The kinetic energy of the fragment ion formed is given by

$$E_{kf} = m_f v_2 = E_k''(m_f/m_p) \quad (5.3a)$$

or

$$E_{kf} = z(m_f/m_p)(V_{acc} - V_{cell} - \Delta V) \quad (5.4)$$

As this fragment ion exits the collision cell it is accelerated by the voltage on the cell. Its final kinetic energy is given by

$$E_{kf}' = m_f v_3 = z(m_f/m_p)(V_{acc} - V_{cell} - \Delta V) + zV_{cell} \quad (5.5)$$

For the ESA to transmit the fragment ion along its axis, its field must be reduced. The initial ESA field is set to transmit ions accelerated from the ion source. The ESA field is reduced by the ratio of the kinetic energy of the fragment and precursor ions:

$$E_1/E_0 = (m_f/m_p)(V_{acc} - V_{cell} - \Delta V)/V_{acc} + V_{cell}/V_{acc}$$

or

$$E_1/E_0 = (m_f/m_p)(1 - V_{cell}/V_{acc} - \Delta V/V_{acc}) + V_{cell}/V_{acc} \quad (5.6)$$

This equation is true for all of the scans described.

For the fragment ion to be transmitted by the magnetic sector, the magnetic field must be reduced. The magnetic field required is derived below.

$$m_f v_f = B_1 z r \qquad (5.7)$$

But from equation (5.5) one can eliminate the velocity of the ion, giving

$$2m_f V_{acc}((m_f/m_p)(1 - V_{cell}/V_{acc} - \Delta V/V_{acc}) + V_{cell}/V_{acc}) = B_1^2 z r^2 \qquad (5.8)$$

The derivation of the individual scan laws requires the knowledge of the mass of a particular species; the precursor ion for fragment ion scans, the fragment ion for precursor ion scans and the mass of the neutral molecule for constant neutral loss scans. Each of these scan laws is derived below.

5.2.2. Fragment Ion Scan.

Initially the magnetic field is set to focus precursor ions formed in the ion source, on the collector slit. This magnetic field is related to the mass of the ion by

$$m_p = B_0^2 z r^2 / 2V_{acc} \qquad (5.9)$$

(c.f. Chapter1).

Eliminating r from equations (5.8) and (5.9) gives

$$B_1^2/B_0^2 = (m_f/m_p)((m_f/m_p)(1 - V_{cell}/V_{acc} - \Delta V/V_{acc}) + V_{cell}/V_{acc}) \qquad (5.10)$$

But from equation (5.6) this can be written

$$B_1^2/B_0^2 = (m_f/m_p)(E_1/E_0) \qquad (5.11)$$

Eliminating (m_f/m_p) using equation (5.6) gives

$$B_1^2/B_0^2 = (E_1/E_0)(E_1/E_0 - V_{cell}/V_{acc})/(1 - V_{cell}/V_{acc} - \Delta V/V_{acc})$$

This is the fragment ion scan law.

5.2.3. Precursor Ion Scan.

For a precursor ion scan, the magnet is initially set to focus fragment ions formed in the ion source, on the collector slit. So

$$m_f v = B_0 z r \qquad (5.12)$$

But

$$m_f v = zV_{acc} \quad (5.13)$$

Eliminating v from equations (5.12) and (5.13) gives

$$m_f = B_0 zr/2V_{acc} \quad (5.14)$$

Eliminating r from equations (5.8) and (5.14) gives

$$B_1/B_0 = (m_f/m_p)(1 - V_{cell}/V_{acc} - \Delta V/V_{acc}) + \Delta V/V_{acc}$$

But, from equation (5.6), this reduces to

$$B_1/B_0 = E_1/E_0$$

This is the precursor ion scan law.

5.2.4. Constant Neutral Loss Scan.

Initially the magnetic field is set to focus ions of mass m_n, formed in the ion source, on the collector slit. So

$$m_n = B_1 zr/2V_{acc} \quad (5.15)$$

Eliminating r from equations (5.8) and (5.15) gives

$$B_1/B_0 = (m_f/m_n)((m_f/m_p)(1 - V_{cell}/V_{acc} - \Delta V/V_{acc}) + V_{cell}/V_{acc}) \quad (5.16)$$

But from equation (5.6) this can be written

$$B_1/B_0 = (E_1/E_0)(m_f/m_n) \quad (5.17)$$

But

$$m_n = m_p - m_f$$

So equation (5.17) can be written

$$B_1/B_0 = (E_1/E_0)(m_f/(m_p - m_f))$$

Or, by inverting and simplifying

$$B_0/B_1 = ((m_p/m_f) - 1)(E_0/E_1) \quad (5.18)$$

Eliminating m_p/m_f using equation (5.6) and rearranging gives

$$B_1/B_0 = (E_1/E_0)(E_1/E_0 - V_{cell}/V_{acc})/(1 - \Delta V/V_{acc} - E_1/E_0)$$

This is the constant neutral loss scan law.

5.3. Implementation of Calibration Software.

The scan laws were derived with the intention of using them in the control of a Kratos Analytical, Concept II HH, four-sector mass spectrometer, equipped with an electrically floated collision cell between the two mass analyzers. Since selection of the precursor ion takes place using the first mass analyzer, the only scan law of value is that for fragment ion scans.

The existing software used for the calibration and control of two sector mass spectrometers, is written in the FORTRAN language for Data General computers. The additional software required for the control of four sector instruments must include the following:

(i) floated cell and translational energy loss calculations,

(ii) the ability to easily select MS1 or MS2 acquisitions,

and (iii) the possibility of still using the software with two sector instruments.

The first version of the software was used to calculate the data necessary to control the digital-to-analogue converter (DAC) which sets the ESA potential as required during a linked scan. After this software was written, the control hardware of the four sector instrument was modified such that the calculation of the effect of collision cell voltage on the ESA potential was performed by the hardware itself, given the uncorrected values. These values are easily calculated given the precursor and fragment ion masses, equation 5.3a. In this case, the calculation of translational energy losses can still be included by modifying the fragment ion mass.

5.3.1. Selection of MS1 or MS2 Calibration and Acquisition.

Since a four sector mass spectrometer has two mass analyzers, a unique set of calibrated reference files must be calculated and stored for each analyzer. The DS-90 software creates reference files for each type of acquisition possible. The filename of each reference file is built up using the characteristics of the acquisition to which it refers. These characteristics are scan-type, start mass, scan speed and resolution. This is shown in figure 5.3.

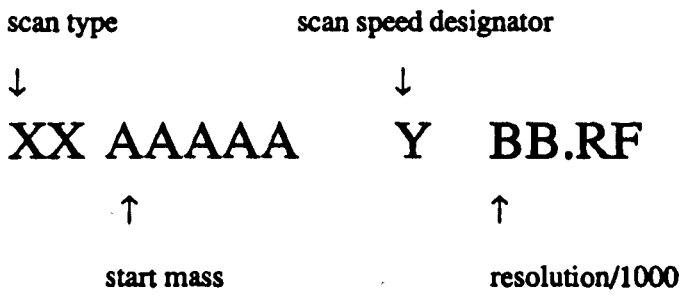

e.g. LR10000H03.RF for a low resolution scan at 30 seconds per decade starting at mass 10000 Daltons with a resolution of 3000.

Figure 5.3. The construction of calibrated reference file names for the DS-90 data system.

There are two possible ways in which identification of the analyzer to which the reference file refers could be made:

(i) addition of a character to the beginning of the filename to distinguish between MS1 and MS2 acquisitions,

or (ii) changing of the second letter of the filename to the next letter in the alphabet when an MS2 acquisition is to be performed.

The first of these methods was discounted since it would require a major re-write of the DS-90 system to cope with the lengthened filename. The latter solution was employed since the necessary changes are simple to implement because of the way in which the filenames are constructed. The effect of these changes is shown in table 5.1.

ACQUISITION TYPE	MS1	MS2
LRP	LR	LS
HRP	HR	HS
SLRP	SL	SM
Magnet	MC	MD
Metastable	MS	MT
Field-to-Mass	FT	FU

Table 5.1. Designators for scan types for CONCEPT II HH mass spectrometer.

The construction of the new filename involves adding one unit to the string variable representing the pair of letters if MS2 is to be scanned. The variable EXPTYPE, stored in the COMMON block MARM.CO, represents which half of the instrument is in operation; EXPTYPE = 0 for MS1 and EXPTYPE = 1 for MS2. The simple solution to the problem is to add this variable to the letter pair in all cases. i.e. in FORTRAN

LETTERS = LETTERS + EXPTYPE

This is the case for metastable, magnet and field-to-mass calibrations. For the remaining calibrations, an algorithm was developed to select the correct letters from an array. Originally, all of the necessary letters are stored in the array DTYPE() as shown in table 5.2. This array was extended to include the new codes, table 5.3.

Array number, n	DTYPE(n)
1	SL
2	LR
3	HR

Table 5.2. Array DTYPE() in original software.

Array number, n	DTYPE(n)
4	SM
5	LS
6	HS

Table 5.3. Extension to the array DTYPE() in new software.

Selection of the calibration type was originally performed using a variable CALEXP, which has one of three values; 1 for SLRP, 2 for LRP and 3 for HRP. Using this variable and the value of EXPTYPE, selection of the correct pair of letters can be achieved using the FORTRAN line:

LETTERS = DTYPE(CALEXP + 3*EXPTYPE)

e.g. for an MS2 LRP acquisition

EXPTYPE = 1 and CALEXP = 2

so CALEXP + 3*EXPTYPE = 5

thus the fifth member of the array 'LS' will be selected. This selection is performed in the MCALMAIN.FR program.

5.3.2. Addition of the New Calibration Software.

The new calibration software were added to the existing software, following the same style of programming. The selection of these new routines is enabled by extending the allowed range of values of the variable which is used to flag which type of scan is being calibrated.

The calibrated reference file for a metastable acquisition contains two sets of information. The first is a set of coefficients related to the ESA DAC setting at any given point during a scan. The second is a list of (mass, time) pairs, starting at the first mass calibrated point, which for a fragment ion scan is the next unit mass above the mass of the precursor ion. The calibration software provides the series of ESA DAC values and a time-to-mass calibration, given the constant mass (i.e. the mass of the precursor ion for a fragment ion scan) and a low resolution calibrated reference file.

5.3.2.1. Calculation of ESA DAC Values Within the DS-90 Software.

In the first version of the new software, terms relating to the collision cell voltage and the translational energy loss were also included in the calculations. Since the ESA DAC value is required, the equations derived in section 5.2 had to be rearranged. The resulting equation used for this calculation is shown as equation 5.19.

$$E_1/E_0 = (V_{cell}/2V_{acc}) + \sqrt{[(V_{cell}/2V_{acc})^2 + (m^*/m_p)(1 - V_{cell}/V_{acc} - \Delta V/V_{acc})]} \qquad (5.19)$$

Once the hardware modification was made, this calculation becomes unnecessary. The calculation of the ESA DAC value is reduced to

$$E_1 = E_0(m_f/m_p)$$

where m_f is calculated from the precursor ion mass, apparent mass, collision cell voltage and translational energy loss using equation 5.20.

$$m_f = \frac{\sqrt{[C^2 + 4(m^*/m_p)(1 - C - \Delta)]} - C}{(2/m_p)(1 - C - \Delta)} \qquad (5.20)$$

where $C = V_{cell}/V_{acc}$

and $\Delta = \Delta V/V_{acc}$

Within the FORTRAN program this equation is split into several lines with temporary variables for simplicity. Figure 5.4 shows the relationship between the ESA potential and magnetic fields strength (note that this axis is mass calibrated), for fragment ion scans of m/ 700 at collision cell voltages of 0, 20, 40, 60, 80 and 100% of the accelerating voltage. In each case the translational energy loss parameters were set to zero.

The remaining calculations, involving the creation of a time-to-mass calibration, are unaffected by the hardware changes and are discussed below.

5.3.2.2. Mass Calibration of Fragment Ion Scans.

The mass calibration of a fragment ion scan is achieved by calculating the time after the start of the scan at which a fragment ion of specific nominal mass will be transmitted through the analyzer to the detector. This calculation is performed for each nominal mass starting with the precursor ion and ending at the lower limit of the low resolution calibrated reference file. The process involves finding the lowest and highest masses in the low resolution calibrated reference file which are applicable, i.e. the precursor ion mass and the last mass in the reference file, and converting them to real, fragment ion masses. In the new version of the software, the conversion of the lowest mass of the low resolution calibrated reference file, which is the lowest apparent or metastable mass which it is possible to transmit, is done using equation 5.20. Once these mass limits have been defined, each nominal, real, fragment ion mass is converted to an apparent mass using equation 5.21, which is derived from equation 5.8.

$$m^* = m_f[(m_f/m_p)(1 - V_{cell}/V_{acc} - \Delta V/V_{acc}) + V_{cell}/V_{acc}] \qquad (5.21)$$

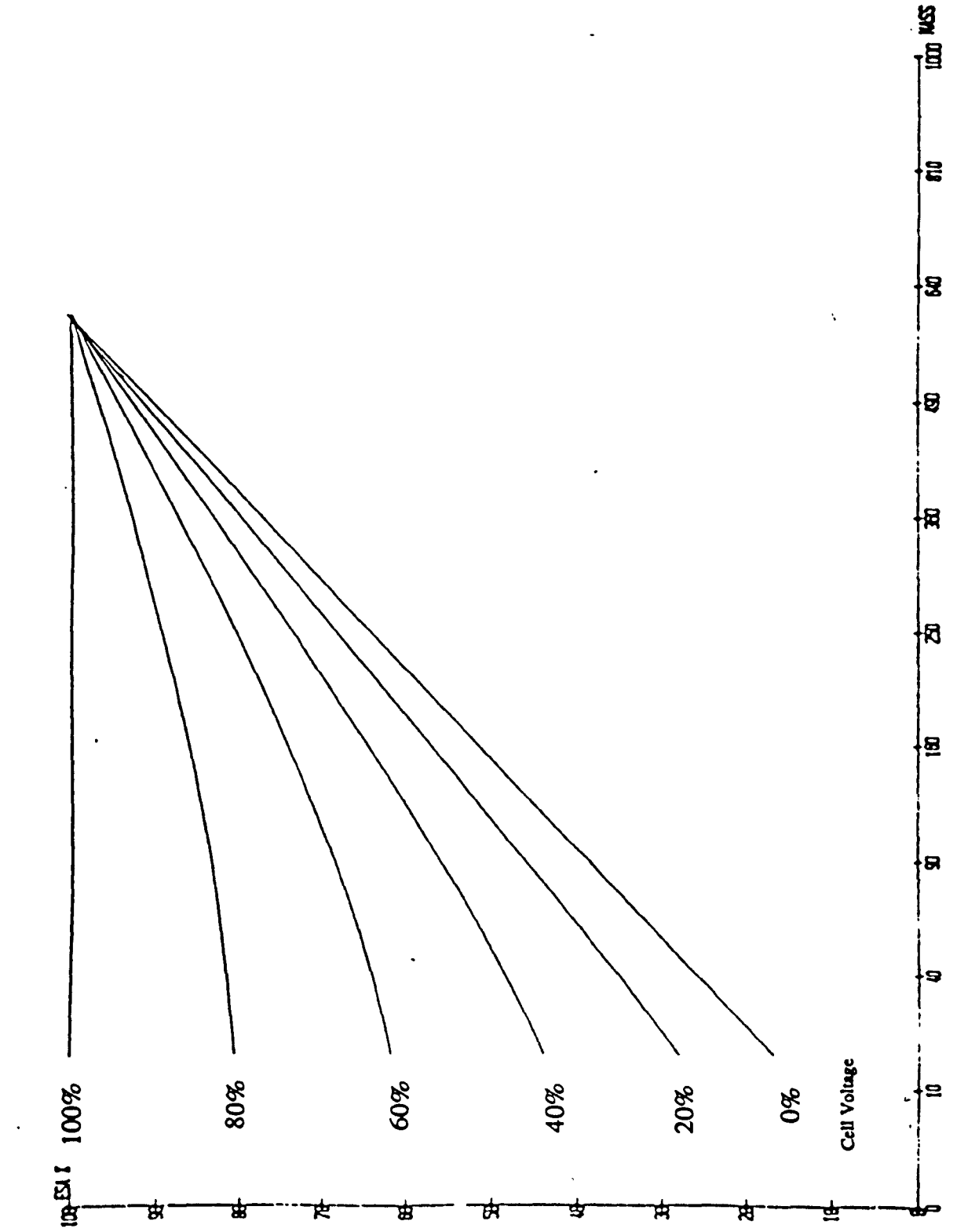

Figure 5.4. Graph of ESA potential against apparent mass, for fragment ion scans of m/z 700 at collision cell voltages of 0, 20, 40, 60, 80 and 100% of the accelerating voltage.

The next procedure locates the nearest higher and lower nominal mass in the low resolution calibrated reference file and their associated times, and performs an interpolation to find the time at which the exact apparent mass, i.e. the nominal real mass, will be transmitted to the detector. The (real mass, time) pair is then written to the metastable calibrated reference file. This is repeated for each nominal mass between the previously determined mass limits.

5.3.3. Calculation of ΔV.

The nature of the ΔV term cannot easily be defined using mathematical models. Derrick and co-workers[1], showed that for gramicidin-A, the translational energy losses caused by CID varied with fragment ion mass. This variation was non-linear, figure 5.5, so the ΔV term included in the new software was also made non-linear. The ΔV term, it was suggested[7], should be parameterized, so that the variation of ΔV with fragment ion mass could be optimized for any given compound and experimental conditions. The calculation of ΔV in the DS-90 software is based on equation 5.22.

$$\Delta V/V_{acc} = a + b[(m_p - m_f)/m_p]^c \qquad (5.22)$$

The parameters a, b and c are set in the calibration parameters menu of the DS-90 data system. The range of allowed values is shown in table 5.4.

Parameter	Range
a	0 - 5% V_{acc}
b	0 - 5% V_{acc}
c	0 - 2

Table 5.4. The range of permitted values for the translational energy loss parameters in the DS-90 metastable calibration software.

It should be noted that it is necessary to calculate the real fragment ion mass before the $\Delta V/V_{acc}$ term can itself be determined. This is facilitated by using a temporary variable OLDMASS, which is initially set to the first mass of the calibration range, usually the

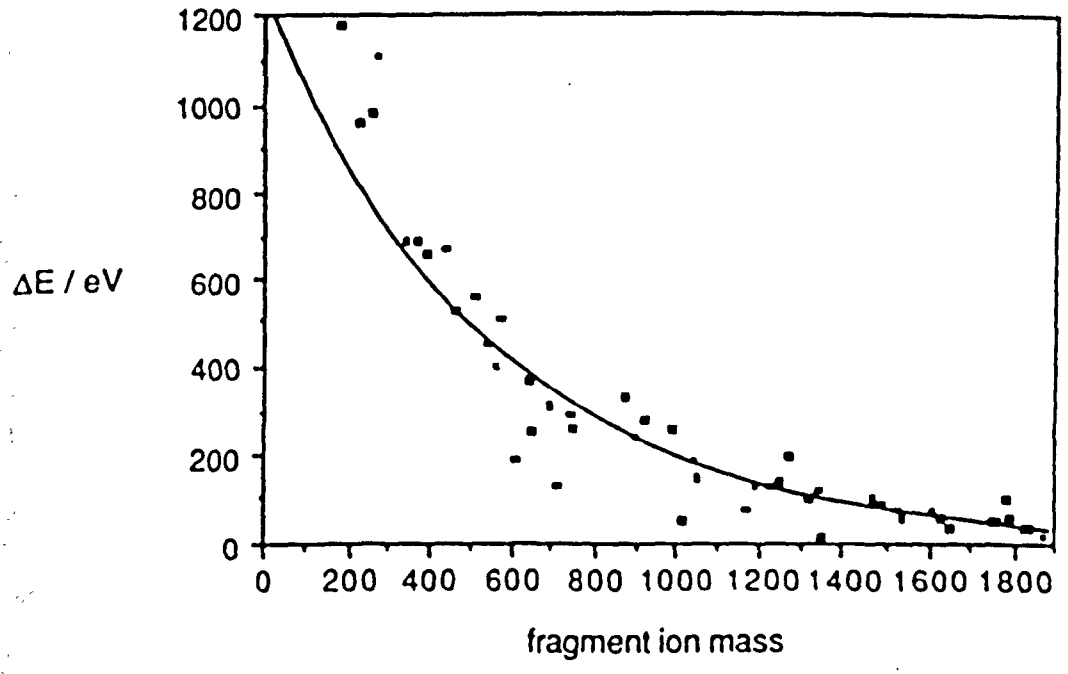

Figure 5.5. A graph illustrating the variation of translational energy loss with fragment ion mass in the CID-MIKES spectrum of gramicidin-A. (Reproduced from ref. 1).

precursor ion mass, and is changed to the fragment ion mass each time this mass is calculated. A flow diagram, figure 5.6, is used to illustrate this point for the calculation of ESA DAC values.

5.4. A Method to Investigate The Nature of the Translational Energy Loss Parameters.

A Kratos Analytical Concept II HH four-sector mass spectrometer, figure 5.7, can be used in two modes of fragment ion scan. Firstly, using PAD 3 as the detector, a MIKES scan can be recorded for a precursor ion selected with high resolution using MS1. The second type is a full four-sector scan, involving high resolution selection of the precursor ion using the first analyzer and a linked scan of the MS2 analyzer.

The effects of translational energy losses of fragment ions formed by CID will be different in both of these spectra. For the MIKES scan, the peaks due to fragment ions which have lost kinetic energy in the CID processes, will appear at a lower ESA potential than would be normally expected. The effect of this on a linked-scan spectrum, for small tranlational energy losses, will be much less drastic because of the double focusing properties of the mass spectrometer. A minor shift to higher mass may occur because of the change in peak shape caused by the loss of ions due to collisions with the inner ESA plate. The centroid of such a peak will be at a slightly higher mass than expected. This can be avoided by using peak-top mass assignment, since changing the shape of the peak will not change the position of the top of the peak. These effects are illustrated in figure 5.8, which shows the relative positions of peaks due to normal (a) and energy deficient (b) ions. If the kinetic energy loss is sufficiently large, the effect on a linked scan will be quite dramatic. It may be possible for some of the energy deficient fragment ions to go undetected. If their trajectory is so far off the ion optical axis, it is conceivable that the ions may not be transmitted to the magnetic analyzer, despite double focusing properties. Recent work by Tomer and Verma have shown this to be the case when translational energy losses are large[8].

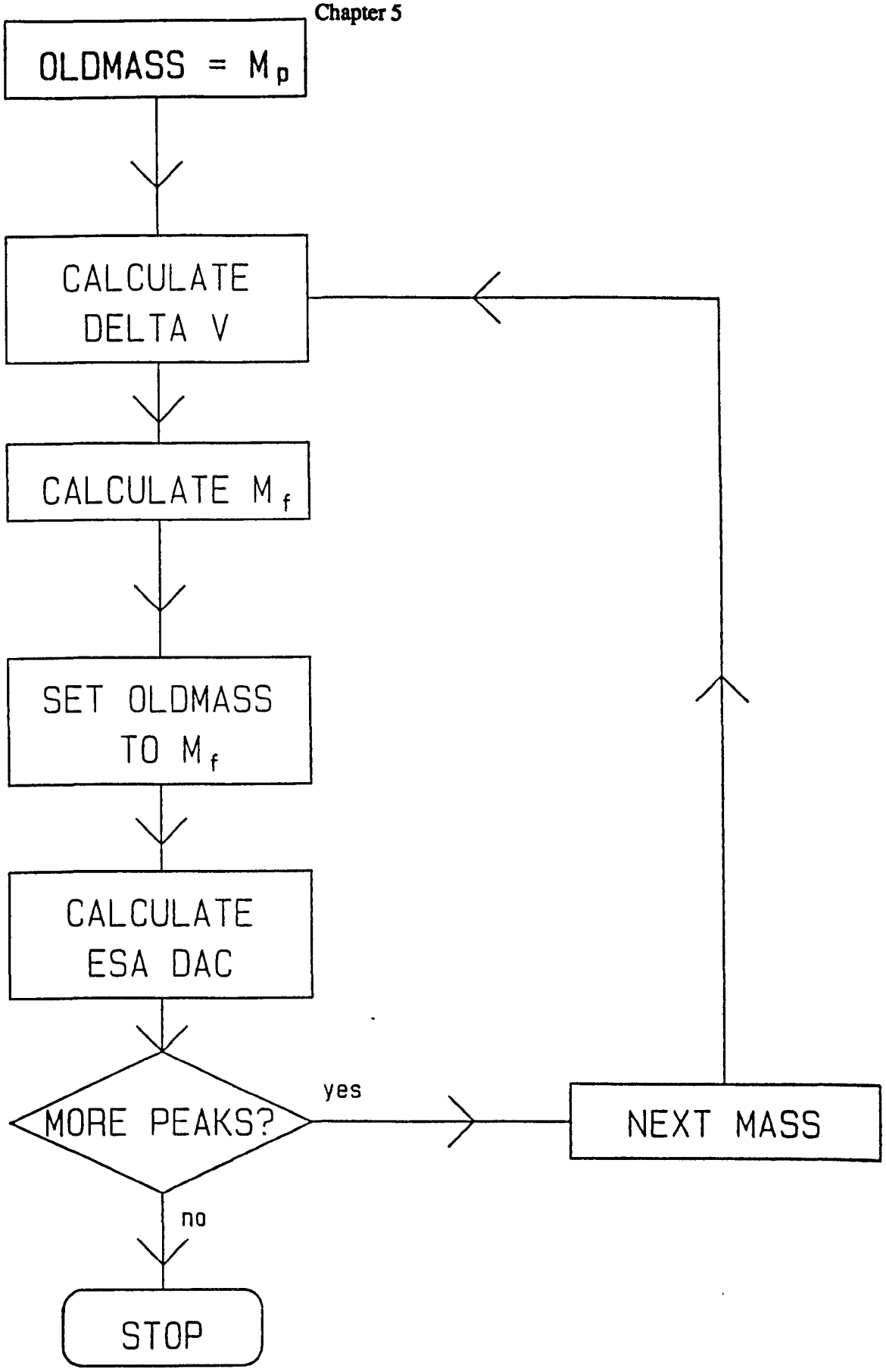

Figure 5.6. Flow diagram illustrating the calculation of ESA DAC values including translational energy losses.

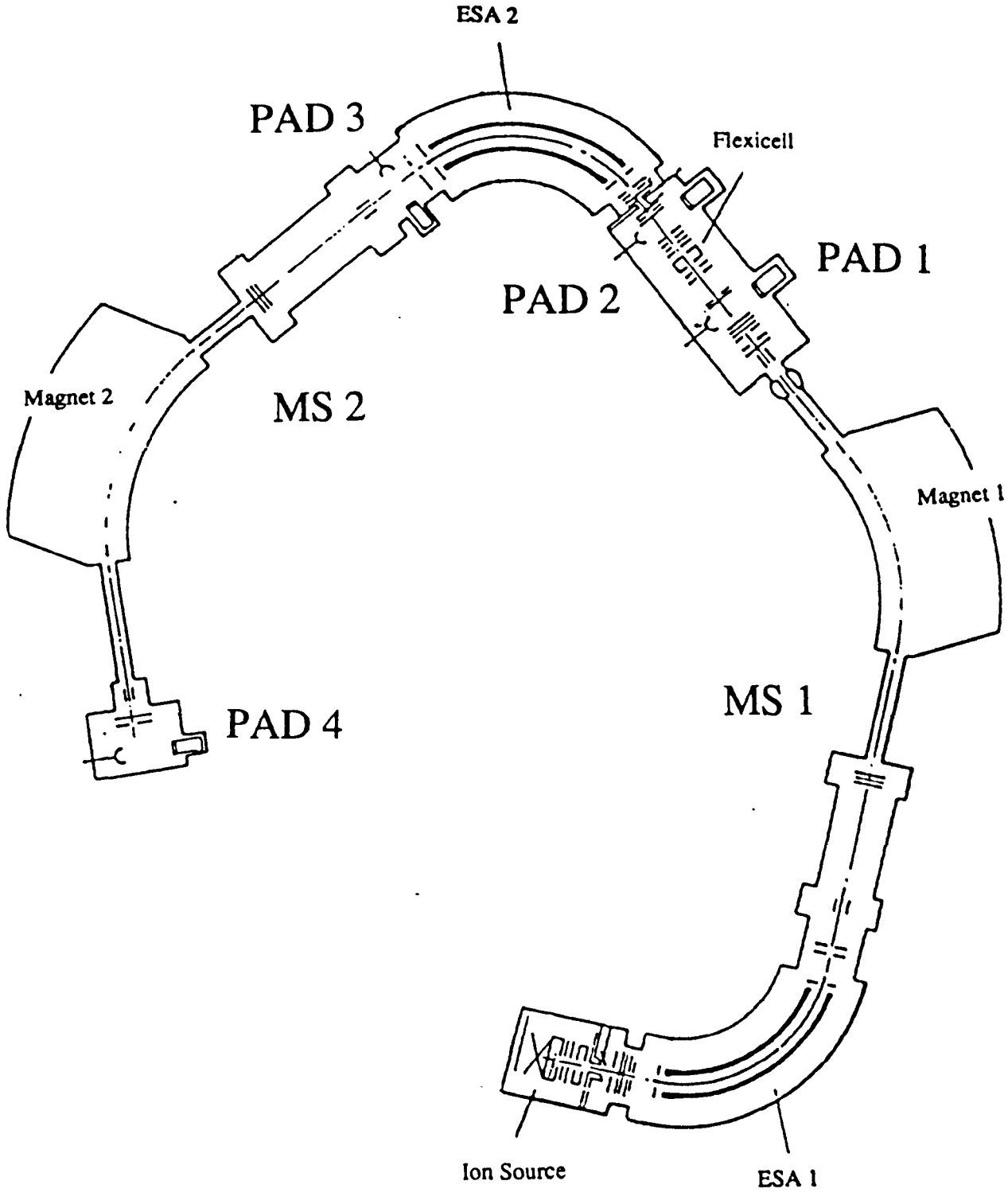

Figure 5.7. Layout of a Kratos Analytical Concept II HH mass spectrometer illustrating the position of the four post acceleration detectors (PADs).

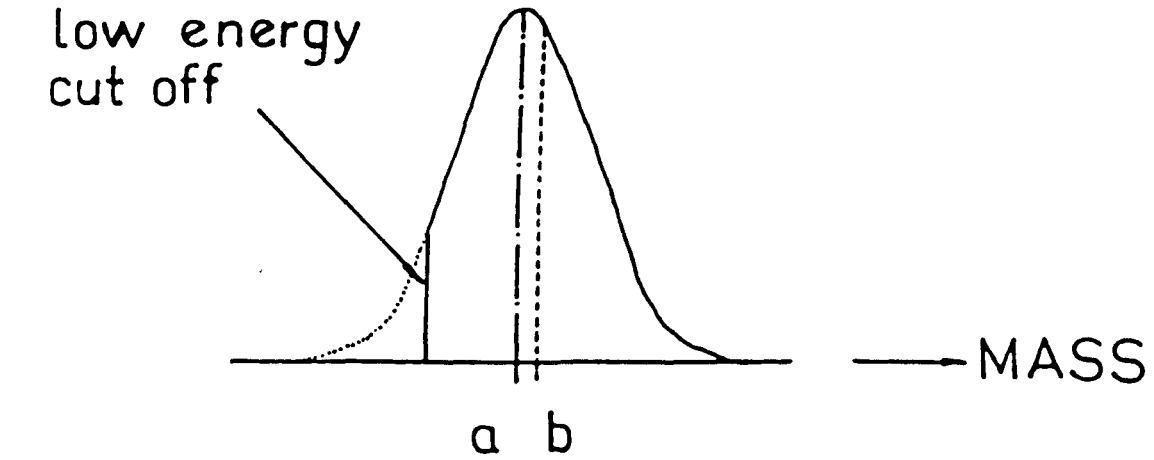

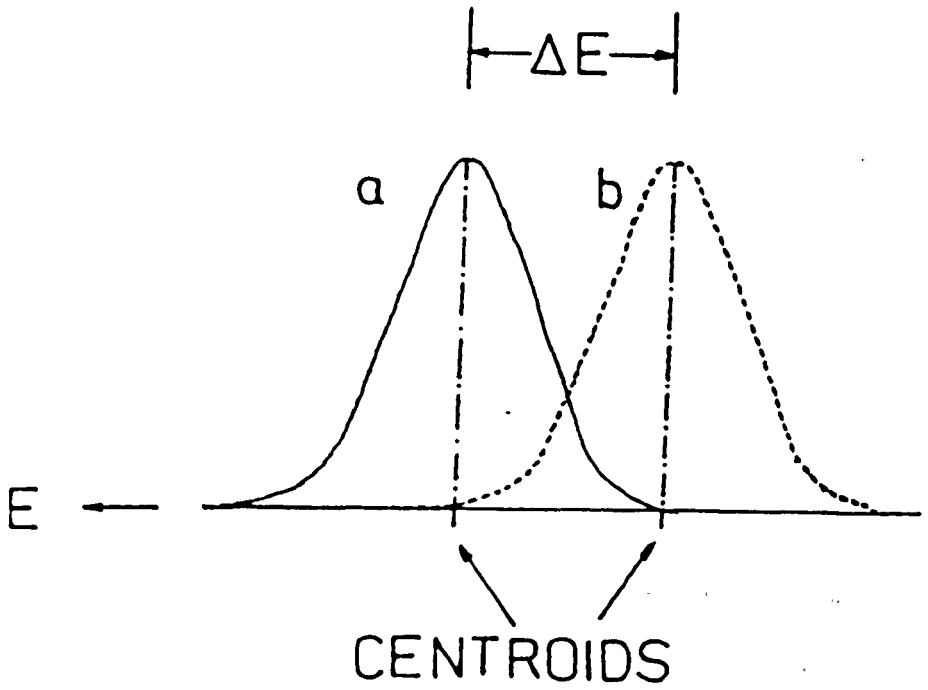

Figure 5.8. The effects of kinetic energy losses on the position of peak centroids in linked-scan and MIKES spectra

In order to determine the TEL parameters, both a MIKES scan and a full linked-scan are required. The MIKES scan will contain peaks shifted in energy due to translational energy losses. The linked-scan spectrum should be correctly mass assigned and so by comparing the masses of the fragment ions in both of the spectra, a value for the translational energy loss can be determined. If this is done for each fragment ion observed, a graph of ΔV against fragment ion mass, similar to that obtained by Shiel and Derrick can be plotted and used to calculate the required TEL parameters a, b and c. This could be performed using a non-linear, least squares, curve fitting program. It may be shown that using this procedure, that the equation used to calculate ΔV is not capable of generating the required values. In this case, a simple modification to the existing software could be made.

5.5. Conclusions.

The software dealing with calculation of ESA DAC values and mass calibrations has been thoroughly tested at several collision cell voltages[9] with all of the TEL parameters set to zero. As yet, the effect on CID mass spectra, of varying the three TEL parameters has not been tested. Initial investigations, whilst writing the software, revealed no major problems in the operation of the modified calibration software.

5.6. References.

1. M.M. Shiel and P.J. Derrick, *Org. Mass Spectrom.*, **23**, 429 (1988).
2. G.M. Neumann and P.J. Derrick, *Org. Mass Spectrom.*, **19**, 165 (1984).
3. G.M. Neumann M.M. Shiel and P.J. Derrick, *Z. Naturforsch.*, **39a**, 584 (1984).
4. "Tandem Mass Spectrometry", Ed. F.W. McLafferty, Wiley, New York, 1983.
5. R. Guevremont and R.K. Boyd, *R. Comms. in Mass Spectrom.*, **2**, 1 (1988).
6. R.K.Boyd, *International Journal of Mass Spectrometry and Ion Processes*, **75**, 243 (1978)
7. Personal communication from Prof. P.J. Derrick.
8. K.B. Tomer and S. Verma, 36th A.S.M.S. Conference on Mass Spectrometry and Allied Topics, San Fransisco, U.S.A., 1988.

9. Unpublished results obtained by J. Bordas-Nagy and D. Despeyroux at Warwick University.